Title:

Biosynthesis of gibberellin-related compounds modulates far-red light responses in the liverwort *Marchantia polymorpha*

Authors:

Rui Sun (孙 芮)[1], Maiko Okabe (岡部 麻衣子)[1], Sho Miyazaki (宮崎 翔)[2], Toshiaki Ishida (石田 俊晃)[3], Kiyoshi Mashiguchi (増口 潔)[3], Keisuke Inoue (井上 佳祐)[1], Yoshihiro Yoshitake (吉竹 良洋)[1], Shohei Yamaoka (山岡尚平)[1], Ryuichi Nishihama (西浜 竜一)[1,4], Hiroshi Kawaide (川出 洋)[5], Masatoshi Nakajima (中嶋 正敏)[6], Shinjiro Yamaguchi (山口 信次郎)[3], Takayuki Kohchi (河内 孝之)[1,*]

[1] Graduate School of Biostudies, Kyoto University, Kyoto 606-8502, Japan.

[2] Institute of Global Innovation Research, Tokyo University of Agriculture and Technology, Fuchu, 183-8509, Japan.

[3] Institute for Chemical Research, Kyoto University, Uji 611-0011, Japan.

[4] Department of Applied Biological Science, Faculty of Science and Technology, Tokyo University of Science, Noda 278-8510, Japan.

[5] Institute of Agriculture, Tokyo University of Agriculture and Technology, Tokyo 183-8509, Japan.

[6] Department of Applied Biological Chemistry, The University of Tokyo, Tokyo 113-8657, Japan.

[*] Correspondence: tkohchi@lif.kyoto-u.ac.jp

Short title:

GA biosynthesis in *M. polymorpha*

The author responsible for distribution of materials integral to the findings presented in this article in accordance with the policy described in the Instructions for Authors (https://academic.oup.com/plcell/pages/General-Instructions) is: Takayuki Kohchi (tkohchi@lif.kyoto-u.ac.jp).

ABSTRACT

The phytohormone gibberellins (GAs) are key regulators of growth, development and environmental responses in angiosperms. From an evolutionary perspective, all major steps of GA biosynthesis are conserved among vascular plants, while GA biosynthetic intermediates such as *ent*-kaurenoic acid (KA) are also produced by bryophytes. Here we show that in the liverwort *Marchantia polymorpha*, KA and GA_{12} are synthesized by evolutionarily conserved enzymes, which are required for developmental responses to far-red light (FR). Under FR-enriched conditions, mutants of various biosynthesis enzymes consistently altered thallus growth allometry, delayed the initiation of gametogenesis, and affected the morphology of gamete-bearing structures (gametangiophores). By chemical treatments and LC-MS/MS analyses, we confirmed these phenotypes were caused by deficiency of some GA-related compounds derived from KA, but not bioactive GAs from vascular plants. Transcriptome analysis showed that FR enrichment induced the up-regulation of genes related to stress responses and secondary metabolism in *M. polymorpha*, which was largely dependent on the biosynthesis of GA-related compounds. Due to the lack of the canonical GA receptors in bryophytes, we hypothesize that GA-related compounds are commonly synthesized in land plants but co-opted independently to regulate responses to light quality change in different lineages during the past 450 million years of evolution.

INTRODUCTION

Throughout evolution, plants developed various chemical tools to optimize growth and development, and to cope with environmental changes. Gibberellins (GAs) are a group of tetracyclic diterpenoid compounds broadly produced by many plants and plant-associated microbes. Among the more than 130 identified GAs, a few of them (GA_1, GA_3, GA_4, and GA_7) are considered as commonly bioactive in angiosperms (reviewed in Sponsel, 2016), stimulating seed germination (Koornneef and van der Veen, 1980; Toyomasu et al., 1998; Yamaguchi et al., 1998a; Ogawa et al., 2003; Gabriele et al., 2009) and promoting growth of various plant organs (Kurosawa, 1926; Koornneef and van der Veen, 1980; Wenzel et al., 2000; Ubeda-Tomás et al., 2008, 2009; Achard et al., 2009; Nelissen et al., 2012).

In *Arabidopsis thaliana*, the biosynthesis of GAs starts with the production of *ent*-kaurene from geranylgeranyl diphosphate (GGDP) by two terpene synthases (TPSs), *ent*-copalyl diphosphate

synthase (CPS) and *ent*-kaurene synthase (KS) (Sun and Kamiya, 1994; Yamaguchi et al., 1998b). Next, *ent*-kaurene is oxidized by two cytochrome P450 monooxygenases (CYPs), first into *ent*-kaurenoic acid (KA) by *ent*-kaurene oxidase (KO), then into GA_{12} by *ent*-kaurenoic acid oxidase (KAO) (Helliwell et al., 1998, 1999, 2001a, 2001b). Finally, GA_{12} is converted into the bioactive form GA_4 through sequential oxidation by two 2-oxoglutarate-dependent dioxygenases (2-OGDs), GA 20-oxidase (GA20ox) and GA 3-oxidase (GA3ox) (Chiang et al., 1995; Yamaguchi et al., 1998a; Williams et al., 1998). A second bioactive GA, GA_1, is different from GA_4 by one additional hydroxyl group on C-13, which is possibly introduced to GA_{12} or KA before the subsequent oxidation steps (Talon et al., 1990; Nomura et al., 2013) (Supplemental Figure 1).

Bioinformatic and chemical analyses revealed that this biosynthetic pathway producing GA_4 and/or GA_1 is conserved among vascular plants (Hirano et al., 2007; Tanaka et al., 2014; Cannell et al., 2020). In several fern species, GA-derived compounds modulate sexual differentiation of gametophytes and spore germination in the darkness (Yamane, 1998; Schneller, 2008; Tanaka et al., 2014; Hornych et al., 2021). Bryophytes have no *bona fide* 2-OGD-family members of GA biosynthesis enzymes, thus considered as lacking the production of common bioactive GAs (Kawai et al., 2014; Bowman et al., 2017; Miyazaki et al., 2018). However, homologs for CPS, KS, KO and KAO still exist in bryophytes, which suggested an ancestral capacity to synthesize the GA precursors KA and GA_{12} in all land plants (Cannell et al., 2020). In the moss *Physcomitrium patens* which lacks KAO, KA is synthesized by a bifunctional CPS/KS and a single KO homolog (Hayashi et al., 2006, 2010; Miyazaki et al., 2011, 2015). The KA derivative, *ent*-3β-OH-KA, is known as a bioactive molecule to regulate protonema differentiation and blue light avoidance in *P. patens* (Hayashi et al., 2010; Miyazaki et al., 2014, 2015, 2018).

In the liverwort *Marchantia polymorpha*, homologs for CPS, KS, KO and KAO were identified in genome-wide analyses (Kumar et al., 2016; Bowman et al., 2017). Also, MpCPS/DTPS3 and MpKS/DTPS4 (hereafter referred to as MpCPS and MpKS) have been reported to catalyze the production of *ent*-copalyl diphosphate and *ent*-kaurene (Kumar et al., 2016; Jia et al., 2022). In transcriptome analysis, upregulation of GA biosynthesis gene homologs was observed under far-red light (FR) enriched conditions, suggesting a role for this pathway in the response to light quality change (Briginshaw et al., 2022). However, no empirical knowledge has been established yet about the exact physiological function of GA-related compounds in liverworts.

FR enrichment mimics the proximity of competitive neighbors in the nature habitat. In many angiosperms, this is perceived by phytochrome (phy) photoreceptors and triggers shade-avoiding responses, including elongation of stem-like structures, hyponastic growth of petioles and acceleration of flowering (Downs et al., 1957; Holmes and Smith, 1975; Morgan and Smith, 1978, 1979; Whitelam and Johnson, 1982; Whitelam and Smith, 1991). GA biosynthesis is often evoked in this process, and is required for the induction of elongative growth (García-Martínez et al., 1987; Beall et al., 1996; Van Tuinen et al., 1999; Hisamatsu et al., 2005; Djakovic-Petrovic et al., 2007; Dubois et al., 2010). For example, in *A. thaliana*, a local FR enrichment at the leaf tip induced the expression of GA biosynthesis genes in both the leaf tip and the petiole, which modulates the hyponastic growth of the petiole (Sessa et al., 2005; Hisamatsu et al., 2005; Djakovic-Petrovic et al., 2007; Bou-Torrent et al., 2014; Kohnen et al., 2016; Küpers et al., 2023). In the gymnosperm *Pinus tabuliformis*, FR-induced shoot elongation was also accompanied with and dependent on the accumulation of bioactive GAs (Li et al., 2020).

As a liverwort, the life cycle of *M. polymorpha* is dominated by the thalloid gametophyte. End-of-day FR irradiation is known to cause hyponastic growth of thallus tips and decrease in chlorophyll (Fredericq, 1964; Ninnemann and Halbsguth, 1965; Fredericq and de Greef, 1966; Fredericq and Greef, 1968). FR enrichment also induced hyponastic thallus growth (Briginshaw et al., 2022), accompanied by the growth activity change of apical meristems and the transition to sexual reproduction (Chiyoda et al., 2008; Inoue et al., 2019; Streubel et al., 2023). Similar to *A. thaliana* and other land plants, these responses in *M. polymorpha* are mediated by the sole phytochrome (Mpphy) and the single-copy transcription factor PHYTOCHROME-INTERACTING FACTOR (MpPIF) (Fredericq, 1964; Inoue et al., 2016, 2019; Streubel et al., 2023). In this study, we characterized evolutionarily conserved GA biosynthesis enzymes in *M. polymorpha* with genetic approach, showing that they were indispensable for developmental and gene expression responses to FR enrichment.

RESULTS

Mp*CPS* is required for thallus morphological changes induced by FR enrichment

To explore the function of GA-related hormones in *M. polymorpha*, we used the CRISPR/Cas9^{D10A} nickase system (Hisanaga et al., 2019; Koide et al., 2020) to create large-deletion mutants of Mp*CPS* (Mp2g07200), which encodes the first enzyme of the biosynthesis

pathway. Two different mutant alleles (Mp*cps-4*^{ld} and Mp*cps-27*^{ld}) with complete loss of the coding sequence (CDS) were isolated from Tak-1, a male wild-type accession (Supplemental Figure 2A). As Mp*CPS* was shown to be up-regulated by FR enrichment (Briginshaw et al., 2022), we observed the thallus morphology of 12-day-old plants grown from gemmae under two different light conditions, either the continuous white light (cW), or cW supplemented with continuous far-red light (cW+cFR). FR enrichment under cW+cFR induced morphological changes in Tak-1 wild-type plants, marked by increased growth angles (hyponasty) and slenderer thallus shapes, the latter shown as the increase of length-width ratio measured from half of the thallus (Figure 1A-C). Such an increase was not observed in Mp*cps*^{ld} mutants, suggesting a role for Mp*CPS* in modulating FR-induced growth responses. Furthermore, Mp*cps*^{ld} mutants were significantly larger in thallus size than wild-type plants, particularly under cW+cFR conditions (Figure 1A,D). It is likely that MpCPS acts in a pathway producing compounds inhibiting growth, rather than promoting growth like bioactive GAs in angiosperms. To complement the mutation, we expressed the CDS of Mp*CPS* with C-terminal Citrine fusion under the control of a cauliflower mosaic virus 35S promoter ($_{pro}$*35S:*Mp*CPS-Cit*) in Mp*cps-4*^{ld}, generating two independent transgenic lines. The complementation lines recovered the hyponastic growth, the thallus shape and the thallus size of Mp*cps-4*^{ld}, confirming that the phenotypes were caused by Mp*CPS* loss-of-function (Figure 1A-D). As a further verification, Mp*cps*^{ld} mutant alleles and complementation lines were constructed in the female wild-type accession (Tak-2). Similarly, Mp*cps*^{ld} mutations resulted in decrease of thallus hyponasty and the length-width ratio, but increased the thallus area drastically under cW+cFR (Supplemental Figure 3).

To examine the influence of Mp*cps*^{ld} on growth activity at the tissue level, we labelled 7-day-old plants grown under cW+cFR with 5-ethynyl-2'-deoxyuridine (EdU), which could be incorporated into actively dividing cells during DNA synthesis. In the wild-type plants, we observed a relatively narrow distribution of EdU-positive nuclei in the slender thallus, dispersing from the apical meristem to the basal region along the midrib. By assigning different pseudo-colors to signals acquired at different depths by confocal microscopy, we found different distributions of dorsal and ventral signals in these plants. Ventral EdU signals along the midrib extended further in the basal direction, suggesting excessive cell divisions specific to the ventral side, which might contribute to the hyponastic growth induced by FR enrichment (Figure 1E).

While in Mp*cps*^{ld} mutants, EdU signals indicated active cell divisions in a broader range. Two fully separated apical meristems were usually seen from the observed region, and the total numbers of EdU-positive nuclei were significantly higher than those of wild-type plants or complementation lines (Figure 1E-F). In addition, dorsal and ventral EdU signals showed similar distribution ranges in Mp*cps*^{ld} mutants, which was consistent with their flat morphology under cW+cFR (Figure 1E).

Mp*CPS* has a role in modulating gametangiophore development

Continuous FR irradiation is known to induce sexual reproduction in *M. polymorpha*, i.e. the formation of sexual branches called gametangiophores, and the differentiation of sexual organs called gametangia (Yamaoka et al., 2018; Inoue et al., 2019). To observe this process, plants were grown from gemmae under cW for 7 days, then transferred to cW+cFR for gametangiophore induction. As a liverwort, *M. polymorpha* undergoes vegetative growth with dichotomous branching, periodically multiplying the number of apical meristems through bifurcation. Generally, all apical meristems remain indeterminate under white light conditions, while a proportion of them become dormant or differentiate into gametangiophores under FR-enriched light conditions (Streubel et al., 2023). During the induction under cW+cFR, we observed higher numbers of total apical meristems in Mp*cps*^{ld} mutants than in wild-type or complementation lines, which is in line with their more active vegetative growth (Figure 2A-B; Supplemental Figure 4A). If the potential for apical meristems to form gametangiophores was similar between the mutants and wild-type plants, higher number of gametangiophore-bearing apexes would be expected in Mp*cps*^{ld} mutants. However, Mp*cps*^{ld} mutants formed fewer gametangiophores than wild-type plants and complementation lines during the first 16 days after FR irradiation, suggesting that gametangiophore formation is inhibited in these mutants (Figure 2A-B; Supplemental Figure 4A).

In addition, the morphology of gametangiophores was distorted in Mp*cps*^{ld} mutants. As *M. polymorpha* is a dioicous species, gametangiophores are sexually dimorphic among plants with different sex chromosomes. The male gametangiophores (antheridiophores) of wild-type plants had roundish, disc-like receptacles, which were ventrally connected to a relatively long and thin stalk at the center. While for Mp*cps*^{ld} mutants, the male receptacles were fan-shaped, attaching to a short and thick stalk(s) at the basal end (Fig 2C,E; Supplemental Figure 4B). Transverse

sectioning revealed thallus-like features in the stalks of Mp*cps*^{ld} antheridiophores. Usually, no air chambers could be observed in the near-cylindric antheridiophore stalks of wild-type plants. In contrast, Mp*cps*^{ld} antheridiophore stalks had a flat dorsal surface beneath which air chambers with photosynthetic filaments were clearly formed (Supplemental Figure 5A), quite similar to the tissue organization in the vegetative thallus (Shimamura, 2016). Besides, Mp*cps*^{ld} antheridiophore stalks frequently have more canals with pegged rhizoids in the ventral side, possibly reflecting additional bifurcation events during gametangiophore morphogenesis (Supplemental Figure 5A).

The female gametangiophores (archegoniophores) of wild-type plants were also stalked and had 9-11 finger-like structure (digitate rays) in the receptacle, which radially arranged like umbrella ribs. Two marginal digitate rays could be recognized as no involucres were produced between them (Figure 2D,F; Supplemental Figure 4B) (Cao et al., 2013). The female receptacles of Mp*cps*^{ld} were palm-like, positioning the two marginal rays at opposite ends. Excessive number of digitate rays and/or bifurcation in the stalk were often observed in late-stage receptacles (Figure 2D,F; Supplemental Figure 4B). In extreme cases from aseptic culture, the archegoniophore of Mp*cps*^{ld} remained the form of bifurcated thalloid branches, with digitate rays formed at the thallus tips (Supplemental Figure 4C). If the relatively fixed number of digitate rays in wild-type receptacles represents a determinate fate for the apical meristem, such excessive bifurcation or additional digitate rays in Mp*cps*^{ld} mutants might suggest a loose transition from the indeterminate vegetative growth. Similar to the male case, the stalks of Mp*cps*^{ld} archegoniophores were shorter and thicker than the wild-type counterparts, bearing more rhizoid canals in the ventral side (Figure 2D; Supplemental Figure 5C).

Since gametangium differentiation accompanies the morphogenesis of gametangiophores, we investigated this progress by examining Citrine-labelled MpBONOBO proteins (MpBNB-Cit), which specifically accumulate in the initial cells and immature gametangia (Yamaoka et al., 2018). To keep the consistency in genetic background, large-deletions of Mp*CPS* were introduced into Mp*BNB-Cit* knock-in lines through thallus transformation (Supplemental Figure 2), again using the CRISPR/Cas9^{D10A} nickase system (Hisanaga et al., 2019). As expected, the gametangiophore morphogenesis was delayed by Mp*cps*^{ld} mutation. After 11 or 14 days of growth under cW+cFR, dome-shaped gametangiophore primordia already formed, respectively, in male and female Mp*BNB-Cit* plants carrying the wild-type Mp*CPS* allele. Under fluorescence

microscopes, arrays and/or clusters of Citrine signals appeared at the edge of primordia, indicating on-going gametangium differentiation in these plants. In contrast, no gametangiophore primordium was yet visible in Mp*cps*^{ld} Mp*BNB-Cit* lines of the same ages. Few or no Citrine-positive nuclei could be found in the apical regions of these plants, suggesting that Mp*cps*^{ld} also caused a delay in gametangium differentiation (Figure 2G-J). Despite such delay, male and female gametangia of normal morphology eventually formed in Mp*cps*^{ld} mutants, as shown by the longitudinal sections of the receptacles (Supplemental Figure 5B,D). Crossing experiments further confirmed the fertility of gametes, as mature spores could be produced from all combinations among Mp*cps*^{ld} and wild-type plants (Supplemental Figure 5E-F).

Mp*cps*^{ld} phenotypes can be rescued by *ent*-kaurenoic acid (KA)

To explore the GA biosynthesis pathway possibly blocked by Mp*cps*^{ld}, we first investigated if common GAs from angiosperms could be detected endogenously in *M. polymorpha*. The plants were cultured for 10 days under cW, then 4 days under cW+cFR before harvested for analysis with liquid chromatography-tandem mass spectrometry (LC-MS/MS). In the Tak-1 wild-type plants, GA_{12} but not any downstream compounds from the angiosperm GA biosynthesis pathway could be detected (Figure 3A-B; Supplemental Figures 1 and 6A). The endogenous level of GA_{12} is 28.9 ± 6.5 pg/g fresh weight on average, which is much lower than the levels in the seedlings of *Arabidopsis thaliana* (Nomura et al., 2013). In Mp*cps-4*^{ld} plants cultured under the same conditions, endogenous GA_{12} did not reach the detection limit, which supported the loss of GA biosynthesis in this mutant (Figure 3B).

Next, we tested the effect of GA-related compounds on *M. polymorpha*. For thallus morphology observation, gemmae were planted on agar medium containing different GAs or the solvent control, then cultured under cW+cFR for 12 days. For gametangiophore induction, plants were transferred onto agar medium containing chemicals at the onset of cW+cFR induction. Several bioactive GAs in vascular plants and the GA biosynthesis precursor, KA, were tested on wild-type and Mp*cps-4*^{ld} mutants. GA_{12} was not included in the assay due to its limited availability. As a result, 2-μM KA application fully complemented Mp*cps-4*^{ld} phenotypes. The thallus shape, the progress of gametangiophore formation and the gametangiophore morphology were all restored to the manner of wild-type plants (Figure 3C-F). Furthermore, KA treatment altered the thallus morphology of Mp*cps-4*^{ld} in a dose-dependent manner under cW+cFR. 100-nM KA was

sufficient to induce clear changes in the size, shape and hyponasty of the mutant thallus (Supplemental Figure 7A, C-E). Compared to Mp*cps-4*^{ld}, wild-type plants are less sensitive to the same concentration of KA (Figures 3C-F, 4F-I). Such difference could be explained by an endogenous KA sink in the wild-type plants, but also suggested that KA is likely a biosynthetic intermediate rather than being directly bioactive. No active GAs in angiosperms (GA_1, GA_3 or GA_4) rescued Mp*cps-4*^{ld} as efficiently as KA, which was consistent with their absence in *M. polymorpha*. GA_9 methyl ester (GA_9-Me), which is released by several ferns as a pheromone and could rescue Pp*cps/ks* phenotype in the moss *P. patens* (Yamauchi et al., 1996; Tanaka et al., 2014; Hayashi et al., 2010), did not work on Mp*cps-4*^{ld} in *M. polymorpha* (Figure 3C-F).

Taken together, these data indicated that Mp*cps*^{ld} phenotypes were likely caused by the deficiency in one or more GA-related diterpenoid compounds, which are derived from KA but different from bioactive GAs in vascular plants. For convenience, hereafter we refer to these putative bioactive compounds collectively as GA_{Mp}.

MpKOL1 and MpKAOL1 catalyze the biosynthesis of KA and GA_{12}, respectively

The enzymatic activities for MpCPS to produce *ent*-copalyl diphosphate and MpKS (Mp6g05950) to produce *ent*-kaurene have been biochemically confirmed in the previous research (Kumar et al., 2016). To find the downstream enzymes catalyzing KA and GA_{12} biosynthesis in *M. polymorpha*, we tested the enzymatic activity of KO and KAO homologs (Figure 4A). Three KO homologs were identified by phylogenetic analysis in *M. polymorpha* (Supplemental Figure 8), and each of them was expressed in the methylotrophic yeast *Pichia pastoris* together with the *Arabidopsis* CYTOCHROME P450 REDUCTASE 1 (AtCPR1, AT4G24520). The yeasts were co-cultured with the substrate (*ent*-kaurene) for two days, then the culture infiltrates were extracted and analyzed with gas chromatography-mass spectrometry (GC-MS). KA was generated as a major product in the yeast culture expressing MpKOL1 (Mp3g18320), but not detected in cultures expressing MpKOL2 (Mp2g01950) or MpKOL3 (Mp2g01940) (Figure 4B; Supplemental Figure 6B).

All currently known plant-type KAOs belong to the CYP88 family, in which two *M. polymorpha* members (MpKAOL1, Mp4g23680; and MpKAOL3, Mp2g10420) were confirmed by our phylogenetic analysis. Previous analysis considered the protein encoded by Mp1g25410 as a KAO homolog and named it MpKAOL2 (Bowman et al., 2017). In our current analysis, this

protein and its liverwort homologs were closely related to CYP729 family members, which are distinctively different from CYP88 proteins (Supplemental Figures 9-10). After two day's culturing, *Pichia* cells expressing MpKAOL1 showed a clear consumption of KA and production of GA_{12}, which displayed identical retention time and mass spectra with the major product from the AtKAO1-expressing culture, i.e. the positive control. While in the MpKAOL3-expressing culture, consumption of KA was limited and no GA_{12} production was detected (Figure 4C-D, Supplemental Figure 6B). Although we were not able to thoroughly investigate all the products, it seems that MpKOL1 and MpKAOL1, but not their *M. polymorpha* homologs, harbor catalytic activities similar to angiosperm GA biosynthesis enzymes.

By expressing Citrine-fused proteins under the control of the 35S promoter, we observed the subcellular localization of the four *M. polymorpha* enzymes which showed catalytic activities related to GA biosynthesis (Supplemental Figure 11). MpCPS-Cit and MpKS-Cit proteins were localized in the chloroplasts, most likely in the stroma as the Citrine signal intensities displayed complementary patterns to the thylakoid-enriched chlorophyll (Supplemental Figure 11A-B). The signals of MpKOL1-Cit proteins were also associated with chloroplasts, being strongest in chloroplast envelopes (Supplemental Figure 11C). On the other hand, MpKAOL1-Cit proteins seemed to aggregate in the endomembrane system and could be observed near the nuclear envelope and the plasma membrane (Supplemental Figure 11D). Overall, the subcellular distribution of these proteins were similar to their homologs in *A. thaliana* (Sun and Kamiya, 1994; Helliwell et al., 2001b), supporting them as being evolutionary conserved in land plants.

KA is a pivotal intermediate in the biosynthesis of GA-related hormone

To validate the physiological role of GA biosynthesis enzymes other than MpCPS *in vivo*, we created loss-of-function mutants for all KS, KO and KAO homologs in *M. polymorpha*, using the CRISPR/Cas9^{D10A} nickase or the CRISPR/Cas9 system (Supplemental Figure 2B-D; Supplemental Figure 12). Consistent with the enzymatic activities in yeast or *in vitro* (Kumar et al., 2016), Mp*ks-14*^{ld}, Mp*kol1-7*^{ld}, and Mp*kaol1-7*^{ge} mutants completely lost the ability to produce GA_{12} endogenously (Figure 4E; Supplemental Figure 6C-D). Under cW+cFR conditions, the phenotypes of Mp*ks*^{ld} and Mp*kol1*^{ld} mutants were similar to that of Mp*cps*^{ld}. The thalli of these mutants were significantly larger, wider and flatter than those of wild-type plants (Figure 4F-G). Mp*ks*^{ld} and Mp*kol1*^{ld} mutants were delayed in gametangiophore formation, and their

antheridiophores had fan-shaped receptacles and short thick stalks (Figure 4H-I). As MpKS and MpKOL1 catalyze reactions prior to KA biosynthesis, we tested if KA could rescue the phenotypes of Mp*ks*^{ld} and Mp*kol1*^{ld}. Indeed, 2-μM KA application fully restored the thallus morphology and gametangiophore formation in these mutants, which further supported that KA biosynthesis has a pivotal role in the FR response of *M. polymorpha* (Figure 4F-I).

In addition to MpKS, the other TPS-e/f clade member, MpTPS1 (Mp6g05430), is known to produce *ent*-kaurene as a minor product (Kumar et al., 2016). However, Mp*tps1*^{ld} mutants showed similar morphology to wild-type plants under cW or cW+cFR conditions, suggesting that Mp*TPS1* is not a major gene required for GA_{Mp} biosynthesis (Supplemental Figure 12A; Supplemental Figure 13). Mp*KOL2* and Mp*KOL3*, the homologs of Mp*KOL1*, are tandemly arranged in the genome, so we removed the whole genomic fragment containing both genes with CRISPR/Cas9^{D10A} nickase (Supplemental Figure 12B). Again, no phenotype related to FR response was observed, which is consistent with the lack of KA-producing activity for both enzymes (Supplemental Figure 13).

As MpKAOL1 could catalyze the KA to GA_{12} conversion, we hypothesized that this is a reaction leading to the biosynthesis of GA_{Mp} in *M. polymorpha*. As a fact, Mp*kaol1*^{ge} mutants were defective in FR response, in a manner similar to the KA biosynthesis mutants. After 12 days of growth under cW+cFR, large wide and flat thallus was observed in Mp*kaol1*^{ge} mutants (Figure 4F-G). Since MpKAOL1 is likely to act downstream of KA synthesis, these mutants were not supposed to be very sensitive to KA treatment. In the experiments, although 2 μM of KA slightly altered the thallus morphology under cW+cFR, while no significant changes could be observed at concentrations equal to or lower than 1 μM (Figure 4F-G; Supplemental Figure 7B-E). Mp*kaol1*^{ge} mutants also showed a moderate delay in gametangiophore formation, which was insensitive to KA treatment. However, the antheridiophore morphology of Mp*kaol1*^{ge} mutants was similar to that of wild-type plants, suggesting that the biosynthesis of GA_{Mp} might not be completely abolished by Mp*kaol1*^{ge} (Figure 4H-I). Complete deletion of the other KAO homolog, Mp*kaol3*^{ld}, failed to show any severe defects in FR response, yet double mutants would be needed for future research to carefully examine the redundancy with MpKAOL1 (Supplemental Figures 12C and 13).

FR enrichment induced GA biosynthesis in a Mp*PIF*-dependent manner

Recent research reported that several GA biosynthesis genes were up-regulated under FR-enriched light conditions (Briginshaw et al., 2022). In our previous transcriptome data (Hernández-García et al., 2021), irradiation solely with FR light significantly increased the expression of Mp*KOL1* within 1 h, and the expression of Mp*CPS* and Mp*KAOL1* after 4 h of treatment. Such responses were only seen in the wild-type plants but not the Mp*pif*^{ko} mutant, indicating that it is a process controlled by the Mpphy-MpPIF signaling module (Supplemental Figure 14A). Similarly, when we transferred 7-day-old plants grown under cW conditions to cW+cFR, Mp*PIF*-dependent up-regulation of Mp*CPS*, Mp*KS*, Mp*KOL1* and Mp*KAOL1* expression could be detected by quantitative polymerase chain reaction (qPCR) within 24 h (Figure 5A, Supplemental Figure 14B). Interestingly, Mp*KOL1* showed a slightly different expression pattern to the other three genes. MpKOL1 expression peaked at 8 h after induction but slightly decreased at the 24-h time point, while the expression of Mp*CPS*, Mp*KS* and Mp*KAOL1* gradually increased in the 24 h after induction, which might reflect different modes of transcriptional regulation. Consistent with the gene expression, we detected a higher level of endogenous GA_{12} in plants induced with cW+cFR than those kept under cW conditions, which suggested the accumulation of GA-related compounds under FR-enriched conditions (Figure 5B).

GA-related hormone regulated transcriptional responses to FR enrichment

To explore gene expression changes related to GA biosynthesis in *M. polymorpha*, we analyzed transcriptomes from thalli grown under cW or cW+cFR for 12 days, either of wild-type plants, or of Mp*cps-4*^{ld} mutants with or without 2-μM KA treatment. In agreement with the mild change in thallus morphology, only a few genes were differentially expressed between Mp*cps-4*^{ld} and wild-type plants under cW conditions (Figure 5C; Supplemental Data Set 1). In particular, the expression of Mp*TPS6*, which encodes an enzyme producing *cis*-kolavenol (Jia et al., 2022), was significantly decreased in Mp*cps-4*^{ld} and rescued by KA under cW. In contrast, 780 and 257 genes were down- and up-regulated, respectively, in Mp*cps-4*^{ld} mutants under cW+cFR, suggesting a more active function of GA_{Mp} under FR-enriched conditions. A proportion of the differentially expressed genes could be rescued by KA application (Figure 5C; Supplemental Data Set 1). For most of the Mp*cps*^{ld}-affected genes, the expression was strongly altered by FR

enrichment in the wild-type plant, and the differential expression in Mp*cps-4*^{ld} was essentially the reduction in FR-induced gene expression change (Figure 5D). If we compare the transcriptomes between cW+cFR and cW, the numbers of up- and down-regulated genes both declined by more than 60% in the Mp*cps-4*^{ld} mutant (Figure 5E).

Using fussy gene ontology (GO) annotations generated with the Blast2GO algorithm (Conesa and Götz, 2008; Hernández-García et al., 2021), we performed GO enrichment analyses for biological processes on differentially expressed genes in Mp*cps-4*^{ld} under cW+cFR (Figure 5F; Supplemental Data Set 2). Although KA application rescued only a limited proportion of gene expression changes in Mp*cps*^{ld}, the patterns of enriched GO terms were quite similar in both comparisons. Mp*cps-4*^{ld} down-regulated or KA-upregulated genes were enriched in GO terms related to stress response and secondary metabolism, among which top-ranked the phenylpropanoid metabolic process. When we carefully checked gene homologs, 23 genes putatively catalyzing biosynthesis of auronidins, bibenzyls or lignin monomers were up-regulated by FR enrichment in a Mp*CPS*-dependent manner (Supplemental Figure 15A). In the Mp*cps-4*^{ld} down-regulated gene set, we also found 30 CYPs, 12 2-OGDs and 7 uridine 5'-diphospho-glucuronosyltransferases (UGTs), all of which were mostly homologs specific to *M. polymorpha* or liverworts, possibly associated with lineage-specific metabolites (Supplemental Figure 15B-D). It seemed that *M. polymorpha* was allocating more resources to stress and defense responses under FR-enriched conditions, yet less doing so when GA_{Mp} biosynthesis was defective. On the other side, GO enrichment captured photosynthetic genes in the Mp*cps-4*^{ld} up-regulated gene set (Figure 5F), which suggested that this mutant might be more resistant to FR-induced chlorophyll reduction (Fredericq and de Greef, 1966). Cell-wall related enzymes and peroxidases were found in both down- and up-regulated gene sets, which was in agreement with the change in thallus growth allometry caused by FR enrichment or Mp*cps*^{ld}, but might also be related to stress and defense responses (Supplemental Figure 15E-F).

Gene expressions of several phytohormone pathways were altered by Mp*cps*^{ld} under cW+cFR. First of all, FR-induction of Mp*KS* and Mp*KAOL1* was reduced in Mp*cps-4*^{ld}, which suggested that GA biosynthesis might be regulated by positive feedback in *M. polymorpha* (Supplemental Figure 15G). Such an effect was confirmed with qPCR, in which 3 days of KA treatment partially restored Mp*KS* and Mp*KAOL1* expression (Figure 5G). Mp*KOL1* expression was not affected by Mp*cps*^{ld} or KA treatment, suggesting that it is not a target for such feedback regulation. For

cytokinin, the biosynthesis enzymes Mp*IPT2* and Mp*LOG*, and the deactivation enzyme Mp*CKX2* were down-regulated in Mp*cps-4*^{ld} (Supplemental Figure 15G). Previous research showed that Mp*CKX2* overexpression reduced the level of cytokinins, restricted thallus growth and increased thallus hyponasty under cW (Aki et al., 2019). It is possible that FR enrichment changed the thallus growth via coordinated deactivation of cytokinins and accumulation of GA_{Mp}. Furthermore, expression of three abscisic acid (ABA) metabolic genes (MpABA4, MpNCED, MpCYP707A) and more than 40 ABA-responsive, LATE EMBRYOGENESIS ABUNDANT-like (LEA-like) proteins were induced by FR enrichment, similar to the response in *A. thaliana* (Michaud et al., 2023) (Supplemental Figure 15H). Such induction was reduced in Mp*cps-4*^{ld} and restored by KA application, which showed similar tendency as the overall stress response.

DISCUSSION

Light quality, i.e. the ratio of red and far-red lights, is an important environmental clue for nearly all land plants to optimize their growth and photosynthesis efficiency. Using a reverse-genetic approach, we showed that biosynthesis of gibberellin-related diterpenoids is required for many aspects of FR response in the liverwort *M. polymorpha*. Under FR-enriched conditions, wild-type plants often develop narrow and hyponastic thallus and begin to form gametangiophores, which is accompanied with increased expression of GA biosynthesis genes and accumulation of GA_{12} (Figures 1, 2, 5) (Fredericq and de Greef, 1966; Briginshaw et al., 2022). In contrast, Mp*cps*^{ld} and other GA biosynthesis mutants developed wide and flat thallus, with a delay in the gametangiophore formation (Figures 1, 2, 4). Application of the biosynthesis intermediate KA rescued all mutants deficient of its biosynthesis (Figures 3, 4), indicating that these phenotypes were likely caused by the deficiency of some KA-derived diterpenoid compound(s), which we named GA_{Mp}. In angiosperms, GA constantly modulates growth and development throughout the life cycle, mostly by promoting growth via cell elongation and/or cell division (Hedden, 2020). But in *M. polymorpha*, GA_{Mp} deficiency had little influence on the vegetative growth under white light conditions. The bioactivity of GA_{Mp} was observed only after its induced accumulation under FR-enriched conditions, suggesting that it served as a hormone coping with environmental changes, rather than constitutively regulating growth. Moreover, the thallus size was increased in GA_{Mp} biosynthesis mutants under cW+cFR (Figures 1, 4), implying that GA_{Mp} actively inhibits rather than promotes growth in the gametophyte of *M. polymorpha*.

FR enrichment induced hyponastic growth in the thallus of *M. polymorpha*, which is comparable to the increase of leaf hyponasty in shade-avoiding angiosperms. In *A. thaliana*, FR enrichment triggers the hyponastic growth by preferentially enhancing cell elongation in the abaxial side of the petiole (Küpers et al., 2023). While in *M. polymorpha*, such response relies on the regional growth driven by apical meristems. In previously reported end-of-day FR irradiation experiments, if the treatment was discontinued after several cycles, the newly-grown apical region resumed pleiotropic orientation, while the basal part remained hyponastic (Fredericq and Greef, 1968). With EdU analysis, we observed cell division patterns under FR-enriched conditions, which was most active near the apical meristem. The hyponastic growth in wild-type plants were marked with excessive cell division in the ventral side of the thallus, implying a role for differential cell proliferation in this process. The large and flat thallus of Mp*cps*^{ld} mutants have more actively dividing cells in total, which showed no dorsiventrally biased distribution (Figure 1). Since Mp*cps*^{ld} phenotypes could be complemented by expression of Mp*CPS* using the constitutive 35S promoter, which was equally active in dorsal and ventral tissues (Althoff et al., 2014), it is unlikely that FR-induced hyponasty is established directly by differential biosynthesis of GA_{Mp}. This is similar to the situation in *A. thaliana* petioles, where GA served as a modulator for FR-induced hyponasty but showed no biased adaxial-abaxial activity (Küpers et al., 2023).

The erected, stalked gametangiophores of *M. polymorpha* could be considered as an extreme form of hyponastic growth, and dorsal tissues were evidently reduced in the cylindrical stalks of wild-type plants (Shimamura, 2016). The stalks of Mp*cps*^{ld} gametangiophores were relatively short and thick, bearing dorsal air chambers similar to the vegetative thallus, which showed less biased dorsoventral growth (Figure 2; Supplemental Figure 5). This phenotype resembled that of Mp*kanadi* (Mp*kan*), which was depleted of the sole *M. polymorpha* homolog for KANADI, a family of transcription factors regulating tissue polarity in angiosperms (Briginshaw et al., 2022). Under cW+cFR, both Mp*kan* and Mp*cps*^{ld} mutants were reduced in hyponasty, formed thallus-like gametangiophores with delay but generated fertile gametes, which could be explained by the dysfunction of Mp*kan* to up-regulate the expression of GA_{Mp} biosynthesis genes in response to FR irradiation (Briginshaw et al., 2022).

By tracing germ cell progenitors with MpBNB accumulation, we found that Mp*cps*^{ld} mutants were delayed in germline differentiation (Figure 2). Many fern species use GA-related

pheromones, i.e. antheridiogens, to control germline differentiation in the population. Particularly, antheridiogens promote the formation of male antheridia, and inhibits female archegonia in undifferentiated gametophytes (Näf et al., 1975; Tanaka et al., 2014; Hornych et al., 2021). In *M. polymorpha*, sexual differentiation is known to be determined by a sex chromosome-located gene (Iwasaki et al., 2021), and MpBNB accumulation was similarly delayed in both male and female Mp*cps*^{ld} gametophytes, suggesting no sexual bias in the function of GA_{Mp}.

We partially elucidated the biosynthetic pathway of GA_{Mp} with biochemical and genetic approaches. Previous bioinformatic research suggested that early steps of GA biosynthesis are conserved in land plants, and the *M. polymorpha* genome contains multiple homologs for KO and KAO (Bowman et al., 2017; Cannell et al., 2020; Yoshida et al., 2020). Using the yeast expression system, we detected the production of KA by MpKOL1 and GA_{12} by MpKAOL1, showing the two enzymes possessing enzymatic activities similar to their angiosperm homologs. Genetic analyses also supported that KA is synthesized via the sequential action of three single enzymes (Mp*CPS*, Mp*KS*, and Mp*KOL1*), as their mutants were consistently defective in FR light responses (Figure 4). Intriguingly, although GA_{12} production was almost completely blocked in Mp*kaol1*^{ge} mutants, we only saw morphological phenotypes in the vegetative thallus, but not in the gametangiophores. As monooxygenases, it takes three sequential steps for CYP enzymes to catalyze the KA-to-GA_{12} conversion, first from KA to *ent*-7-hydroxy-kaurenoic acid (7OH-KA), then from 7OH-KA to GA_{12}-aldehyde, and finally from GA_{12}-aldehyde to GA_{12} (Helliwell et al., 2001a). In the GA-producing fungus *Fusarium fujikuroi*, even though GA_{12} production still occurs, it is largely bypassed through 3β-hydroxylation of GA_{12}-aldehyde to form GA_{14}-aldehyde, which is then converted into GA_{14} and other gibberellin compounds (Hedden et al., 1974; Urrutia et al., 2001; Rojas et al., 2001). Therefore, we could not conclude that Mp*kaol1*^{ge} mutant phenotypes were caused by deficiency in GA_{12} production, and MpKAOL1 might work redundantly with other enzymes to produce other intermediates, synthesizing GA_{Mp} in a GA_{12}-independent pathway.

Despite the conserved activities of MpKOL1 and MpKAOL1, we detected no KA synthesis activity for MpKOL2 or MpKOL3, and no GA_{12} production by MpKAOL3 (Figure 4). Also, no morphological abnormality related to far-red light response was observed in their loss-of-function mutants, suggesting that they are not major enzymes required for GA_{Mp} biosynthesis (Supplemental Figure 13). In the phylogenetic tree of KOs (CYP701s) (Supplemental Figure 8), all liverwort homologs formed a monophyletic clade with two major subclades, both containing

sequences from Jungermanniopsida and Marchantiopsida species. MpKOL2 and MpKOL3 belong to a subclade different from MpKOL1, suggesting these KO homologs were diverged soon after the emergence of the most recent liverwort common ancestor. The phylogenetic relationship of KAOs (CYP88s) from liverworts and hornworts is less clear, but similarly, MpKAOL1 and MpKAOL3 belong to different clades deeply diverged in liverworts (Supplemental Figure 9). It remains to be explored if such divergence contributes to the diversification of diterpenoid metabolism in liverworts.

Comparing the biosynthesis of GA-related diterpenoids between *M. polymorpha* and *P. patens*, we see both conservation and divergence of this pathway in evolution. On the one hand, both bryophyte species share the biosynthesis route for KA with vascular plants. A recent study proposed that the ancestral *TPS* gene in land plants encoded a bifunctional CPS/KS enzyme (Jia et al., 2022), and KO is present in almost all genomes and transcriptomes included in our phylogenetic analysis. It is possible that the production of KA is conserved in all major lineages of land plants. On the other hand, *M. polymorpha* and *P. patens* seem to take different routes to synthesize bioactive compounds from KA. Consistent with the lack of KAO (CYP88) homologs in all mosses, *P. patens* produced *ent*-3β-hydroxy-kaurenoic acid (3OH-KA) and *ent*-2α-hydroxy-kaurenoic acid (2OH-KA) from KA, with the former having physiological activities on protonemal cell differentiation (Miyazaki et al., 2018). Meanwhile, the production of GA_{12} in *M. polymorpha* opened the possibility of using C20-GAs in growth regulation, although no common GA from angiosperms was detected in either bryophyte species (Figure 3) (Hayashi et al., 2010).

In vascular plants, GAs are perceived by GIBBERELLIN-INSENSITIVE DWARF1 (GID1) receptors, which interacts with and promotes the degradation of DELLA proteins to regulate gene expression (Ueguchi-Tanaka et al., 2005; Hirano et al., 2007; Yasumura et al., 2007; Tanaka et al., 2014). Although DELLA proteins broadly exist and interact with multiple transcription factors in a conserved manner across land plants (Hernández-García et al., 2019; Briones-Moreno et al., 2023), the lack of GID1 receptors in bryophytes suggested that GA-related hormones in *M. polymorpha* or *P.* patens are not likely perceived via this pathway. Previously we reported that overexpression of Mp*DELLA* inhibited MpPIF-mediated FR responses, reducing gemma dormancy and delaying the formation of gametangiophores (Hernández-García et al., 2021). However, Mp*DELLA* overexpression strongly inhibited cell

division and thallus growth, which was opposite to the effect of GA_{Mp} deficiency. It is possible that the functions of GA_{Mp} and MpDELLA remain uncoupled in *M. polymorpha*.

Gene expression analysis confirmed that Mp*CPS*, Mp*KS*, Mp*KOL1* and Mp*KAOL1* were induced by FR enrichment in an Mp*PIF*-dependent manner (Figure 5). The regulatory role of Mp*PIF* is further supported by phenotypic similarities between GA_{Mp} biosynthesis mutants and Mp*pif*. Under FR enriched conditions, Mp*pif* mutants developed wider, flatter and larger thallus, and failed to form any gametangiophores (Inoue et al., 2019; Streubel et al., 2023). In angiosperms, FR enrichment also activates the expression GA biosynthesis enzymes, yet more frequently regulating 2-OGD family genes such as GA20ox or GA3ox (Hisamatsu et al., 2005; Kohnen et al., 2016; Küpers et al., 2023), of which no reliable homolog was reported in bryophytes. Considering the putatively different mechanism for GA perception, GA biosynthesis might be independently incorporated into the gene regulatory network by liverworts and angiosperms in evolution, in response to the common threat of a FR-enriched environment.

METHODS

Plant materials and maintenance

The *M. polymorpha* subsp. *ruderalis* accessions Takaragaike-1 (Tak-1) and Takaragaike-2 (Tak-2) were used as male and female wild-type materials, respectively (Ishizaki et al., 2008). For maintenance, *M. polymorpha* plants were cultured aseptically on half-strength Gamborg's B5 medium (Gamborg et al., 1968) with 1% agar at 22°C under continuous white light (40-50 µmol photons m^{-2} s^{-1}), which was supplemented by cold cathode fluorescent lamps (CCFLs, OPT-40C-N-L from Optrom, Japan). If not specified, this medium and temperature was used for all aseptic cultures for *M. polymorpha*.

Light sources

In all the experiments, plants were cultured under continuous white light conditions (cW, approximately 40 µmol photons m^{-2} s^{-1}) with or without continuous far-red light (cFR, approximately 25 µmol photons m^{-2} s^{-1}). For thallus morphology observation, cW and cFR were supplemented by CCFLs and light-emitting diodes (LEDs), respectively, in the multi-chambered incubator (LH-80CCFL-6CT from NK systems, Japan). For gametangiophore induction of aseptic cultures, cW was supplemented by CCFLs (ST-40C-BN, Shinshu Trading, Japan) and

cFR was supplemented by LEDs (IR LED STICK, NAMOTO, Japan). For plants grown on the vermiculite, cW was supplemented by fluorescent tubes (FLR40SN/M/36, Toshiba, Japan) and cFR was supplemented by LEDs (VBL-TFL600-IR730, Valore, Japan).

Construction of mutants and transgenic plants

To create large-deletion mutants of a target gene, four guide RNAs (gRNAs) with target sequences flanking the CDS were first cloned separately into pMpGE_En04, pBCGE12, pBCGE23 and pBCGE34 (Hisanaga et al., 2019; Koide et al., 2020) by ligation of BsaI-digested vectors with annealed complementary DNA oligos. Then the fragments containing the MpU6-1 promoter and gRNAs were digested from the pBCGE12, pBCGE23 and pBCGE34 constructs and inserted between the BglI sites of the pMpGE_En04 construct to create a multiplex entry vector. Finally, this entry vector was recombined with pMpGE017 or pMpGE018 (Hisanaga et al., 2019) using Gateway LR Clonase II (Thermo Fisher Scientific) to generate the binary vector for plant transformation. To generate the Mp*kaol1*^{ge} mutants, the gRNA was designed to target sequences near the start codon of Mp*KAOL1*. The corresponding DNA oligos were annealed and ligated into the BsaI sites of pMpGE_En03, then subcloned to the binary vector pMpGE011 (Sugano et al., 2018).

For the complementation of mutants and/or subcellular localization observations, CDSs of Mp*CPS*, Mp*KS*, Mp*KOL1* and Mp*KAOL1* were amplified from the complementary DNA (cDNA) of Tak-1 plants and directionally cloned into pENTR/D-TOPO (Thermo Fisher Scientific) to create entry vectors without stop codon. To mutate the gRNA target sequence in Mp*KAOL1*, the whole plasmid of pENTR-MpKAOL1-CDS was amplified with the site-directed mutagenesis primers MpKAOL1-mut-F and MpKAOL1-mut-R, then re-circularized to generate pENTR-MpKAOL1-CDSmut. All the CDSs were then subcloned from entry vectors to pMpGWB106 or pMpGWB306 using Gateway LR reactions, which were used for expressing the target proteins under the 35S promoter with an in-frame Citrine fusion at the C terminus (Ishizaki et al., 2015).

All the binary vectors were introduced into *M. polymorpha* by transformation of regenerating thalli using the *Agrobacterium tumefaciens* strain GV2260 as previously described (Kubota et al., 2013). Successful mutations were identified by genotyping PCR and Sanger-sequenced to confirm non-identical alleles. See Supplemental Tables 1-3 for full lists of plant materials generated by this research, and the plasmids and DNA oligos used for construction.

Measurement of thallus morphology

For thallus morphological observation, plants were grown from gemmae on the medium containing 1% sucrose under cW or cW+cFR in a multi-chambered incubator (LH-80CCFL-6CT from NK systems, Japan). After 12 days of growth, camera photos of the plants were taken vertically from the top. Then medium blocks with individual plants were carefully cut out, aligned at a certain distance to a fixed camera for taking side-view photos. Typically, the two apical meristems from one gemma both develop into mature thallus branches, and we define the part developed from a single gemma meristem as a "half thallus". These half thalli were cut apart, flattened on a filter paper and photographed for the measurements of length, width and area. All the measurements were done in Fiji (Schindelin et al., 2012) as describe in Supplemental Figure 16 with in-house macro scripts, which are available at https://github.com/dorrenasun/Mp_GA_biosynthesis. Data was excluded for a whole plant if more than two apical meristems were active in the gemma, or for a half thallus if it showed severe defects in dorsoventral differentiation.

EdU assay

To analyze the cell division activity, plants were grown on the medium containing 1% sucrose under cW+cFR for 7 days, then soaked for 2 h in liquid half-strength Gamborg's B5 medium containing 20 mM 5-ethynyl-2'-deoxyuridine (EdU). Then the samples were fixed in 3.7% formaldehyde for 1 h, washed twice with phosphate buffer saline (PBS, 5 min each), and treated with 0.5% Triton X-100 in PBS for 20 min. After two washes with 3% bovine serum albumin (BSA) in PBS, the samples were kept in the reaction mixture from the Click-iT EdU Imaging Kit with Alexa Fluor 555 (Thermo Fisher Scientific, #C10338) for 1 h in darkness, then washed twice with PBS before soaked overnight in 20% caprylyl sulfobetaine (#D4246, TCI, Japan) to remove the chlorophyll. After another two washes with PBS, the thalli were treated with 75.5% (w/v) iohexol (GE Healthcare Pharma) for 1 h and mounted on glass slides following the iTOMEI protocol (Sakamoto et al., 2022). Image stacks of the apical regions were obtained with a confocal laser scanning microscope (Olympus FLUOVIEW FV1000) at 5-μm steps in the z direction. Excitation and emission wavelengths were 543 nm and 505-605 nm, respectively.

Numbers of EdU-positive nuclei were quantified in the Z-projections of the image stacks using the StarDist plugin of Fiji and in-house scripts (Schmidt et al., 2018; Schindelin et al., 2012).

Observation of gametangiophores

To observe the progress of gametangiophore formation in aseptic culture, plants were first grown from gemmae on the medium containing 1% sucrose under cW for 7 days, then half thalli developed from single gemma meristems were cut apart and cultured on fresh medium plates under cW+cFR. Chemical treatments were included in the medium of second-stage culturing, starting together with the FR irradiation. Apical regions of each plant were observed under a stereoscope (Olympus SZX16) every day, and the emergence of gametangiophores was recorded if a stalk or dark-green primordia was formed. Images of gametangiophores were taken with stereoscopes (Olympus SZX16 or Leica M205C). For morphological observation of gametangiophores, the plants were also grown on the vermiculite in the open air. After an initial culturing of 7-14 days from gemmae under aseptic maintenance conditions, thallus fragments were planted in pots containing vermiculite and grown under cW+cFR conditions with regular watering. For sectioning of gametangiophores, fresh stalks or receptacles were embedded in 5-6% agar and sectioned with a vibratome (DOSAKA LinearSlicer Pro7) at the desired thickness. Images of the sections were obtained with the microscope under bright field (Keyence BZ-X710).

Microscopy of MpBNB-Cit

To capture the early stage of gametangium differentiation, male and female plants carrying the Mp*BNB-Cit* knock-in locus were cultured from gemmae on the medium containing 1% sucrose under cW+cFR for 11 and 14 days, respectively. For male plants, half thalli developed from single gemma meristems were collected for observation. For female plants, the second bifurcation has already occurred, so one of the four apical regions was selected randomly on each plant for observation. Thallus fragments were fixed with 4% paraformaldehyde (PFA) for 1 h at room temperature, washed twice with PBS and soaked in the ClearSeeAlpha solution (Kurihara et al., 2021) for 2 days to remove chlorophyll. After that, the samples were washed twice with PBS, stained with 1 mg/mL calcofluor white for 10 min and washed again twice with PBS. Finally, the samples were infiltrated with 75.5% (w/v) iohexol (GE Healthcare Pharma) for 1 h and mounted onto slides. Image stacks were obtained with the fluorescent microscope

(Keyence BZ-X710) at 5-μm steps and processed into full-focus projections with BZ-X Analyzer, and the number of Citrine-positive nuclei was counted in Fiji (Schindelin et al., 2012). The BZ-X DAPI (Excitation: 360±20 nm; Emission: 460±25 nm; Dichroic mirror: 400 nm) and customized (Excitation: 500±10 nm; Emission: 535±15 nm; Dichroic mirror: 515 nm) filters were used for acquiring signals from calcofluor white and Citrine, respectively.

LC-MS/MS analysis of endogenous GAs

To analyze the endogenous GAs, most plants were cultured from gemmae on the medium containing 1% sucrose under cW for 10 days, then under cW+cFR for another 4 days. Tak-1 wild-type plants were also cultured under cW for 14 days to examine the effect of FR enrichment. For each sample, 3 g of thallus tissue was harvested, frozen with liquid nitrogen, and stored at -80 °C before extraction. To prepare samples for LC-MS/MS analysis, each frozen sample was homogenized in 15 mL acetone with $^{2}H_{2}$-labelled authentic compounds, then left at 4 °C for a 2-h extraction. After filtering with defatted cotton, the acetone extract was concentrated to approximately 1 mL with nitrogen blow and mixed with 1 mL acetonitrile. The mixture was extracted for 3 times with 2 mL hexane, and the remaining aqueous phase was alkalified with 1 mL saturated solution of $NaHCO_3$. After two more extractions with 2 mL chloroform, the aqueous phase was passed through a cartridge filled with polyvinylpyrrolidone (PVP), acidified to pH2-3 with HCl (6 M), and sequentially purified with a reverse-phase cartridge (Oasis HLB 3 cc/60 mg, Waters), an anion-exchange cartridge (Bond Elut DEA 100 mg/1 mL, Agilent), and a silica cartridge (Sep-Pak Silica 1 cc Vac Cartridge, Waters). The final elute was dried up with a vacuum centrifuge concentrator and dissolved in 1% acetic acid before loading to the LC-MS/MS.

The LC-MS/MS system consisted of an ultra-performance LC (ExionLC, Sciex) equipped with a reverse-phase column (CORTECS UPLC C18+, φ1.6 μm, 2.1×100 mm, Waters) and a quadrupole time-of-flight mass spectrometer (X500R QTOF, Sciex). LC separations were performed at 40 °C with a flow rate of 0.3 mL/min using solvent A (0.05% acetic acid in water) and solvent B (0.05% acetic acid in acetonitrile) and the following program: a linear gradient of B from 3% to 65% over 17 min, followed by an isocratic elution with 98% of B for 2 min. Quantification of GAs was performed in the multiple reaction monitoring (MRM) mode, and the mass spectrum of GA_{12} was confirmed in the TOF-MS/MS mode.

Phylogenetic analysis

For the phylogenetic analysis of KO and KAO homologs, the known protein sequences from *A. thaliana* and *Oryza sativa* were used as the input for BLAST (Altschul et al., 1990) search in the annotated proteins from published genomes and transcriptomes (See Supplemental Data Set 3 for a full list of species and references). Considering the relative low redundancy of these enzymes, the top 20 BLAST hits from each species were retrieved and aligned with MAFFT using the progressive FFT-NS-2 algorithm (Katoh and Standley, 2013). After removing the positions with >80% gaps, an initial maximum likelihood phylogenetic tree was built with all candidate sequences using IQ-TREE 2 with automatic substitution model selection (ModelFinder) and 1000 bootstraps from the ultrafast bootstrap approximation (UFBoot) (Minh et al., 2020; Kalyaanamoorthy et al., 2017; Hoang et al., 2018). Highly-relevant candidate sequences and outgroup sequences were selected from the initial tree and re-aligned with MAFFT using the L-INS-I algorithm (Katoh and Standley, 2013) and trimmed off positions with >98% gaps. The final maximum likelihood tree was inferred using IQ-TREE 2 with automatic substitution model selection (LG+I+G4 for both KOs and KAOs) and 1000 standard non-parametric bootstraps (Minh et al., 2020; Kalyaanamoorthy et al., 2017; Hoang et al., 2018; Guindon et al., 2010). The complete pipeline including scripts, sequence alignments, and the data file for the phylogenetic trees are available at https://github.com/dorrenasun/Mp_GA_biosynthesis. The ggtree R package suite was used for visualization (Yu, 2022; Xu et al., 2022; Yu, 2020b; Yu et al., 2018, 2017).

Enzymatic assay in *P. pastoris* and GC-MS analysis

To express MpKOLs and MpKAOLs in the yeast *P. pastoris*, the CDSs were amplified from pENTR-CDS entry vectors and inserted into the pPICZA vector (Thermo Fisher Scientific) with homologous recombination using the seamless ligation cloning extract (SLiCE) from *Escherichia coli* (Zhang et al., 2012; Motohashi, 2015). The CDSs of At*KO* (AT5G25900) and At*KAO1* (AT1G05160) were amplified from the cDNA of 14-day-old Col-0 seedlings and cloned into pPICZA with the same method. All these plasmids were transformed into a previously described *P. pastoris* X-33 strain carrying the *A. thaliana* cytochrome reductase gene, At*ATR1* (AT4G24520) (Katsumata et al., 2008), following the manufacturer's protocol. The selected transformants were incubated in 2 mL of BMG medium (100 mM potassium phosphate (pH 6.0),

1.34% yeast nitrogen base (YNB), 4×10^{-5}% biotin, 1% glycerol) with shaking at 30 °C until they reached an OD_{600} value of 2. Cells were collected by centrifugation and resuspended in 50 mL of MM medium (1.34% YNB, 4×10^{-5}% biotin, 0.5% methanol), and cultured at 30 °C with shaking and addition of methanol every 24 h (final concentration: 0.5% v/v) to maintain protein induction. After 24 h of initial culturing, substrates (7 μg of *ent*-kaurene, or 15 μg of KA) were added into the medium. After another 48 h of incubation, the supernatants were isolated with centrifugation and extracted two times with equal volume of ethyl acetate. The organic phase from the two extractions were combined together, concentrated *in vacuo*, and derivatized with diazomethane in ether solution. After that, the samples were concentrated to approximately 100 μL with nitrogen blow and subjected to GC-MS analysis with a GC (Agilent 6890) equipped with a DB-1 capillary column (15 m/0.25 mm/0.25 μm, Agilent J&W) and a mass selective detector (Agilent 5975C MSD, ionization energy at 70 eV). The oven temperature was programmed as described previously (Hayashi et al., 2006).

Subcellular localization of proteins

To observe the subcellular localizations of GA_{MP} biosynthesis enzymes, plants were grown from gemmae on the medium containing 1% sucrose under cW+cFR conditions for 7 days. The thallus tissues were fixed with 4% PFA at room temperature for 20 min, washed twice with PBS, and stained with 1 mg/mL calcofluor white for 10 min at room temperature or 1 μg/mL 4′,6-diamidino-2-phenylindole (DAPI) for 8 h at 4 °C. After another two washes with PBS, the samples were soaked in 75.5% (w/v) iohexol (GE Healthcare Pharma) for 1 h and mounted onto slides. For all experiments, complementation lines which used the 35S promoter to express target proteins fused with Citrine in the C-teminus were used for observation, and the parent lines of genetic mutants were used as the negative control.

Fluorescent images were acquired using a confocal microscope (Leica TCS SP8X Falcon) equipped with a hybrid detector (HyD). For the observation of MpCPS-Cit, calcofluor white signals were excited with the 405 nm UV laser, and obtained in the xyz mode within the 425-435 nm wavelength region; the Citrine signals were excited with the the pulsed white light laser (WLL) at 488 nm, and obtained at 500-541 nm with time gating (1.8-12 ns); the autofluorescence from chlorophyll was excited with the WLL at 592 nm, and obtained at 680-700 nm. For the observation of MpKS-Cit and MpKOL1-Cit, calcofluor white signals were excited with the 405

nm UV laser, and obtained at 425-475 nm; the Citrine signals were excited with the WLL at 495 nm, and obtained at 500-530 nm with time gating (1.2-6.0 ns); the autofluorescence from chlorophyll was excited with the WLL at 649 nm, and obtained at 655-755 nm. For the observation of MpKAOL1-Cit, DAPI signals were excited with the 405 nm UV laser, and obtained at 430-480 nm; the Citrine signals were excited with the WLL at 495 nm, and obtained at 500-530 nm with time gating (1.2-6.0 ns); the autofluorescence from chlorophyll was excited with the WLL at 649 nm, and obtained at 655-755 nm.

RNA extraction and qPCR

For qPCR experiments, 50-100 mg of whole thallus was collected for each sample, which is frozen with liquid nitrogen and crashed into fine powders with metal beads in a shaking device (Shake Master Auto, BMS-A20TP, Bio Medical Science, Japan). The total RNA was extracted with the TRIzol reagent (Thermo Fisher Scientific) following the manufacturer's protocol. After treatment with RQ1 RNase-Free DNase (Promega), the total RNA was reverse-transcribed using ReverTra Ace (Toyobo Life Science) and the $(dT)_{20}$ oligo. Quantitative real-time PCR reactions with Taq polymerase prepared following (Pluthero, 1993) and SYBR Green I Nucleic Acid Gel Stain (Lonza) was performed in triplicates using the CFX96 real-time PCR detection system (Bio-Rad) with the following program: an initial denaturation for 30 s at 95 °C, then 40 cycles of 5 s at 95 °C followed by 30 s at 60 °C. A standard melting curve analysis was performed at the end of the program to validate amplified products. Mp*EF1* (Mp3g23400) was used as the reference gene for quantification, and the relative gene expression levels were calculated following the method in (Hellemans et al., 2008). All primers for target and reference genes were listed in Supplemental Table 3, and the amplification efficiency for each primer pair was measured with serial dilution of mixed cDNA samples.

Transcriptome analysis

For transcriptome analysis, plants were cultured from gemmae on the medium with 1% sucrose, either containing 2 μM KA or the solvent control. After 12 days of growth under cW or cW+cFR, ~50 mg whole thallus was collected for each sample, frozen with liquid nitrogen and homogenized with metal beads in a shaking device (Shake Master Auto, BMS-A20TP, Bio Medical Science, Japan). The total RNA was isolated with the RNeasy Plant Mini Kit (QIAGEN),

and the RNA quality was confirmed using the Bioanalyzer RNA 6000 pico assay (Agilent). The mRNA was enriched with the NEBNext Poly(A) mRNA Magnetic Isolation Module (New England Biolabs, #E7490). The library was prepared with the NEBNext Ultra II Directional RNA Library Prep Kit for Illumina (New England Biolabs, #E7760) and amplified using NEBNext Multiplex Oligos for Illumina (96 Unique Dual Index Primer Pairs Set 2, New England Biolabs, #E6442). After quality check with the Bioanalyzer High Sensitivity DNA assay (Agilent), the samples were sequenced with the NextSeq 500 system using the NextSeq 500/550 High Output Kit v2.5 for 75 cycles (Illumina). Approximately 7.8 million of single-end reads were obtained for each sample, and automatically de-multiplexed by the BaseSpace Sequence Hub (Illumina).

The sequence reads were quasi-mapped to the *M. polymorpha* MpTak_v6.1 genome (Iwasaki et al., 2021) and quantified using Salmon (v1.9.0) (Patro et al., 2017), with U-chromosome transcripts excluded from the index. After that, differential gene expression analysis was performed in R (v4.2.2) with the package DESeq2 (v1.38.3) in default settings (Love et al., 2014). Gene ontology enrichment analyses was performed with the R package topGO (v2.50.0) (Alexa and Rahnenfuhrer, 2022) using annotations previously described (Hernández-García et al., 2021) and the classic Fisher's exact test, and *p*-values were left unadjusted following the package's instructions. To visualize the enriched terms, semantic similarities were calculated using the R package GOSemSim (v2.24.0) (Yu et al., 2010; Yu, 2020a), and used for building a two-dimensional map with the package Rtsne (Krijthe, 2015).

Accession numbers

M. polymorpha genes investigated in this research can be found in the MarpolBase (https://marchantia.info) with the following accession numbers: Mp*CPS* (Mp2g07200/Mapoly0015s0008); Mp*KS* (Mp6g05950/Mapoly0097s0049); Mp*TPS1* (Mp6g05430/Mapoly0167s0025); Mp*KOL1* (Mp3g18320/Mapoly0140s0010); Mp*KOL2* (Mp2g01950/Mapoly0130s0003); Mp*KOL3* (Mp2g01940/Mapoly0130s0002); Mp*KAOL1* (Mp4g23680/Mapoly0020s0131); Mp*KAOL3* (Mp2g10420/Mapoly0023s0011); Mp*BNB* (Mp3g23300/ Mapoly0024s0106). The transcriptome data obtained in this research is deposited to the Sequence Read Archive at the DNA Data Bank of Japan (DDBJ) under the Bioproject PRJDB15786. The scripts for data analysis are available at GitHub: https://github.com/dorrenasun/Mp_GA_biosynthesis.

Supplemental Data

Supplemental Figure 1. Gibberellin (GA) biosynthesis pathway in vascular plants, showing compounds analyzed or used for treatment in this research.

Supplemental Figure 2. Genotype information for Mp*cps*^{ld}, Mp*ks*^{ld}, Mp*kol1*^{ld}, and Mp*kaol1*^{ge} mutants.

Supplemental Figure 3. Thallus morphology of Mp*cps*^{ld} mutants in Tak-2 background under cW+cFR.

Supplemental Figure 4. Morphology of Mp*cps*^{ld} plants during gametangiophore formation in the aseptic culture.

Supplemental Figure 5. Sections of gametangiophores in wild-type and Mp*cps*^{ld} plants, as well as the fertility test.

Supplemental Figure 6. LC-MS/MS and GC-MS profiles for KA and GA_{12} detection.

Supplemental Figure 7. Response of Mp*cps-4*^{ld} and Mp*kaol1-5*^{ge} to different concentrations of KA.

Supplemental Figure 8. Phylogenetic tree of KO homologs in land plants.

Supplemental Figure 9. Phylogenetic tree of KAO and closely-related CYP enzymes in land plants.

Supplemental Figure 10. Heatmap of percentage identity for KAO and closely-related CYP enzymes in land plants.

Supplemental Figure 11. Subcellular localizations of GA biosynthesis enzymes in *M. polymorpha*.

Supplemental Figure 12. Genotype information for Mp*tps1*^{ld}, [Mp*kol2* Mp*kol3*]^{ld} and Mp*kaol3*^{ld} mutants.

Supplemental Figure 13. Phenotypes of Mp*tps1*^{ld}, [Mp*kol2* Mp*kol3*]^{ld} and Mp*kaol3*^{ld} mutants.

Supplemental Figure 14. Up-regulation of GA biosynthesis genes by FR irradiation.

Supplemental Figure 15. Heatmaps of genes from selected pathways or gene families, showing differential expression in Mp*cps-4*^{ld} under cW+cFR.

Supplemental Figure 16. Quantification method for thallus morphology.

Supplemental Table 1. List of plant materials

Supplemental Table 2. List of plasmids

Supplemental Table 3. List of DNA oligos

Supplemental Data Set 1. Differentially expressed genes in the transcriptome analysis

Supplemental Data Set 2. Enriched gene ontology (GO) terms in the transcriptome analysis

Supplemental Data Set 3. List of genome and transcriptome sources for phylogenetic analysis

Supplemental Data Set 4. Summary of statistics

Supplemental References.

AKNOWLEDGEMENTS

The authors thank Ryunosuke Kusunoki for plasmid construction and collecting initial experimental data; Wakako Fukuda for data collection during GC-MS analysis; Takefumi Kondo and Yukari Sando for the support on RNA sequencing; Megumi Iwano for the help on confocal microscopy and Chikako Inoue for plant maintenance. This work has been supported by MEXT KAKENHI Grant Number JP19H05675 and JSPS KAKENHI Grant Numbers JP17H07424, JP22H00417 to T.K.; JSPS KAKENHI Grant Numbers JP 24380060, JP15H04492 to M.N. and H.K.; JSPS KAKENHI Grant Number JP16K18693 to S.M.; as well as the International Collaborative Research Program of Institute for Chemical Research, Kyoto University (Grant Numbers 2020-53, 2021-60, 2022-63, 2023-74) to T.K. and S.Yamaguchi.

AUTHOR CONTRIBUTIONS

R.S. and M.O. collected and analyzed most of the final data with the help and supervision from K.M., Y.Y., S.Yamaoka., R.N. and T.K.. M.O., S.M., T.I., K.M., M.N. and S.Yamaguchi analyzed endogenous GAs. S.M. and H.K. assayed enzymatic activity. R.K. performed initial experiments that conceptualized the research. H.K., M.N., S.Yamaguchi and T.K. organized the project. R.S., S.Yamaoka., R.N and T.K. wrote the paper with the review and editing from all authors.

REFERENCES

Achard, P., Gusti, A., Cheminant, S., Alioua, M., Dhondt, S., Coppens, F., Beemster, G.T.S., and Genschik, P. (2009). Gibberellin Signaling Controls Cell Proliferation Rate in Arabidopsis. Current Biology 19: 1188–1193.

Aki, S.S., Mikami, T., Naramoto, S., Nishihama, R., Ishizaki, K., Kojima, M., Takebayashi, Y., Sakakibara, H., Kyozuka, J., Kohchi, T., and Umeda, M. (2019). Cytokinin Signaling Is Essential for Organ Formation in Marchantia polymorpha. Plant and Cell Physiology 60: 1842–1854.

Alexa, A. and Rahnenfuhrer, J. (2022). topGO: Enrichment Analysis for Gene Ontology. R package version 2.50.0.

Althoff, F., Kopischke, S., Zobell, O., Ide, K., Ishizaki, K., Kohchi, T., and Zachgo, S. (2014). Comparison of the MpEF1α and CaMV35 promoters for application in Marchantia polymorpha overexpression studies. Transgenic Res 23: 235–244.

Altschul, S.F., Gish, W., Miller, W., Myers, E.W., and Lipman, D.J. (1990). Basic local alignment search tool. Journal of Molecular Biology 215: 403–410.

Beall, F.D., Yeung, E.C., and Pharis, R.P. (1996). Far-red light stimulates internode elongation, cell division, cell elongation, and gibberellin levels in bean. Can. J. Bot. 74: 743–752.

Bou-Torrent, J., Galstyan, A., Gallemí, M., Cifuentes-Esquivel, N., Molina-Contreras, M.J., Salla-Martret, M., Jikumaru, Y., Yamaguchi, S., Kamiya, Y., and Martínez-García, J.F. (2014). Plant proximity perception dynamically modulates hormone levels and sensitivity in Arabidopsis. Journal of Experimental Botany 65: 2937–2947.

Bowman, J.L. et al. (2017). Insights into land plant evolution garnered from the *Marchantia polymorpha* genome. Cell 171: 287-304.e15.

Briginshaw, L.N., Flores-Sandoval, E., Dierschke, T., Alvarez, J.P., and Bowman, J.L. (2022). KANADI promotes thallus differentiation and FR-induced gametangiophore formation in the liverwort Marchantia. New Phytologist 234: 1377–1393.

Briones-Moreno, A., Hernández-García, J., Vargas-Chávez, C., Blanco-Touriñán, N., Phokas, A., Úrbez, C., Cerdán, P.D., Coates, J.C., Alabadí, D., and Blázquez, M.A. (2023). DELLA functions evolved by rewiring of associated transcriptional networks. Nat. Plants 9: 535–543.

Cannell, N., Emms, D.M., Hetherington, A.J., MacKay, J., Kelly, S., Dolan, L., and Sweetlove, L.J. (2020). Multiple Metabolic Innovations and Losses Are Associated with Major Transitions in Land Plant Evolution. Current Biology 30: 1783-1800.e11.

Cao, J.-G., Wang, Q.-X., Zou, H.-M., Dai, X.-L., and Cao, T. (2013). New Observations on the Morphology and Structure of *Marchantia polymorpha* Gametophores in Sexual Reproduction Adaption. Plant Science Journal 31: 555.

895 Chiang, H.-H., Hwang, I., and Goodman, H.M. (1995). Isolation of the Arabidopsis *GA4* locus.
896 the Plant Cell 7: 195–201.

897 Chiyoda, S., Ishizaki, K., Kataoka, H., Yamato, K.T., and Kohchi, T. (2008). Direct transformation
898 of the liverwort Marchantia polymorpha L. by particle bombardment using immature thalli
899 developing from spores. Plant Cell Reports 27: 1467–1473.

900 Conesa, A. and Götz, S. (2008). Blast2GO: A comprehensive suite for functional analysis in
901 plant genomics. International Journal of Plant Genomics 2008.

902 Djakovic-Petrovic, T., Wit, M.D., Voesenek, L.A.C.J., and Pierik, R. (2007). DELLA protein
903 function in growth responses to canopy signals. Plant Journal 51: 117–126.

904 Downs, R.J., Hendricks, S.B., and Borthwick, H.A. (1957). Photoreversible Control of Elongation
905 of Pinto Beans and Other Plants under Normal Conditions of Growth. Botanical Gazette
906 118: 199–208.

907 Dubois, P.G., Olsefski, G.T., Flint-Garcia, S., Setter, T.L., Hoekenga, O.A., and Brutnell, T.P.
908 (2010). Physiological and Genetic Characterization of End-of-Day Far-Red Light
909 Response in Maize Seedlings. Plant Physiology 154: 173–186.

910 Fredericq, H. (1964). Influence formatrice de la lumière rouge-foncé sur le développement des
911 thalles de Marchantia polymorpha L. Bull. Soc. Roy. Bot. Belgique 98: 67–76.

912 Fredericq, H. and de Greef, J. (1966). Red (R), Far-red (FR) photoreversible control of growth
913 and chlorophyll content in light-grown thalli of Marchantia polymorpha L. Die
914 Naturwissenschaften 53: 337.

915 Fredericq, H. and Greef, J.D. (1968). Photomorphogenic and Chlorophyll Studies in the
916 Bryophyte Marchantia polymorpha. I. Effect of Red, Far-red Irradiations in Short and
917 Long-term Experiments. Physiol Plant 21: 346–359.

918 Gabriele, S., Rizza, A., Martone, J., Circelli, P., Costantino, P., and Vittorioso, P. (2009). The
919 Dof protein DAG1 mediates PIL5 activity on seed germination by negatively regulating
920 GA biosynthetic gene AtGA3ox1: DAG1 represses seed germination via PIL5 signalling.
921 The Plant Journal 61: 312–323.

922 Gamborg, O.L., Miller, R.A., and Ojima, K. (1968). Nutrient requirements of suspension cultures
923 of soybean root cells. Experimental Cell Research 50: 151–158.

924 García-Martínez, J.L., Keith, B., Bonner, B.A., Stafford, A.E., and Rappaport, L. (1987).
925 Phytochrome Regulation of the Response to Exogenous Gibberellins by Epicotyls of
926 *Vigna sinensis*. Plant Physiol. 85: 212–216.

927 Guindon, S., Dufayard, J.-F., Lefort, V., Anisimova, M., Hordijk, W., and Gascuel, O. (2010).
928 New algorithms and methods to estimate maximum-likelihood phylogenies: Assessing
929 the performance of PhyML 3.0. Systematic Biology 59: 307–321.

Hayashi, K., Horie, K., Hiwatashi, Y., Kawaide, H., Yamaguchi, S., Hanada, A., Nakashima, T., Nakajima, M., Mander, L.N., Yamane, H., Hasebe, M., and Nozaki, H. (2010). Endogenous diterpenes derived from *ent*-kaurene, a common gibberellin precursor, regulate protonema differentiation of the moss *Physcomitrella patens*. Plant Physiology 153: 1085–1097.

Hayashi, K. ichiro, Kawaide, H., Notomi, M., Sakigi, Y., Matsuo, A., and Nozaki, H. (2006). Identification and functional analysis of bifunctional *ent*-kaurene synthase from the moss *Physcomitrella patens*. FEBS Letters 580: 6175–6181.

Hedden, P. (2020). The Current Status of Research on Gibberellin Biosynthesis. Plant and Cell Physiology 61: 1832–1849.

Hedden, P., MacMillan, J., and Phinney, B.O. (1974). Fungal products. Part XII. Gibberellin A14-aldehyde, an intermediate in gibberellin biosynthesis in Gibberella fujikuroi. Journal of the Chemical Society, Perkin Transactions 1: 587–592.

Hellemans, J., Mortier, G., De Paepe, A., Speleman, F., and Vandesompele, J. (2008). qBase relative quantification framework and software for management and automated analysis of real-time quantitative PCR data. Genome Biology 8.

Helliwell, C.A., Chandler, P.M., Poole, A., Dennis, E.S., and Peacock, W.J. (2001a). The CYP88A cytochrome P450, *ent*-kaurenoic acid oxidase, catalyzes three steps of the gibberellin biosynthesis pathway. Proceedings of the National Academy of Sciences of the United States of America 98: 2065–2070.

Helliwell, C.A., Poole, A., James Peacock, W., and Dennis, E.S. (1999). Arabidopsis *ent* -kaurene oxidase catalyzes three steps of gibberellin biosynthesis. Plant Physiology 119: 507–510.

Helliwell, C.A., Sheldon, C.C., Olive, M.R., R.Walker, A., Zeevaart, J.A.D., Peacock, W.J., and Dennis, E.S. (1998). Cloning of the *Arabidopsis ent*-kaurene oxidase gene *GA3*. Proceedings of the National Academy of Sciences of the United States of America 95: 9019–9024.

Helliwell, C.A., Sullivan, J.A., Mould, R.M., Gray, J.C., James Peacock, W., and Dennis, E.S. (2001b). A plastid envelope location of *Arabidopsis ent*-kaurene oxidase links the plastid and endoplasmic reticulum steps of the gibberellin biosynthesis pathway. Plant Journal 28: 201–208.

Hernández-García, J., Briones-Moreno, A., Dumas, R., and Blázquez, M.A. (2019). Origin of gibberellin-dependent transcriptional regulation by molecular exploitation of a transactivation domain in DELLA proteins. Molecular biology and evolution 36: 908–918.

Hernández-García, J., Sun, R., Serrano-Mislata, A., Inoue, K., Vargas-Chávez, C., Esteve-Bruna, D., Arbona, V., Yamaoka, S., Nishihama, R., Kohchi, T., and Blázquez, M.A. (2021). Coordination between growth and stress responses by DELLA in the liverwort Marchantia polymorpha. Current Biology.

968 Hirano, K. et al. (2007). The GID1-mediated gibberellin perception mechanism is conserved in
969 the lycophyte Selaginella moellendorffii but not in the bryophyte *Physcomitrella patens*.
970 The Plant Cell 19: 3058–3079.

971 Hisamatsu, T., King, R.W., Helliwell, C. a, and Koshioka, M. (2005). The involvement of
972 gibberellin 20-oxidase genes in phytochrome-regulated petiole elongation of Arabidopsis.
973 Plant Physiology 138: 1106–1116.

974 Hisanaga, T., Okahashi, K., Yamaoka, S., Kajiwara, T., Nishihama, R., Shimamura, M., Yamato,
975 K.T., Bowman, J.L., Kohchi, T., and Nakajima, K. (2019). A cis -acting bidirectional
976 transcription switch controls sexual dimorphism in the liverwort. The EMBO Journal 38:
977 1–12.

978 Hoang, D.T., Chernomor, O., von Haeseler, A., Minh, B.Q., and Vinh, L.S. (2018). UFBoot2:
979 Improving the Ultrafast Bootstrap Approximation. Molecular Biology and Evolution 35:
980 518–522.

981 Holmes, M.G. and Smith, H. (1975). The function of phytochrome in plants growing in the natural
982 environment. Nature 254: 512–514.

983 Hornych, O., Testo, W.L., Sessa, E.B., Watkins, J.E., Campany, C.E., Pittermann, J., and Ekrt,
984 L. (2021). Insights into the evolutionary history and widespread occurrence of
985 antheridiogen systems in ferns. New Phytologist 229: 607–619.

986 Inoue, K., Nishihama, R., Araki, T., and Kohchi, T. (2019). Reproductive induction is a far-red
987 high irradiance response that is mediated by phytochrome and PHYTOCHROME
988 INTERACTING FACTOR in Marchantia polymorpha. Plant and Cell Physiology 60: 1136–
989 1145.

990 Inoue, K., Nishihama, R., Kataoka, H., Hosaka, M., Manabe, R., Nomoto, M., Tada, Y., Ishizaki,
991 K., and Kohchi, T. (2016). Phytochrome signaling is mediated by PHYTOCHROME
992 INTERACTING FACTOR in the liverwort *Marchantia polymorpha*. The Plant Cell 28:
993 1406–1421.

994 Ishizaki, K., Chiyoda, S., Yamato, K.T., and Kohchi, T. (2008). *Agrobacterium*-mediated
995 transformation of the haploid liverwort *Marchantia polymorpha* L., an emerging model for
996 plant biology. Plant and Cell Physiology 49: 1084–1091.

997 Ishizaki, K., Nishihama, R., Ueda, M., Inoue, K., Ishida, S., Nishimura, Y., Shikanai, T., and
998 Kohchi, T. (2015). Development of Gateway binary vector series with four different
999 selection markers for the liverwort *Marchantia polymorpha*. PLoS ONE 10: e0138876.

1000 Iwasaki, M. et al. (2021). Identification of the sex-determining factor in the liverwort Marchantia
1001 polymorpha reveals unique evolution of sex chromosomes in a haploid system. Current
1002 Biology 31: 5522-5532.e7.

1003 Jia, Q., Brown, R., Köllner, T.G., Fu, J., Chen, X., Wong, G.K.S., Gershenzon, J., Peters, R.J.,
1004 and Chen, F. (2022). Origin and early evolution of the plant terpene synthase family.

Proceedings of the National Academy of Sciences of the United States of America 119: 1–9.

Kalyaanamoorthy, S., Minh, B.Q., Wong, T.K.F., von Haeseler, A., and Jermiin, L.S. (2017). ModelFinder: fast model selection for accurate phylogenetic estimates. Nat Methods 14: 587–589.

Katoh, K. and Standley, D.M. (2013). MAFFT multiple sequence alignment software version 7: Improvements in performance and usability. Molecular Biology and Evolution 30: 772–780.

Katsumata, T., Hasegawa, A., Fujiwara, T., Komatsu, T., Notomi, M., Abe, H., Natsume, M., and Kawaide, H. (2008). Arabidopsis CYP85A2 Catalyzes Lactonization Reactions in the Biosynthesis of 2-Deoxy-7-oxalactone Brassinosteroids. Bioscience, Biotechnology, and Biochemistry 72: 2110–2117.

Kawai, Y., Ono, E., and Mizutani, M. (2014). Evolution and diversity of the 2-oxoglutarate-dependent dioxygenase superfamily in plants. Plant J. 78: 328–343.

Kohnen, M.V., Schmid-Siegert, E., Trevisan, M., Petrolati, L.A., Sénéchal, F., Müller-Moulé, P., Maloof, J., Xenarios, I., and Fankhauser, C. (2016). Neighbor Detection Induces Organ-Specific Transcriptomes, Revealing Patterns Underlying Hypocotyl-Specific Growth. Plant Cell 28: 2889–2904.

Koide, E., Suetsugu, N., Iwano, M., Gotoh, E., Nomura, Y., Stolze, S.C., Nakagami, H., Kohchi, T., and Nishihama, R. (2020). Regulation of Photosynthetic Carbohydrate Metabolism by a Raf-Like Kinase in the Liverwort Marchantia polymorpha. Plant and Cell Physiology 61: 631–643.

Koornneef, M. and van der Veen, J.H. (1980). Induction and analysis of gibberellin sensitive mutants in *Arabidopsis thaliana* (L.) heynh. Theoretical and Applied Genetics 58: 257–263.

Krijthe, J.H. (2015). Rtsne: T-Distributed Stochastic Neighbor Embedding using a Barnes-Hut Implementation.

Kubota, A., Ishizaki, K., Hosaka, M., and Kohchi, T. (2013). Efficient *Agrobacterium*-mediated transformation of the liverwort *Marchantia polymorpha* using regenerating thalli. Bioscience, Biotechnology and Biochemistry 77: 167–172.

Kumar, S. et al. (2016). Molecular diversity of terpene synthases in the liverwort *Marchantia polymorpha*. The Plant Cell 28: 2632–2650.

Küpers, J.J. et al. (2023). Local light signaling at the leaf tip drives remote differential petiole growth through auxin-gibberellin dynamics. Current Biology 33: 75-85.e5.

Kurihara, D., Mizuta, Y., Nagahara, S., and Higashiyama, T. (2021). ClearSeeAlpha: Advanced Optical Clearing for Whole-Plant Imaging. Plant and Cell Physiology 62: 1302–1310.

Kurosawa, E. (1926). Experimental studies on the nature of the substance excreted by the "bakanae" fungus. Trans. Nat. Hist. Soc. Formosa 16: 213–227.

Li, W., Liu, S.-W., Ma, J.-J., Liu, H.-M., Han, F.-X., Li, Y., and Niu, S.-H. (2020). Gibberellin Signaling Is Required for Far-Red Light-Induced Shoot Elongation in *Pinus tabuliformis* Seedlings. Plant Physiol. 182: 658–668.

Love, M.I., Huber, W., and Anders, S. (2014). Moderated estimation of fold change and dispersion for RNA-seq data with DESeq2. Genome Biology 15: 550.

Michaud, O., Krahmer, J., Galbier, F., Lagier, M., Galvão, V.C., Ince, Y.Ç., Trevisan, M., Knerova, J., Dickinson, P., Hibberd, J.M., Zeeman, S.C., and Fankhauser, C. (2023). Abscisic acid modulates neighbor proximity-induced leaf hyponasty in Arabidopsis. Plant Physiology 191: 542–557.

Minh, B.Q., Schmidt, H.A., Chernomor, O., Schrempf, D., Woodhams, M.D., von Haeseler, A., and Lanfear, R. (2020). IQ-TREE 2: New Models and Efficient Methods for Phylogenetic Inference in the Genomic Era. Molecular Biology and Evolution 37: 1530–1534.

Miyazaki, S., Hara, M., Ito, S., Tanaka, K., Asami, T., Hayashi, K., Kawaide, H., and Nakajima, M. (2018). An Ancestral Gibberellin in a Moss Physcomitrella patens. Molecular Plant 11: 1097–1100.

Miyazaki, S., Katsumata, T., Natsume, M., and Kawaide, H. (2011). The CYP701B1 of *Physcomitrella patens* is an ent-kaurene oxidase that resists inhibition by uniconazole-P. FEBS Letters 585: 1879–1883.

Miyazaki, S., Nakajima, M., and Kawaide, H. (2015). Hormonal diterpenoids derived from ent-kaurenoic acid are involved in the blue-light avoidance response of Physcomitrella patens. Plant Signaling and Behavior 10: 1–4.

Miyazaki, S., Toyoshima, H., Natsume, M., Nakajima, M., and Kawaide, H. (2014). Blue-light irradiation up-regulates the *ent*-kaurene synthase gene and affects the avoidance response of protonemal growth in *Physcomitrella patens*. Planta 240: 117–124.

Morgan, D.C. and Smith, H. (1979). A systematic relationship between phytochrome-controlled development and species habitat, for plants grown in simulated natural radiation. Planta 145: 253–258.

Morgan, D.C. and Smith, H. (1978). The relationship between phytochrome-photoequilibrium and Development in light grown Chenopodium album L. Planta 142: 187–193.

Motohashi, K. (2015). A simple and efficient seamless DNA cloning method using SLiCE from Escherichia coli laboratory strains and its application to SLiP site-directed mutagenesis. BMC Biotechnol 15: 47.

Näf, U., Nakanishi, K., and Endo, M. (1975). On the Physiology and Chemistry of Fern Antheridiogens. Botanical Review 41: 315–359.

Nelissen, H., Rymen, B., Jikumaru, Y., Demuynck, K., Van Lijsebettens, M., Kamiya, Y., Inzé, D., and Beemster, G.T.S. (2012). A Local Maximum in Gibberellin Levels Regulates Maize Leaf Growth by Spatial Control of Cell Division. Current Biology 22: 1183–1187.

Ninnemann, H. and Halbsguth, W. (1965). Rolle des Phytochroms beim Etiolement von Marchantia polymorpha. Naturwissenschaften 52: 110–111.

Nomura, T., Magome, H., Hanada, A., Takeda-Kamiya, N., Mander, L.N., Kamiya, Y., and Yamaguchi, S. (2013). Functional analysis of *Arabidopsis* CYP714A1 and CYP714A2 reveals that they are distinct gibberellin modification enzymes. Plant and Cell Physiology 54: 1837–1851.

Ogawa, M., Hanada, A., Yamauchi, Y., Kuwahara, A., Kamiya, Y., and Yamaguchi, S. (2003). Gibberellin Biosynthesis and Response during Arabidopsis Seed Germination. The Plant Cell 15: 1591–1604.

Patro, R., Duggal, G., Love, M.I., Irizarry, R.A., and Kingsford, C. (2017). Salmon provides fast and bias-aware quantification of transcript expression. Nature Methods 14: 417–419.

Pluthero, F.G. (1993). Rapid purification of high-activity Taq DNA polymerase. Nucleic Acids Res 21: 4850–4851.

Rojas, M.C., Hedden, P., Gaskin, P., and Tudzynski, B. (2001). The *P450–1* gene of *Gibberella fujikuroi* encodes a multifunctional enzyme in gibberellin biosynthesis. Proc. Natl. Acad. Sci. U.S.A. 98: 5838–5843.

Sakamoto, Y., Ishimoto, A., Sakai, Y., Sato, M., Nishihama, R., Abe, K., Sano, Y., Furuichi, T., Tsuji, H., Kohchi, T., and Matsunaga, S. (2022). Improved clearing method contributes to deep imaging of plant organs. Commun Biol 5: 12.

Schindelin, J. et al. (2012). Fiji: an open-source platform for biological-image analysis. Nat Methods 9: 676–682.

Schmidt, U., Weigert, M., Broaddus, C., and Myers, G. (2018). Cell Detection with Star-Convex Polygons. In Medical Image Computing and Computer Assisted Intervention – MICCAI 2018, A.F. Frangi, J.A. Schnabel, C. Davatzikos, C. Alberola-López, and G. Fichtinger, eds, Lecture Notes in Computer Science. (Springer International Publishing: Cham), pp. 265–273.

Schneller, J.J. (2008). Antheridiogens. In Biology and Evolution of Ferns and Lycophytes, T.A. Ranker and C.H. Haufler, eds (Cambridge University Press: New York), pp. 134–158.

Sessa, G., Carabelli, M., Sassi, M., Ciolfi, A., Possenti, M., Mittempergher, F., Becker, J., Morelli, G., and Ruberti, I. (2005). A dynamic balance between gene activation and repression regulates the shade avoidance response in *Arabidopsis*. Genes Dev. 19: 2811–2815.

Shimamura, M. (2016). *Marchantia polymorpha*: Taxonomy, phylogeny and morphology of a model system. Plant and Cell Physiology 57: 230–256.

Sponsel, V.M. (2016). Signal achievements in gibberellin research: the second half-century. Annual Plant Reviews: The Gibberellins 49: 1–36.

Streubel, S., Deiber, S., Rötzer, J., Mosiolek, M., Jandrasits, K., and Dolan, L. (2023). Meristem dormancy in Marchantia polymorpha is regulated by a liverwort-specific miRNA and a clade III SPL gene. Current Biology: S0960982222019996.

Sugano, S.S., Nishihama, R., Shirakawa, M., Takagi, J., Matsuda, Y., Ishida, S., Shimada, T., Hara-Nishimura, I., Osakabe, K., and Kohchi, T. (2018). Efficient CRISPR/Cas9-based genome editing and its application to conditional genetic analysis in Marchantia polymorpha. PLoS ONE 13: e0205117.

Sun, T. and Kamiya, Y. (1994). The Arabidopsis *GA1* locus encodes the cyclase *ent*-kaurene synthetase A of gibberellin biosynthesis. the Plant Cell 6: 1509–1518.

Talon, M., Koornneef, M., and Zeevaart, J.A.D. (1990). Endogenous gibberellins in Arabidopsis thaliana and possible steps blocked in the biosynthetic pathways of the semidwarf ga4 and ga5 mutants. Proceedings of the National Academy of Sciences of the United States of America 87: 7983–7987.

Tanaka, J., Yano, K., Aya, K., Hirano, K., Takehara, S., Koketsu, E., Ordonio, R.L., Park, S.-H., Nakajima, M., Ueguchi-Tanaka, M., and Matsuoka, M. (2014). Antheridiogen determines sex in ferns via a spatiotemporally split gibberellin synthesis pathway. Science 346: 469–473.

Toyomasu, T., Kawaide, H., Mitsuhashi, W., Inoue, Y., and Kamiya, Y. (1998). Phytochrome regulates gibberellin biosynthesis during germination of photoblastic lettuce seeds. Plant Physiology 118: 1517–1523.

Ubeda-Tomás, S., Federici, F., Casimiro, I., Beemster, G.T.S., Bhalerao, R., Swarup, R., Doerner, P., Haseloff, J., and Bennett, M.J. (2009). Gibberellin Signaling in the Endodermis Controls Arabidopsis Root Meristem Size. Current Biology 19: 1194–1199.

Ubeda-Tomás, S., Swarup, R., Coates, J., Swarup, K., Laplaze, L., Beemster, G.T.S., Hedden, P., Bhalerao, R., and Bennett, M.J. (2008). Root growth in Arabidopsis requires gibberellin/DELLA signalling in the endodermis. Nat Cell Biol 10: 625–628.

Ueguchi-Tanaka, M., Ashikari, M., Nakajima, M., Itoh, H., Katoh, E., Kobayashi, M., Chow, T., Hsing, Y.C., Kitano, H., Yamaguchi, I., and Matsuoka, M. (2005). *GIBBERELLIN INSENSITIVE DWARF1* encodes a soluble receptor for gibberellin. Nature 437: 693–698.

Urrutia, O., Hedden, P., and Rojas, M.C. (2001). Monooxygenases involved in GA12 and GA14 synthesis in Gibberella fujikuroi. Phytochemistry 56: 505–511.

Van Tuinen, A., Peters, A.H.L.J., Kendrick, R.E., Zeevaart, J. a. D., and Koornneef, M. (1999). Characterisation of the procera mutant of tomato and the interaction of gibberellins with end-of-day far-red light treatments. Physiologia Plantarum 106: 121–128.

Wenzel, C.L., Williamson, R.E., and Wasteneys, G.O. (2000). Gibberellin-Induced Changes in Growth Anisotropy Precede Gibberellin-Dependent Changes in Cortical Microtubule Orientation in Developing Epidermal Cells of Barley Leaves. Kinematic and Cytological Studies on a Gibberellin-Responsive Dwarf Mutant, M489. Plant Physiology 124: 813–822.

Whitelam, G.C. and Johnson, C.B. (1982). PHOTOMORPHOGENESIS IN IMPATIENS PARVIFLORA AND OTHER PLANT SPECIES UNDER SIMULATED NATURAL CANOPY RADIATIONS. New Phytol 90: 611–618.

Whitelam, G.C. and Smith, H. (1991). Retention of Phytochrome-Mediated Shade Avoidance Responses in Phytochrome-Deficient Mutants of Arabidopsis, Cucumber and Tomato. Journal of Plant Physiology 139: 119–125.

Williams, J., Phillips, A.L., Gaskin, P., and Hedden, P. (1998). Function and Substrate Specificity of the Gibberellin 3β-Hydroxylase Encoded by the Arabidopsis GA4Gene. Plant Physiology 117: 559–563.

Xu, S., Li, L., Luo, X., Chen, M., Tang, W., Zhan, L., Dai, Z., Lam, T.T., Guan, Y., and Yu, G. (2022). Ggtree: A serialized data object for visualization of a phylogenetic tree and annotation data. iMeta 1: e56.

Yamaguchi, S., Smith, M.W., Brown, R.G.S., Kamiya, Y., and Sun Tai-ping (1998a). Phytochrome Regulation and Differential Expression of Gibberellin 3β-Hydroxylase Genes in Germinating Arabidopsis Seeds. The Plant Cell 10: 2115–2126.

Yamaguchi, S., Sun, T., Kawaide, H., and Kamiya, Y. (1998b). The *GA2* locus of *Arabidopsis thaliana* encodes *ent*-kaurene synthase of gibberellin biosynthesis. Plant Physiology 116: 1271–1278.

Yamane, H. (1998). Fern Antheridiogens. International Review of Cytology 184: 1–32.

Yamaoka, S. et al. (2018). Generative Cell Specification Requires Transcription Factors Evolutionarily Conserved in Land Plants. Current Biology 28: 479-486.e5.

Yamauchi, T., Oyama, N., Yamane, H., Murofushi, N., Schraudolf, H., Pour, M., Furber, M., and Mander, L.N. (1996). Identification of Antheridiogens in Lygodium circinnatum and Lygodium flexuosum. Plant Physiology 111: 741–745.

Yasumura, Y., Crumpton-Taylor, M., Fuentes, S., and Harberd, N.P. (2007). Step-by-step acquisition of the gibberellin-DELLA growth-regulatory mechanism during land-plant evolution. Current Biology 17: 1225–1230.

Yoshida, H., Takehara, S., Mori, M., Ordonio, R.L., and Matsuoka, M. (2020). Evolution of GA metabolic enzymes in land plants. Plant and Cell Physiology 61: 1919–1934.

Yu, G. (2022). Data Integration, Manipulation and Visualization of Phylogenetic Trees (Chapman and Hall/CRC: New York).

Yu, G. (2020a). Gene ontology semantic similarity analysis using GOSemSim. In Methods in Molecular Biology (Humana Press Inc.), pp. 207–215.

Yu, G. (2020b). Using ggtree to Visualize Data on Tree-Like Structures. Current Protocols in Bioinformatics 69: e96.

Yu, G., Lam, T.T.-Y., Zhu, H., and Guan, Y. (2018). Two Methods for Mapping and Visualizing Associated Data on Phylogeny Using Ggtree. Molecular Biology and Evolution 35: 3041–3043.

Yu, G., Li, F., Qin, Y., Bo, X., Wu, Y., and Wang, S. (2010). GOSemSim: an R package for measuring semantic similarity among GO terms and gene products. Bioinformatics 26: 976–978.

Yu, G., Smith, D.K., Zhu, H., Guan, Y., and Lam, T.T.-Y. (2017). ggtree: an r package for visualization and annotation of phylogenetic trees with their covariates and other associated data. Methods in Ecology and Evolution 8: 28–36.

Zhang, Y., Werling, U., and Edelmann, W. (2012). SLiCE: A novel bacterial cell extract-based DNA cloning method. Nucleic Acids Research 40: 1–10.

Figure Legends

Figure 1 Loss of Mp*CPS* function alters thallus morphology under far-red light (FR) enriched conditions.

A, Morphology of 12-day-old plants grown from gemmae under continuous white light (cW) or continuous white light with far-red light (cW+cFR) conditions. Images were selected randomly from different plants. Bars = 10 mm. B-D, Measurements of the thallus growth angle (B), length-width ratio (C) and thallus area (D) from half plants shown in A. n=21-36. E, Apical regions of plants labelled with 5-ethynyl-2'-deoxyuridine (EdU) after 7-day growth in cW+cFR, showing two-dimensional projections of color-coded z-stacks. White lines mark the boundary of plants or imaging area. F, Number of nuclei with positive EdU signals in the apical regions of 7-day-old plants grown in cW+cFR (n=5). For all figures, WT♂ refer to Tak-1 wild-type plants. For B-D and F, each dot represents data from a “half thallus”, which was developed from a single meristem of the gemma. Horizontal lines represent mean values. Letters represent statistical differences, and groups with no common letters were significantly different (adjusted $p<0.05$). For B-D, non-pooled Welch’s t-test with Benjamini-Hochberg (B-H) adjustment was used due to heterogeneity of variance. Tukey’s HSD test was used in F.

Figure 2 Mp*CPS* is required for delayed sexual reproduction and affected gametangiophore morphology.

A-B, Progress of apical bifurcation and gametangiophore formation in male (A) and female (B) plants, which were cultured aseptically under cW for 7 days before transferred to cW+cFR. Dots and error bars represent means and standard deviations, respectively. n=8. WT♂ and WT♀ refer to Tak-1 and Tak-2 wild-type plants, respectively. C-D, Photos of male (C) and female (D) plants bearing gametangiophores, cultured on vermiculite under cW+cFR from thallus fragments for 81 and 63 days, respectively. E, Ventral view of antheridiophores. F, Dorsal and ventral view of archegoniophores. Arrowheads indicate marginal digitate rays, and the number of digitate rays was labeled in the ventral view. G-J, Fluorescence microscopic images and quantification of MpBNB-Cit accumulation in the apical regions of 11-day-old male (G-H, dorsal view), or 14-day-old female (I-J, ventral view) plants cultured under cW+cFR from gemmae. G and I, Z-projections of image stacks, with cell walls stained with calcofluor white (purple) and Citrine signals shown in green. Arrows indicate apical meristems. H and J, Number of Citrine-positive nuclei counted

from projection of image stacks. Each dot represents data from 1/2 (H) or 1/4 (J) of the thallus, and horizontal lines represent mean values. Asterisks show statistical difference compared to the control group (Mann-Whitney U test; **, p<0.01; ***, p<0.001). n=7 for H, n=8 for J.

Figure 3 Endogenous levels of and responsiveness to KA or GAs in wild-type and Mp*cps*^{ld} plants. A, Endogenous levels of GAs measured in wild-type plants (Tak-1) by LC-MS/MS. B, Selected ion chromatography showing peak of endogenous GA_{12} in comparison with the $^{2}H_{2}$-labeled internal standard. For A-B, plants were cultured under cW for 10 days, then induced under cW+cFR for 3 days. C-D, Effect of 2-μM KA or GAs on the morphology of 12-day-old thalli cultured under cW+cFR from gemmae. Horizontal bars in D represent mean values, and letters represent multiple comparisons with non-pooled Welch's *t*-test and B-H adjustment (adjusted p<0.05 for non-overlapping letters, n=16-18). E-F, Effect of 2-μM KA or GAs on gametangiophore formation (E) and morphology (F). Plants were cultured aseptically under cW for 7 days before transferred to cW+cFR. For (E), dots and error bars represent mean±SD (n=5), and asterisks show statistical difference compared to the mock group (Kruskal- Wallis test; *, p<0.05; **, p<0.01; ***, p<0.001). Data from the mock group is presented repeatedly in each subplot for comparison. Bars = 10 mm in C and 5 mm in F.

Figure 4 Biosynthetic route for GA_{12} production in *M. polymorpha*. A, Proposed enzymatic steps for GA_{12} biosynthesis in *M. poymorpha*. B-D, GC-MS analysis showing conversion of *ent*-kaurene to KA (B), and KA to GA_{12} (C-D) by yeast cultures expressing KO and KAO homologs. E, biosynthesis mutants with GA_{12} below the detection limit. n.d., not detected. F-G, morphlogy of 12-day-old mutants grown under cW+cFR with or without 2 μM KA. Each dot in G represents data from a "half thallus", horizontal bars represent mean values, and letters represent multiple comparisons with non-pooled Welch's t-test and B-H adjustment (adjusted p<0.05 for non-overlapping letters, n=14-18). H-I, Gametangiophore formation progress (H) and morphology (I) of mutants, cultured aseptically under cW for 7 days before transferred to cW+cFR and treated with 2 μM KA. Dots and error bars represent mean±SD in H (n=5), and asterisks show statistical difference (Kruskal-Wallis test; *, p<0.05; **, p<0.01; ***, p<0.001). Bars=10 mm in F and 5 mm in I.

Figure 5 Transcriptional regulation related to GA biosynthesis in *M. polymorpha*. A, Relative expression level of GA biosynthesis genes by qPCR in Mp*pif*^{ko} and its complementation line, cultured under cW for 7 days and then transferred to cW+cFR. B, endogenous level of GA_{12} in Tak-1 plants cultured under cW for 10 days, then under cW or cW+cFR for 4 days. The data for cW+cFR group is the same as in Figure 3A. The *p*-value was calculated by Student's *t*-test. C, Number of differentially expressed genes (DEGs) between 12-day-old Mp*cps-4*^{ld} and Tak-1 plants, or Mp*cps-4*^{ld} plants grown with or without 2-μM KA under indicated light conditions (Wald test with B-H adjustment by DESeq2, DEG defined as adjusted p<0.01 and $|log_2(\text{Fold Change})|>0.585$). D, expression patterns of up- and down- regulated genes in Mp*cps-4*^{ld}. E, Distribution of DEGs induced by FR enrichment in Tak-1 and Mp*cps-4*^{ld} plants, comparing transcriptomes of cW+cFR to cW conditions. F, GO term enrichment analysis of DEG sets shown in (C). Each dot shows a significant enriched biological process term (p<0.01 by Fisher's exact test), and semantically similar terms were plotted in color-coded clusters. Selected terms were highlighted with annotations. metab. proc., metabolic process. See Supplemental Data Set 2 for full lists. G, Relative expression level of GA biosynthesis genes by qPCR in plants cultured under cW for 11 days, then transferred to cW+cFR with or without 2-μM KA treatment. All bar plots with error bars (A-B, G) represent mean±SD from 3 biological replicates (pooled whole thallus tissue). Letters in A and G represent multiple comparisons with Tukey's HSD test (adjusted p<0.05 for non-overlapping letters).

Main Figures

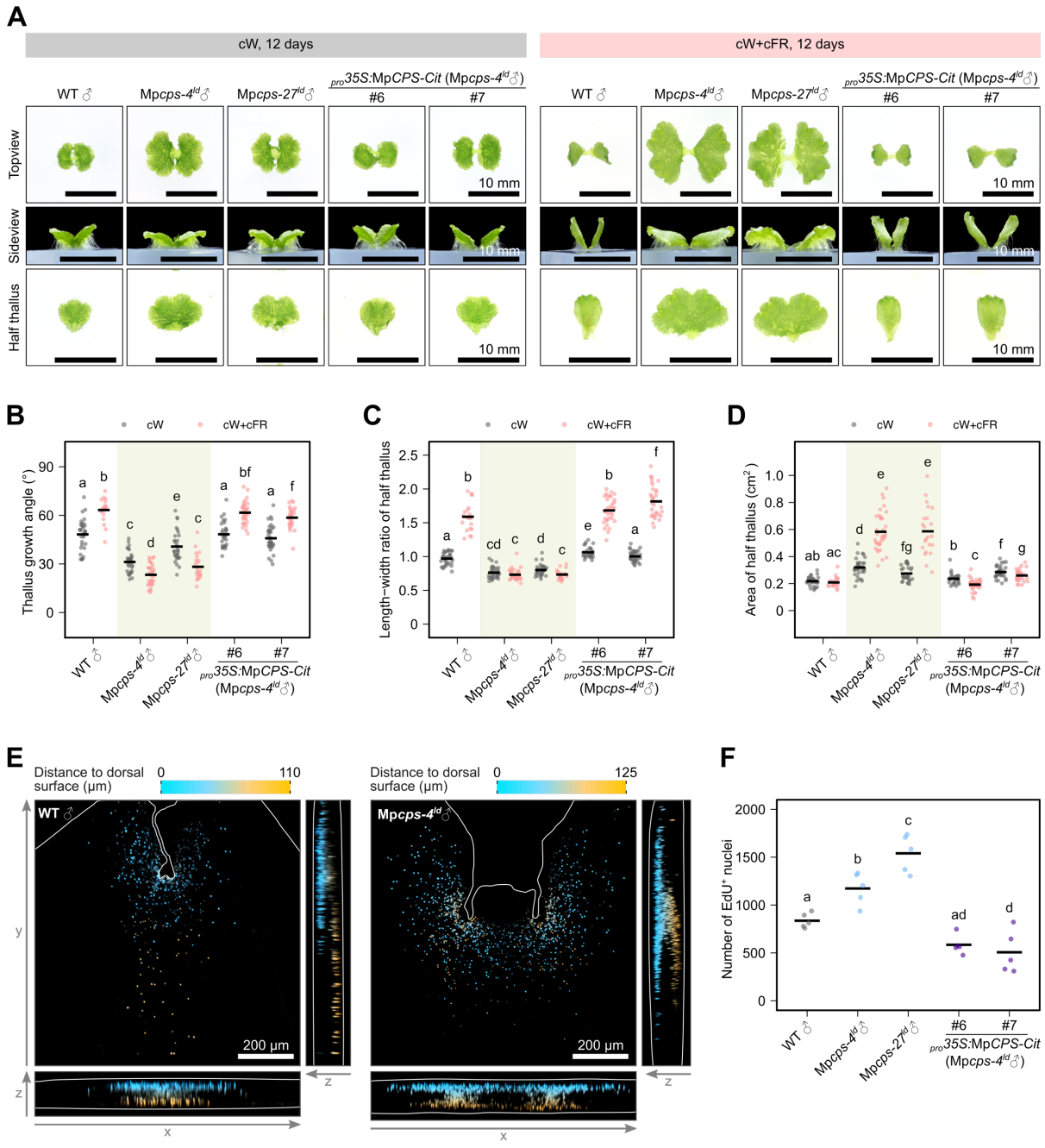

Figure 1 Loss of Mp*CPS* activity alters thallus morphology under far-red light (FR) enriched conditions. A, Morphology of 12-day-old plants grown from gemmae under continuous white light (cW) or continuous white light with far-red light (cW+cFR) conditions. Images were selected randomly from different plants. Bars = 10 mm. B-D, Measurements of the thallus growth angle (B), length-width ratio (C) and thallus area (D) from half plants shown in A. n=21-36. E, Apical regions of plants labelled with 5-ethynyl-2'-deoxyuridine (EdU) after 7-day growth in cW+cFR, showing two-dimensional projections of color-coded z-stacks. White lines mark the boundary of plants or imaging area. F, Number of nuclei with positive EdU signals in the apical regions of 7-day-old plants grown in cW+cFR (n=5). For all figures, WT♂ refer to Tak-1 wild-type plants. For B-D and F, each dot represents data from a "half thallus", which was developed from a single meristem of the gemma. Horizontal lines represent mean values. Letters represent statistical differences, and groups with no common letters were significantly different (adjusted $p<0.05$). For B-D, non-pooled Welch's *t*-test with Benjamini-Hochberg (B-H) adjustment was used due to heterogeneity of variance. Tukey's HSD test was used in F.

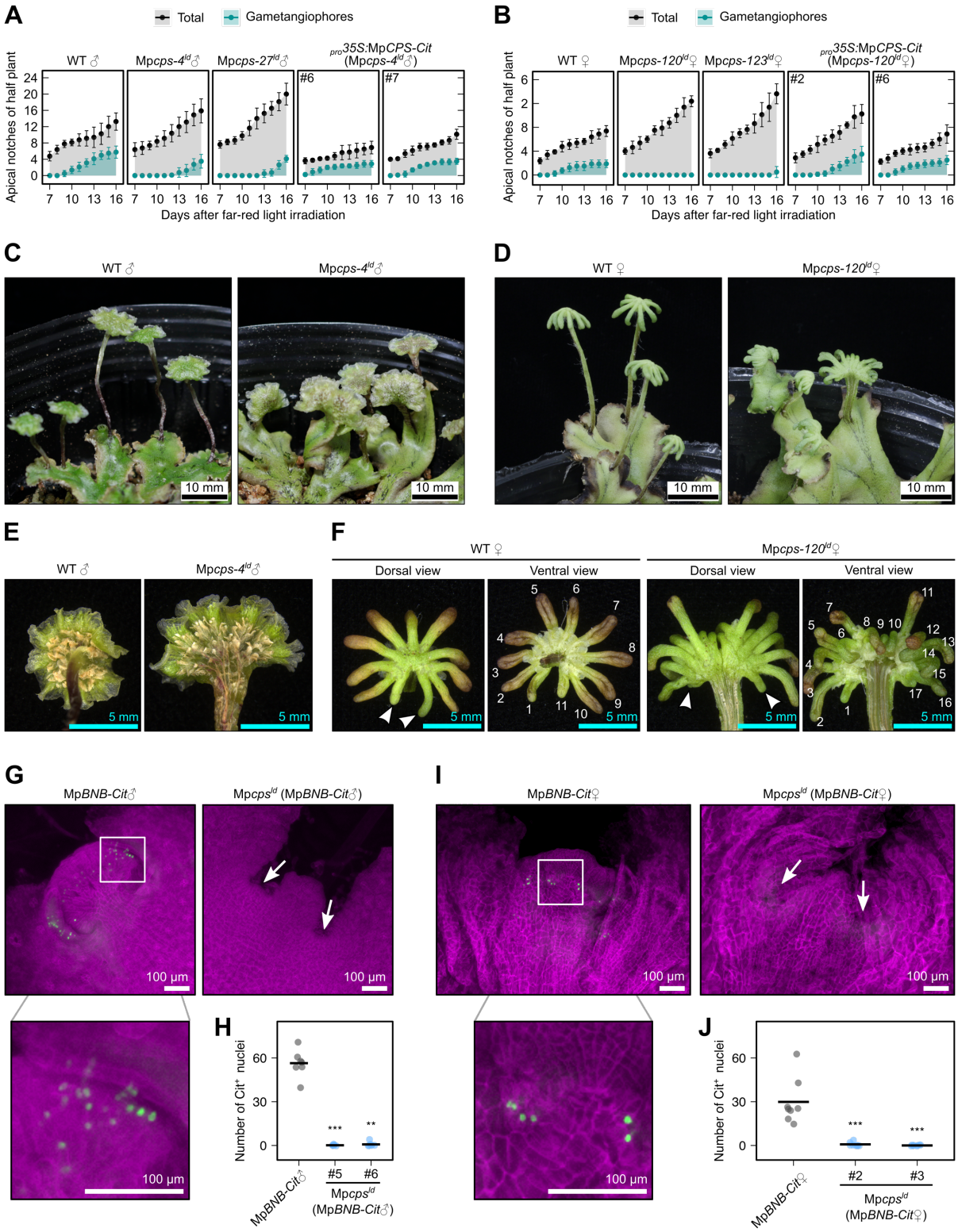
A
Total
Gametangiophores
WT ♂
Mpcps-4ld♂
Mpcps-27ld♂
pro35S:MpCPS-Cit (Mpcps-4ld♂)
#6
#7
Apical notches of half plant
Days after far-red light irradiation
B
WT ♀
Mpcps-120ld♀
Mpcps-123ld♀
pro35S:MpCPS-Cit (Mpcps-120ld♀)
#2
#6
C
D
10 mm
E
5 mm
F
Dorsal view
Ventral view
G
MpBNB-Cit♂
Mpcpsld (MpBNB-Cit♂)
100 µm
H
Number of Cit+ nuclei
***
**
MpBNB-Cit♂
#5
#6
Mpcpsld (MpBNB-Cit♂)
I
MpBNB-Cit♀
Mpcpsld (MpBNB-Cit♀)
J
MpBNB-Cit♀
#2
#3
Mpcpsld (MpBNB-Cit♀)

Figure 2 Mp*CPS* is required for delayed sexual reproduction and affected gametangiophore morphology.
A-B, Progress of apical bifurcation and gametangiophore formation in male (A) and female (B) plants, which were cultured aseptically under cW for 7 days before transferred to cW+cFR. Dots and error bars represent means and standard deviations, respectively. n=8. WT♂ and WT♀ refer to Tak-1 and Tak-2 wild-type plants, respectively. C-D, Photos of male (C) and female (D) plants bearing gametangiophores, cultured on vermiculite under cW+cFR from thallus fragments for 81 and 63 days, respectively. E, Ventral view of antheridiophores. F, Dorsal and ventral view of archegoniophores. Arrowheads indicate marginal digitate rays, and the number of digitate rays was labeled in the ventral view. G-J, Fluorescence microscopic images and quantification of MpBNB-Cit accumulation in the apical regions of 11-day-old male (G-H, dorsal view), or 14-day-old female (I-J, ventral view) plants cultured under cW+cFR from gemmae. G and I, Z-projections of image stacks, with cell walls stained with calcofluor white (purple) and Citrine signals shown in green. Arrows indicate apical meristems. H and J, Number of Citrine-positive nuclei counted from projection of image stacks. Each dot represents data from 1/2 (H) or 1/4 (J) of the thallus, and horizontal lines represent mean values. Asterisks show statistical difference compared to the control group (Mann-Whitney *U* test; **, $p<0.01$; ***, $p<0.001$). n=7 for H, n=8 for J.

A

Metabolite	Endogenous Level	Metabolite	Endogenous Level
GA_1	not detected	GA_{20}	not detected
GA_4	not detected	GA_{24}	not detected
GA_8	not detected	GA_{29}	not detected
GA_9	not detected	GA_{34}	not detected
GA_{12}	28.9±6.5	GA_{44}	not detected
GA_{15}	not detected	GA_{51}	not detected
GA_{19}	not detected	GA_{53}	not detected

(unit: pg/g fresh weight)

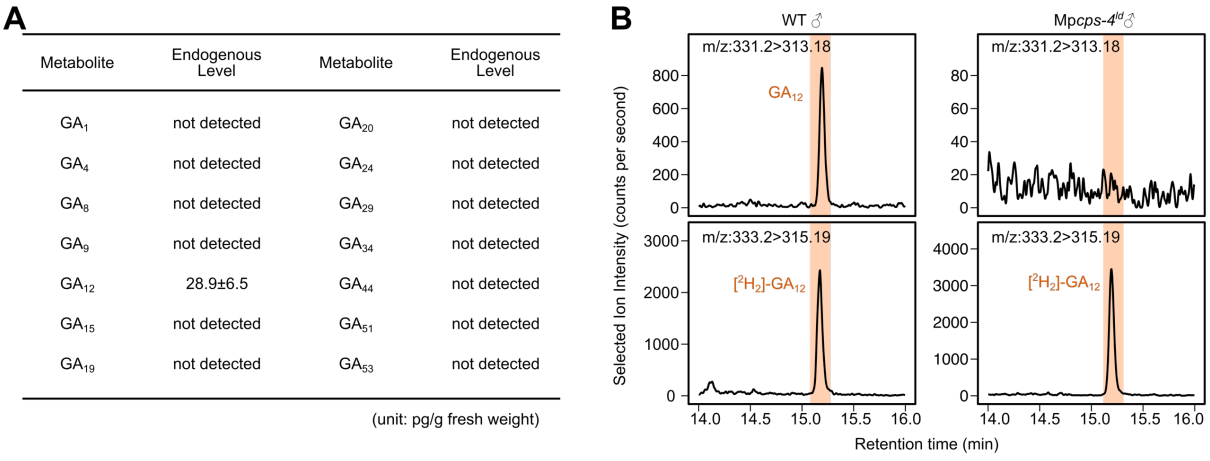

Figure 3 Endogenous levels of and responsiveness to KA or GAs in wild-type and Mp*cps*^{ld} plants.
A, Endogenous levels of GAs measured in wild-type plants (Tak-1) by LC-MS/MS. B, Selected ion chromatography showing peak of endogenous GA_{12} in comparison with the $^{2}H_{2}$-labeled internal standard. For A-B, plants were cultured under cW for 10 days, then induced under cW+cFR for 3 days. C-D, Effect of 2-μM KA or GAs on the morphology of 12-day-old thalli cultured under cW+cFR from gemmae. Horizontal bars in D represent mean values, and letters represent multiple comparisons with non-pooled Welch's *t*-test and B-H adjustment (adjusted $p<0.05$ for non-overlapping letters, n=16-18). E-F, Effect of 2-μM KA or GAs on gametangiophore formation (E) and morphology (F). Plants were cultured aseptically under cW for 7 days before transferred to cW+cFR. For (E), dots and error bars represent mean±SD (n=5), and asterisks show statistical difference compared to the mock group (Kruskal-Wallis test; *, $p<0.05$; **, $p<0.01$; ***, $p<0.001$). Data from the mock group is presented repeatedly in each subplot for comparison. Dots and error bars represent mean±SD in E (n=5). Bars = 10 mm in C and 5 mm in F.

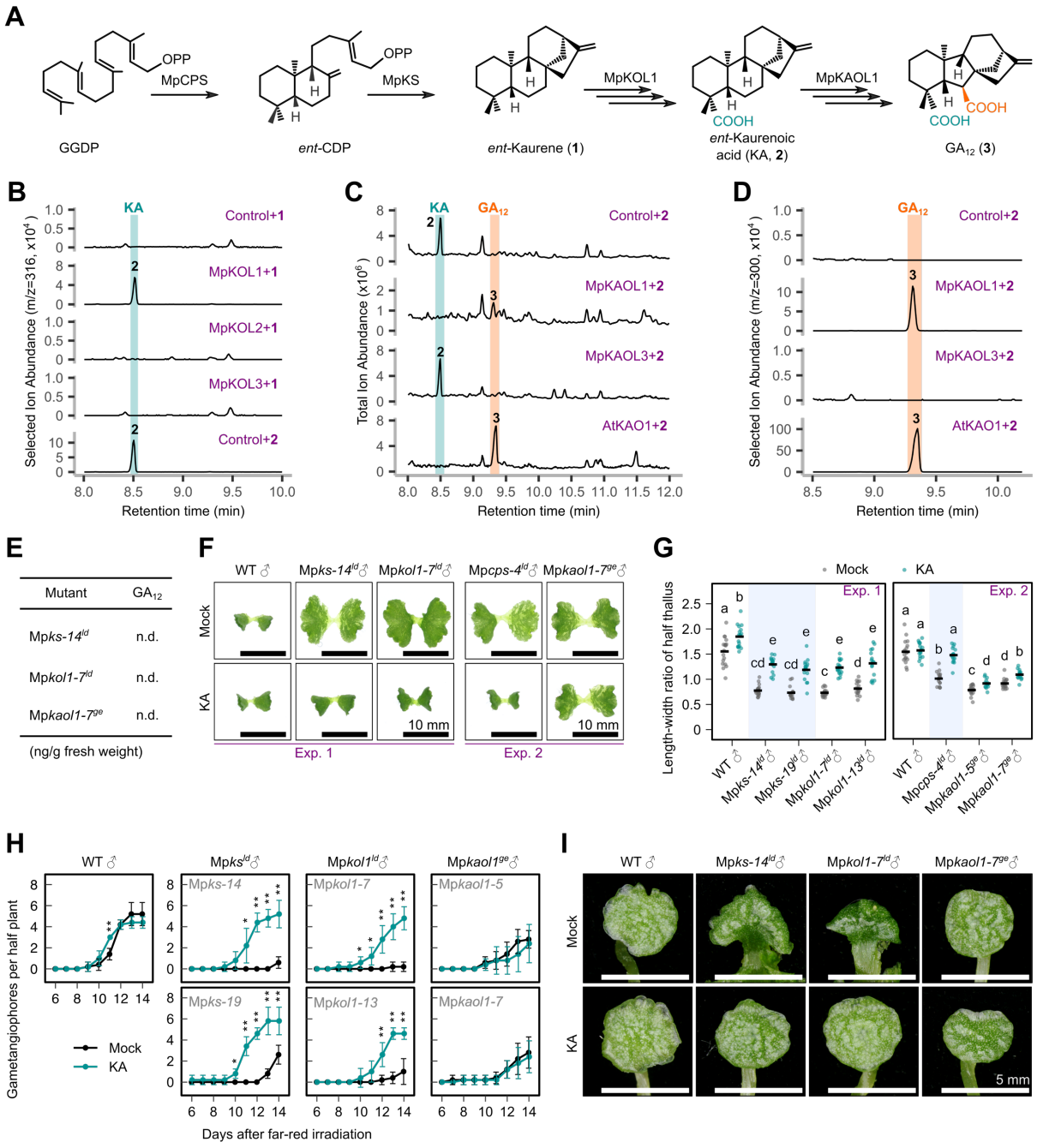
A
OPP
MpCPS
GGDP
ent-CDP
OPP
MpKS
ent-Kaurene (1)
MpKOL1
ent-Kaurenoic acid (KA, 2)
MpKAOL1
GA12 (3)
COOH
B
KA
Control+1
MpKOL1+1
MpKOL2+1
MpKOL3+1
Control+2
Selected Ion Abundance (m/z=316, x10^4)
Retention time (min)
C
KA
GA12
Control+2
MpKAOL1+2
MpKAOL3+2
AtKAO1+2
Total Ion Abundance (x10^6)
Retention time (min)
D
GA12
Control+2
MpKAOL1+2
MpKAOL3+2
AtKAO1+2
Selected Ion Abundance (m/z=300, x10^4)
Retention time (min)
E
Mutant
GA12
Mpks-14ld
n.d.
Mpkol1-7ld
n.d.
Mpkaol1-7ge
n.d.
(ng/g fresh weight)
F
WT ♂
Mpks-14ld♂
Mpkol1-7ld♂
Mpcps-4ld♂
Mpkaol1-7ge♂
Mock
KA
10 mm
Exp. 1
Exp. 2
G
Mock
KA
Exp. 1
Exp. 2
Length-width ratio of half thallus
WT ♂
Mpks-14ld♂
Mpks-19ld♂
Mpkol1-7ld♂
Mpkol1-13ld♂
Mpcps-4ld♂
Mpkaol1-5ge♂
Mpkaol1-7ge♂
H
WT ♂
Mpksld♂
Mpkol1ld♂
Mpkaol1ge♂
Mpks-14
Mpkol1-7
Mpkaol1-5
Mpks-19
Mpkol1-13
Mpkaol1-7
Gametangiophores per half plant
Mock
KA
Days after far-red irradiation
I
WT ♂
Mpks-14ld♂
Mpkol1-7ld♂
Mpkaol1-7ge♂
Mock
KA
5 mm

Figure 4 Biosynthetic route for GA_{12} production in *M. polymorpha*.
A, Proposed enzymatic steps for GA_{12} biosynthesis in *M. poymorpha*. B-D, GC-MS analysis showing conversion of *ent*-kaurene to KA (B), and KA to GA_{12} (C-D) by yeast cultures expressing KO and KAO homologs. E, biosynthesis mutants with GA_{12} below the detection limit. n.d., not detected. F-G, morphlogy of 12-day-old mutants grown under cW+cFR with or without 2 μM KA. Each dot in G represents data from a "half thallus", horizontal bars represent mean values, and letters represent multiple comparisons with non-pooled Welch's *t*-test and B-H adjustment (adjusted $p<0.05$ for non-overlapping letters, n=14-18). H-I, Gametangiophore formation progress (H) and morphology (I) of mutants, cultured aseptically under cW for 7 days before transferred to cW+cFR and treated with 2 μM KA. Dots and error bars represent mean±SD in H (n=5), and asterisks show statistical difference (Kruskal-Wallis test; *, $p<0.05$; **, $p<0.01$; ***, $p<0.001$). Bars = 10 mm in F and 5 mm in I.

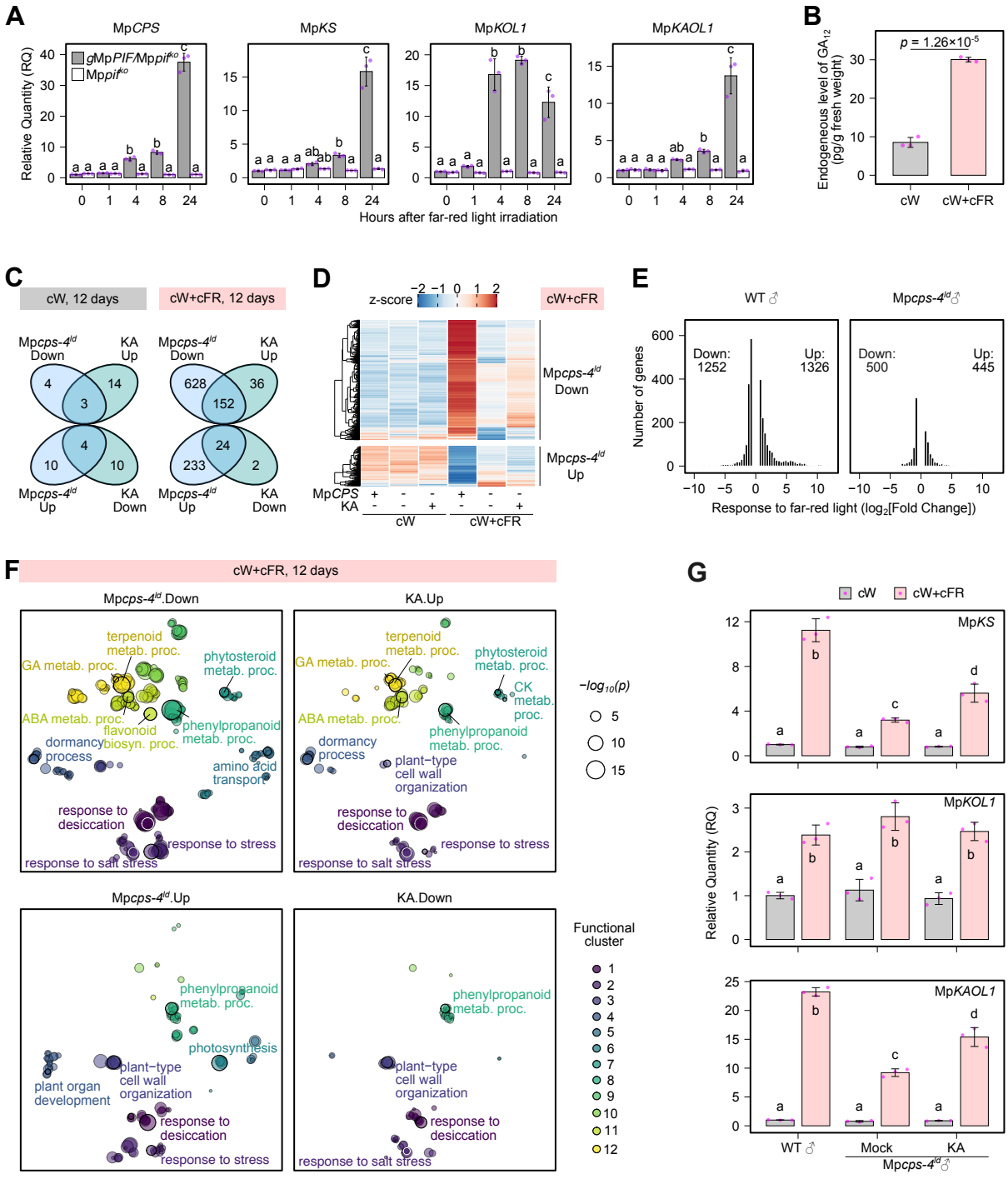
A
MpCPS
MpKS
MpKOL1
MpKAOL1
Relative Quantity (RQ)
gMpPIF/MppifKO
MppifKO
Hours after far-red light irradiation
B
p = 1.26×10-5
Endogeneous level of GA12 (pg/g fresh weight)
cW
cW+cFR
C
cW, 12 days
cW+cFR, 12 days
Mpcps-4ld Down
KA Up
Mpcps-4ld Up
KA Down
4
14
3
4
10
10
628
36
152
24
233
2
D
z-score
cW+cFR
Mpcps-4ld Down
Mpcps-4ld Up
MpCPS
KA
cW
cW+cFR
E
WT ♂
Mpcps-4ld♂
Number of genes
Down: 1252
Up: 1326
Down: 500
Up: 445
Response to far-red light (log2[Fold Change])
F
cW+cFR, 12 days
Mpcps-4ld.Down
KA.Up
Mpcps-4ld.Up
KA.Down
terpenoid metab. proc.
GA metab. proc.
phytosteroid metab. proc.
ABA metab. proc.
flavonoid biosyn. proc.
phenylpropanoid metab. proc.
dormancy process
amino acid transport
response to desiccation
response to stress
response to salt stress
CK metab. proc.
plant−type cell wall organization
photosynthesis
plant organ development
−log10(p)
Functional cluster
G
cW
cW+cFR
MpKS
MpKOL1
MpKAOL1
Relative Quantity (RQ)
WT ♂
Mock
KA
Mpcps-4ld♂

Figure 5 Transcriptional regulation related to GA biosynthesis in *M. polymorpha*.
A, Relative expression level of GA biosynthesis genes by qPCR in Mp*pif*^{ko} and its complementation line, cultured under cW for 7 days and then transferred to cW+cFR. B, Endogenous level of GA_{12} in Tak-1 plants cultured under cW for 10 days, then under cW or cW+cFR for 4 days. The data for cW+cFR group is the same as in Figure 3A. The *p*-value was calculated by Student's *t*-test. C, Number of differentially expressed genes (DEGs) between 12-day-old Mp*cps*^{ld} and Tak-1 plants, or Mp*cps-4*^{ld} plants grown with or without 2-μM KA under indicated light conditions (Wald test with B-H adjustment by DESeq2, DEG defined as adjusted $p<0.01$ and $|\log_2(\text{Fold Change})|>0.585$). D, Expression patterns of up- and down-regulated genes in Mp*cps-4*^{ld}. E, Distribution of DEGs induced by FR enrichment in Tak-1 and Mp*cps-4*^{ld} plants, comparing transcriptomes of cW+cFR to cW conditions. F, GO term enrichment analysis of DEG sets shown in (C). Each dot shows a significant enriched biological process term ($p<0.01$ by Fisher's exact test), and semantically similar terms were plotted in color-coded clusters. Selected terms were highlighted with annotations. metab. proc., metabolic process. See Supplemental Data Set 2 for full lists. G, Relative expression level of GA biosynthesis genes by qPCR in plants cultured under cW for 11 days, then transferred to cW+cFR with or without 2-μM KA treatment. All bar plots with error bars (A-B, G) represent mean±SD from 3 biological replicates (pooled whole thallus tissue). Letters in A and G represent multiple comparisons with Tukey's HSD test (adjusted $p<0.05$ for non-overlapping letters).

Supplemental Figures

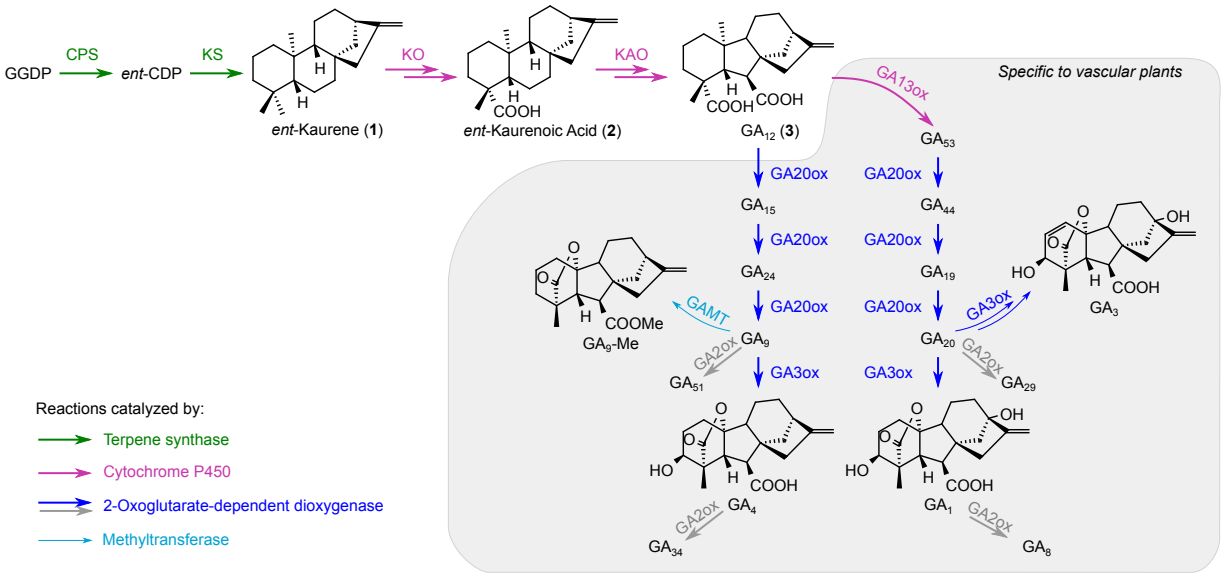

Supplemental Figure 1 Gibberellin (GA) biosynthesis pathway in vascular plants, showing compounds analyzed or used for treatment in this research. GGDP, geranylgeranyl diphosphate; *ent*-CDP, *ent*-copalyl diphosphate; CPS, *ent*-copalyl diphosphate synthase; KS, *ent*-kaurene synthase; KO, *ent*-kaurene oxidase; KAO, *ent*-kaurenoic acid oxidase. GA13ox, GA 13-oxidase; GA20ox, GA 20-oxidase; GA3ox, GA 3-oxidase; GA2ox, GA 2-oxidase; GAMT, GA methyltransferase. Deactivation steps catalyzed by GA2ox was shown with grey arrows. GA_3 is a major product from the fungus *Fusarium fujikuroi*, but could also be produced from GA_{20} by angiosperms like *Zea mays* or *Marah macrocarpa* (Fujioka et al., 1990; Albone et al., 1990). GAMT and GA2ox could act on broader ranges of substrates than shown in the figure, but reactions irrelevant to compounds used in this research were omitted. Related to Figure 3.

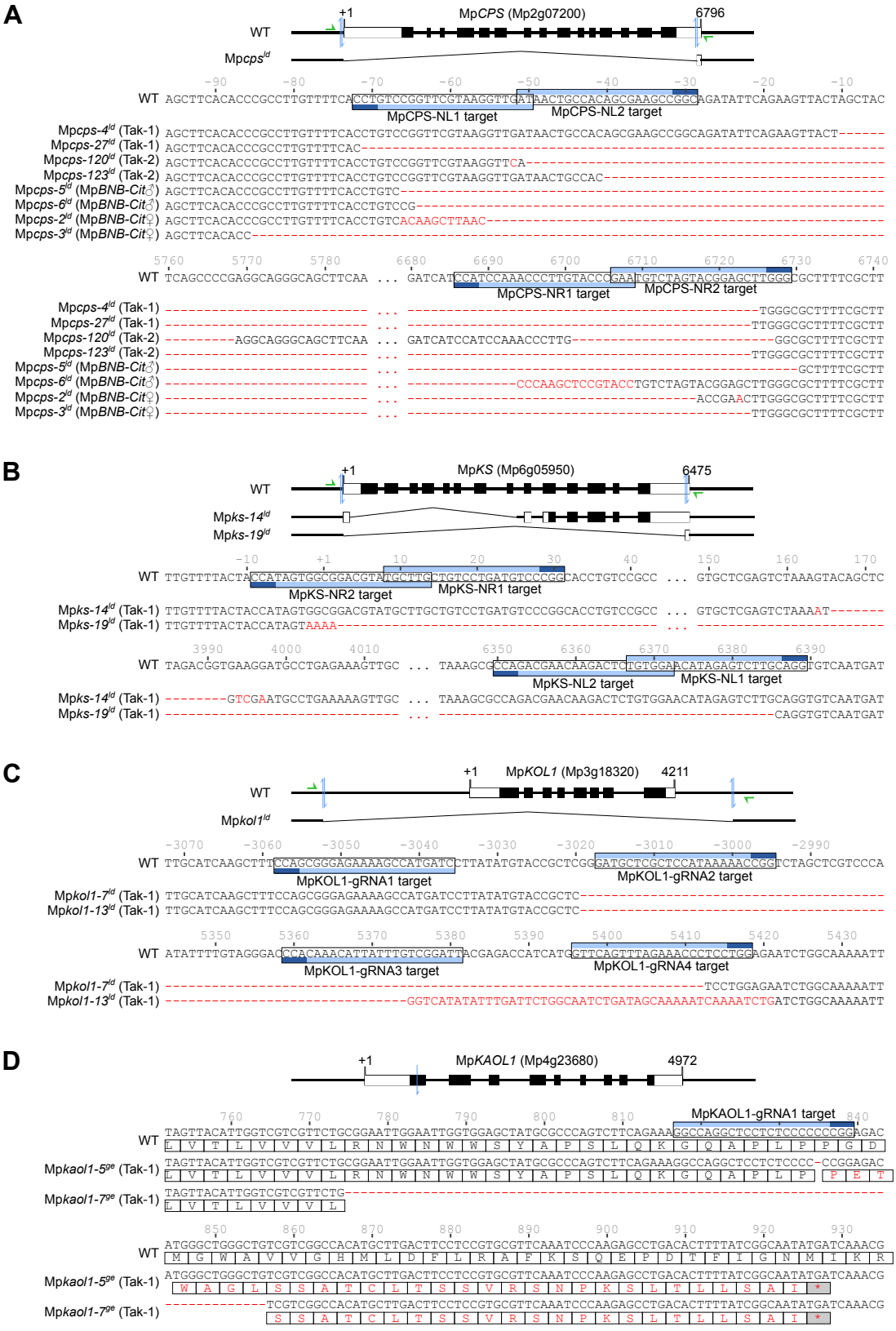

Supplemental Figure 2 Genotype information for Mp*cps*^{ld} (A), Mp*ks*^{ld} (B), Mp*kol1*^{ld} (C), and Mp*kaol1*^{ge} (D) mutants. WT refers to reference sequences from MpTak_v6.1 genome assembly. In the schematic presentations of genomic structures, white and black rectangles represent untranslated and coding regions of exons, respectively. Targets of guide RNAs are indicated by blue arrows in the scheme and

frames in the sequence (dark blue: the protospacer adjacent motif). Green arrows indicate the binding sites of genotyping primers. Indels and substitutions are shown in red letters. Numbers above the sequences indicate positions relative to the transcription start sites (+1). Putative protein translations are shown with framed letters in D, and the premature stop codons are marked with asterisks (*). Related to Figures 1 and 4.

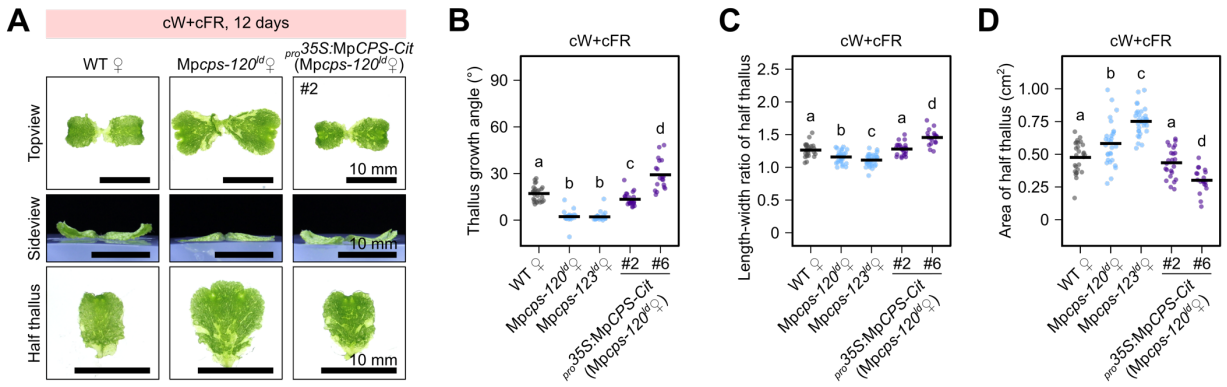

Supplemental Figure 3 Thallus morphology of female Mp*cps*^{ld} mutants in Tak-2 background under cW+cFR. A, Photos of 12-day-old plants grown from gemmae under cW+cFR. Bars = 10 mm. WT♀ refers to Tak-2 wild-type plants. B-D, Measurements of the thallus growth angle (B), length-width ratio (C) and thallus area (D) from half plants shown in A. Each dot represent data from a "half thallus" developed from one apical meristem of the gemma. Horizontal lines represent mean values, and letters represent multiple comparisons with two-sided, non-pooled Welch's *t*-test and B-H adjustment (adjusted p<0.05 for non-overlapping letters, n=19-34). Related to Figure 1.

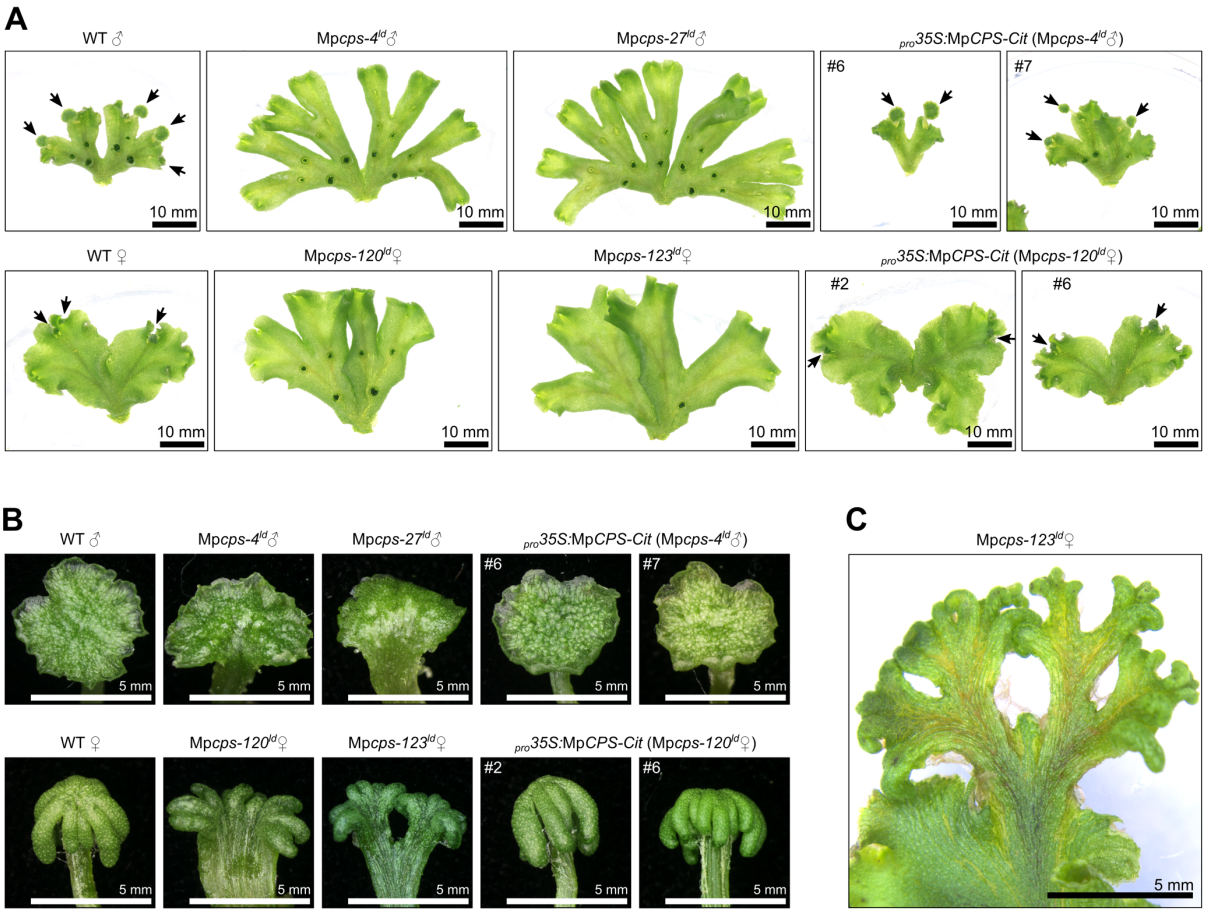

Supplemental Figure 4 Morphology of Mp*cps*^{ld} plants during gametangiophore formation in aseptic culture. A, Morphology of half thalli cultured under cW for 7 days, then under cW+cFR for 16 days. Arrows indicate gametangiophores visible by the naked eye. WT♂ and WT♀ refer to Tak-1 and Tak-2 wild-type plants, respectively. B, Morphology of young gametangiophores from aseptic culture. C, An extreme example of Mp*cps*^{ld} female gametangiophore with indeterminate bifurcation. The dashed line indicates the whole structure equivalent to a single gametangiophore. Related to Figure 2.

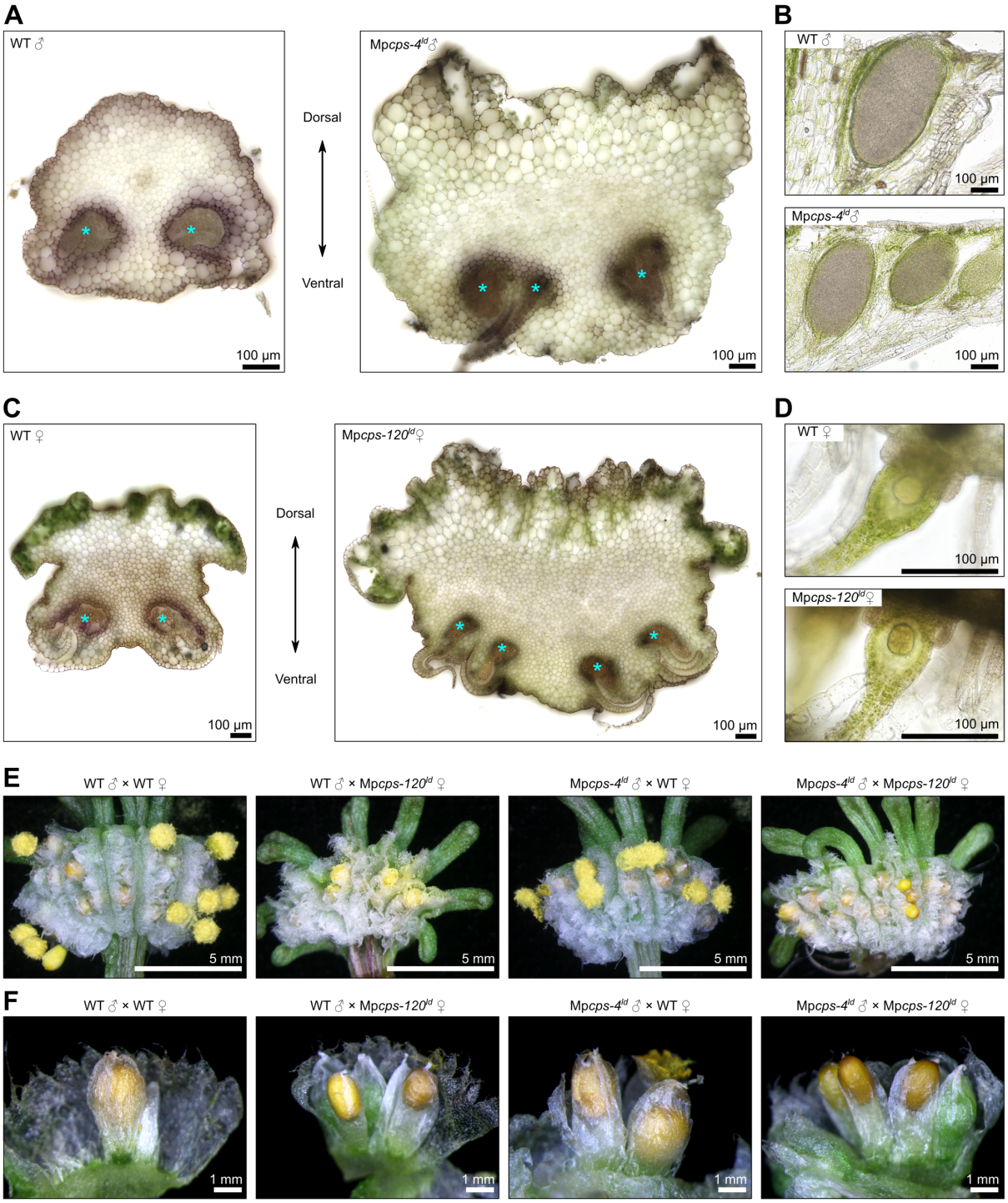

Supplemental Figure 5 Sections of gametangiophores in wild-type and Mp*cps*^{ld} plants, as well as the fertility test. A and C, Transverse sections of antheridiophore (A) or archegoniophore (C) stalks. Asterisks indicate bundles of pegged rhizoids. Thickness: 200 µm. B and D, longitudinal sections of antheridiophore (B) or archegoniophore (D) receptacles, showing the antheridium (B) or the egg cell in archegonium (D). Thickness: 70 µm. E-F, Mature sporangia from crossing experiments with various combinations among wild-type and Mp*cps*^{ld} plants. Related to Figure 2.

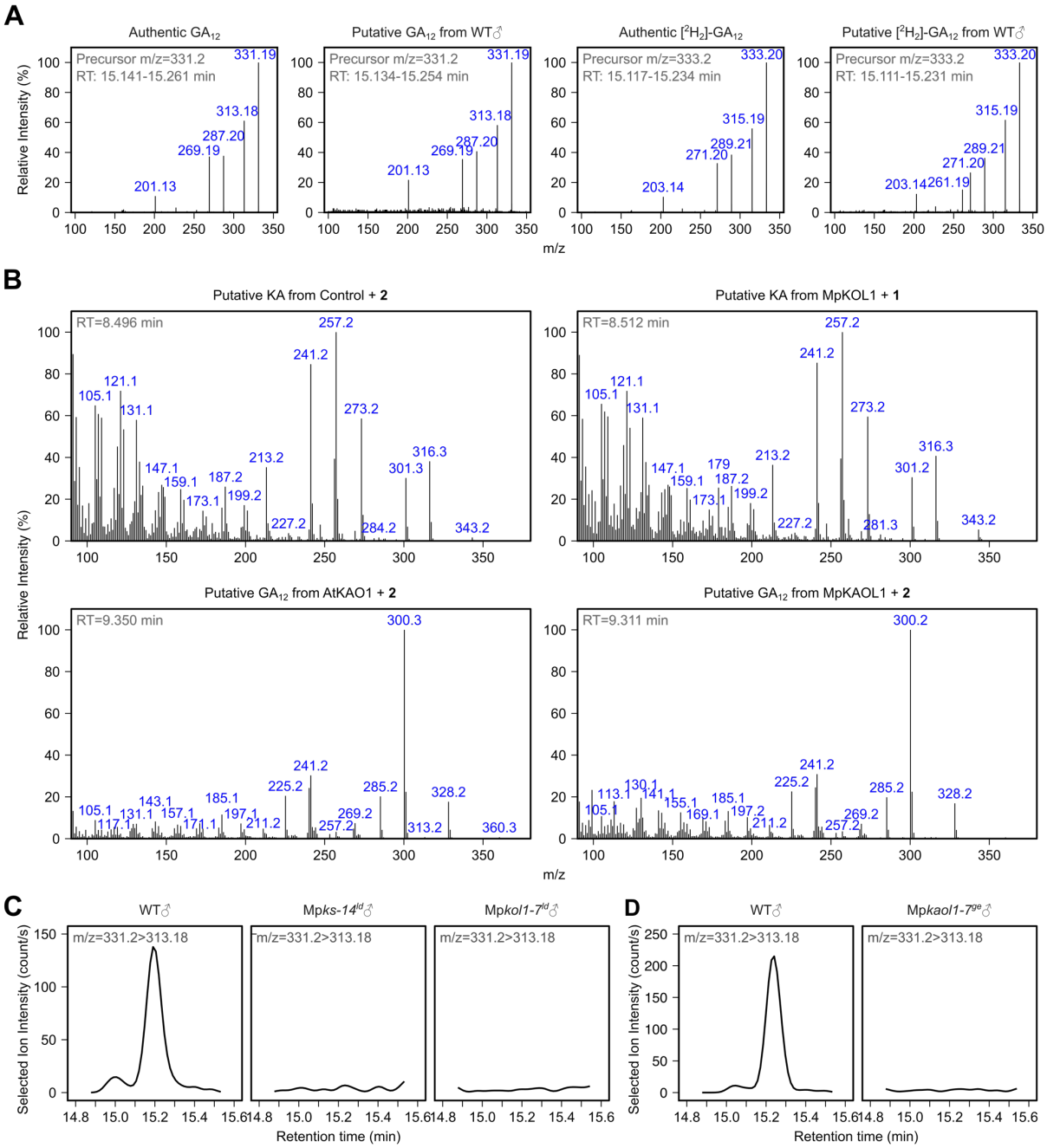

Supplemental Figure 6 LC-MS/MS and GC-MS profiles for KA and GA_{12} detection. A, Mass spectra of GA_{12} and [$^2H_2$]-GA_{12} in wild-type *M. polymorpha* samples were identical to those of authentic compounds. Detected by LC-MS/MS in the product-ion scanning mode. B, Mass spectra of KA and GA_{12} detected by GC-MS in *P. pastoris* cultures expressing MpKOL1 or MpKAOL1, compared to the positive controls. C-D, Selected ion chromatograph showing GA_{12} deficiency in Mp*ks-14*^{ld}, Mp*kol1-7*^{ld} or Mp*kaol1-7*^{ge}, detected by LC-MS/MS with the multiple reaction monitoring (MRM) mode. Related to Figures 3 and 4.

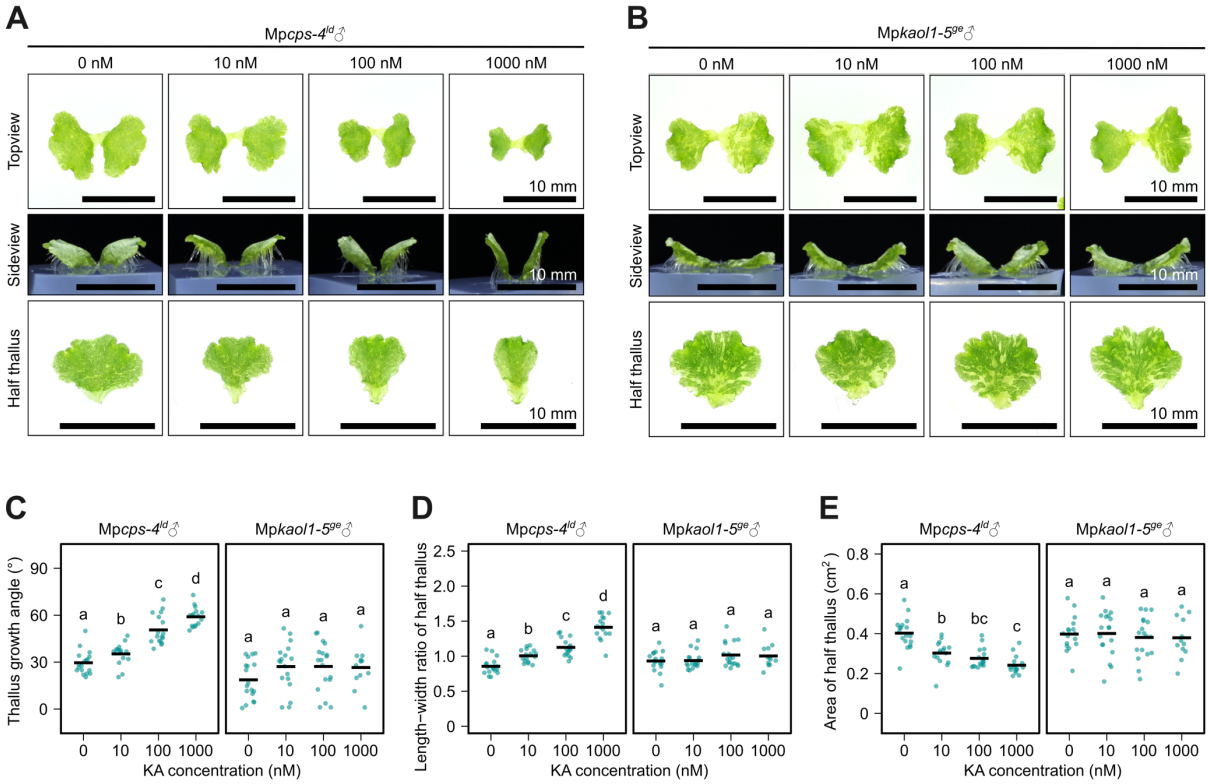

Supplemental Figure 7 Response of Mp*cps-4*^{ld} and Mp*kaol1-5*^{ge} to different concentrations of KA. A-B, Morphology of 12-day-old plants cultured under cW+cFR from gemmae with different concentrations of KA. Bars = 10 mm. C-E, Measurements of the thallus growth angle (C), length-width ratio (D) and thallus area (E) from half plants shown in A-B. Each dot represent data from a "half thallus" developed from one apical meristem of the gemma. Horizontal lines represent mean values, and letters represent multiple comparisons with two-sided, non-pooled Welch's *t*-test and B-H adjustment (adjusted p<0.05 for non-overlapping letters, n=12-18). Related to Figures 3 and 4.

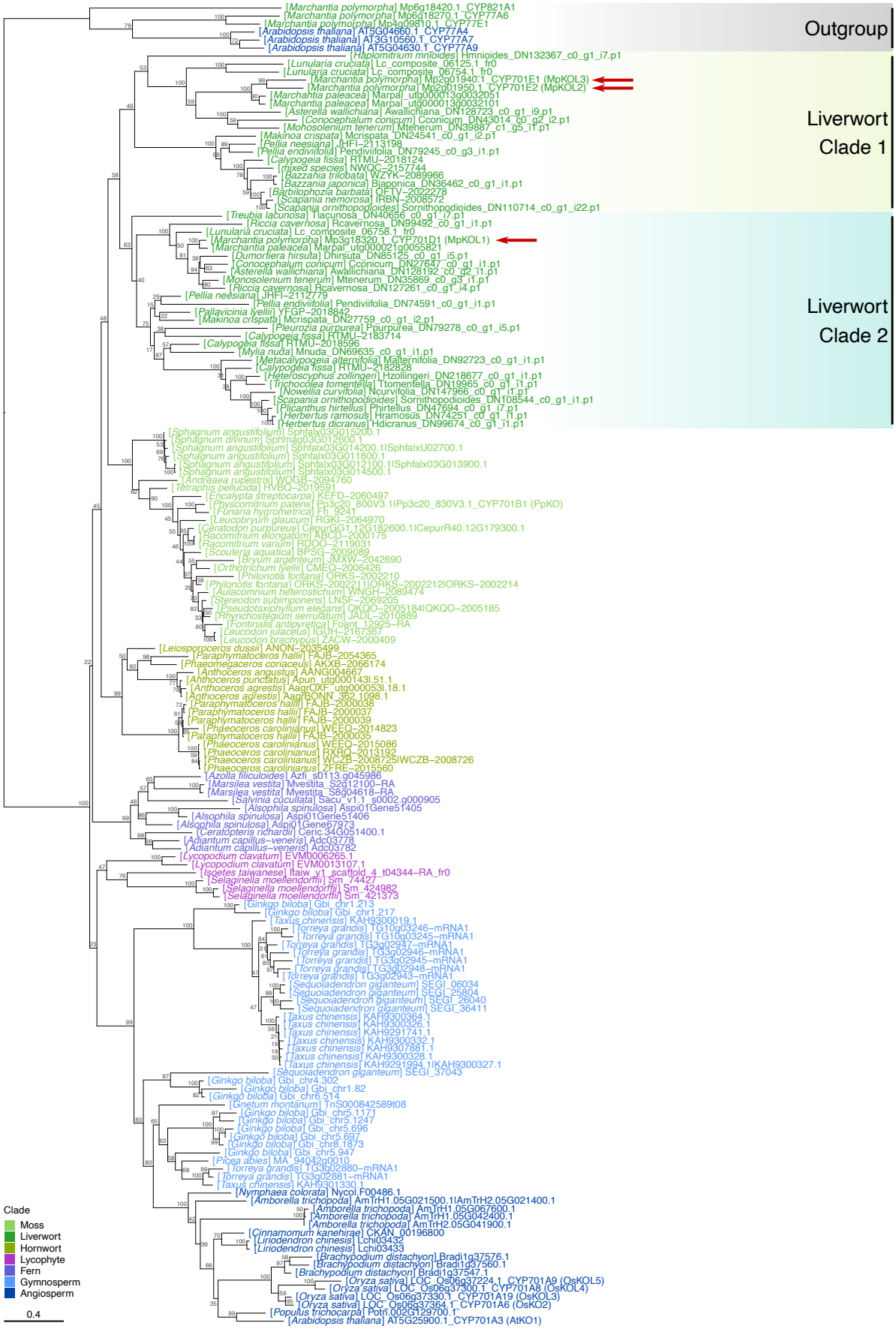
Outgroup
Liverwort Clade 1
Liverwort Clade 2
[Marchantia polymorpha] Mp6g18420.1_CYP821A1
[Marchantia polymorpha] Mp6g18270.1_CYP77A6
[Marchantia polymorpha] Mp4g09810.1_CYP77E1
[Arabidopsis thaliana] AT5G04660.1_CYP77A4
[Arabidopsis thaliana] AT3G10560.1_CYP77A7
[Arabidopsis thaliana] AT5G04630.1_CYP77A9
[Haplomitrium mnioides] Hmnioides_DN132367_c0_g1_i7.p1
[Lunularia cruciata] Lc_composite_06125.1_fr0
[Lunularia cruciata] Lc_composite_06754.1_fr0
[Marchantia polymorpha] Mp2g01940.1_CYP701E1 (MpKOL3)
[Marchantia polymorpha] Mp2g01950.1_CYP701E2 (MpKOL2)
[Marchantia paleacea] Marpal_utg000013g0032051
[Marchantia paleacea] Marpal_utg000013g0032101
[Asterella wallichiana] Awallichiana_DN128723_c0_g1_i9.p1
[Conocephalum conicum] Cconicum_DN43014_c0_g2_i2.p1
[Monosolenium tenerum] Mtenerum_DN39887_c1_g5_i1.p1
[Makinoa crispata] Mcrispata_DN24541_c0_g1_i2.p1
[Pellia neesiana] JHFI–2113198
[Pellia endiviifolia] Pendiviifolia_DN79245_c0_g3_i1.p1
[Calypogeia fissa] RTMU–2018124
[mixed species] NWQC–2157744
[Bazzania trilobata] WZYK–2089966
[Bazzania japonica] Bjaponica_DN36462_c0_g1_i1.p1
[Barbilophozia barbata] QFTV–2022278
[Scapania nemorosa] IRBN–2008572
[Scapania ornithopodioides] Sornithopodioides_DN110714_c0_g1_i22.p1
[Treubia lacunosa] Tlacunosa_DN40656_c0_g1_i7.p1
[Riccia cavernosa] Rcavernosa_DN99492_c0_g1_i1.p1
[Lunularia cruciata] Lc_composite_06758.1_fr0
[Marchantia polymorpha] Mp3g18320.1_CYP701D1 (MpKOL1)
[Marchantia paleacea] Marpal_utg000021g0055821
[Dumortiera hirsuta] Dhirsuta_DN85125_c0_g1_i5.p1
[Conocephalum conicum] Cconicum_DN27647_c0_g1_i1.p1
[Asterella wallichiana] Awallichiana_DN128192_c0_g2_i1.p1
[Monosolenium tenerum] Mtenerum_DN35869_c0_g3_i1.p1
[Riccia cavernosa] Rcavernosa_DN127261_c0_g1_i4.p1
[Pellia neesiana] JHFI–2112779
[Pellia endiviifolia] Pendiviifolia_DN74591_c0_g1_i1.p1
[Pallavicinia lyellii] YFGP–2018842
[Makinoa crispata] Mcrispata_DN27759_c0_g1_i2.p1
[Pleurozia purpurea] Ppurpurea_DN79278_c0_g1_i5.p1
[Calypogeia fissa] RTMU–2183714
[Calypogeia fissa] RTMU–2018598
[Mylia nuda] Mnuda_DN69635_c0_g1_i1.p1
[Metacalypogeia alternifolia] Malternifolia_DN92723_c0_g1_i1.p1
[Calypogeia fissa] RTMU–2182828
[Heteroscyphus zollingeri] Hzollingeri_DN218677_c0_g1_i1.p1
[Trichocolea tomentella] Ttomentella_DN19965_c0_g1_i1.p1
[Nowellia curvifolia] Ncurvifolia_DN147966_c0_g1_i1.p1
[Scapania ornithopodioides] Sornithopodioides_DN108544_c0_g1_i1.p1
[Plicanthus hirtellus] Phirtellus_DN47694_c0_g1_i7.p1
[Herbertus ramosus] Hramosus_DN74251_c0_g1_i1.p1
[Herbertus dicranus] Hdicranus_DN99674_c0_g1_i1.p1
[Sphagnum angustifolium] Sphfalx03G015200.1
[Sphagnum divinum] Sphmag03G012600.1
[Sphagnum angustifolium] Sphfalx03G014200.1|SphfalxU02700.1
[Sphagnum angustifolium] Sphfalx03G011800.1
[Sphagnum angustifolium] Sphfalx03G012100.1|Sphfalx03G013900.1
[Sphagnum angustifolium] Sphfalx03G014500.1
[Andreaea rupestris] WOSB–2094760
[Tetraphis pellucida] HVBO–2019591
[Encalypta streptocarpa] KEFD–2060497
[Physcomitrium patens] Pp3c20_800V3.1|Pp3c20_830V3.1_CYP701B1 (PpKO)
[Funaria hygrometrica] FH_9241
[Leucobryum glaucum] RGKI–2064970
[Ceratodon purpureus] CepurGG1.12G182600.1|CepurR40.12G179300.1
[Racomitrium elongatum] ABCD–2000175
[Racomitrium varium] RDQO–2119031
[Scouleria aquatica] BPSG–2009089
[Bryum argenteum] JMXW–2042690
[Orthotrichum lyellii] CMEQ–2006426
[Philonotis fontana] ORKS–2002210
[Philonotis fontana] ORKS–2002211|ORKS–2002212|ORKS–2002214
[Aulacomnium heterostichum] WNGH–2089474
[Stereodon subimponens] LNSF–2069205
[Pseudotaxiphyllum elegans] QKQO–2005184|QKQO–2005185
[Rhynchostegium serrulatum] JABL–2010889
[Fontinalis antipyretica] Foant_12925–RA
[Leucodon julaceus] IGUH–2167367
[Leucodon brachypus] ZACW–2000409
[Leiosporoceros dussii] ANON–2035499
[Paraphymatoceros hallii] FAJB–2054365
[Phaeomegaceros coriaceus] AKXB–2066174
[Anthoceros angustus] AANG004667
[Anthoceros punctatus] Apun_utg000143l.51.1
[Anthoceros agrestis] AagrOXF_utg000053l.18.1
[Anthoceros agrestis] AagrBONN_362.1098.1
[Paraphymatoceros hallii] FAJB–2000038
[Paraphymatoceros hallii] FAJB–2000037
[Paraphymatoceros hallii] FAJB–2000039
[Phaeoceros carolinianus] WEEQ–2014823
[Paraphymatoceros hallii] FAJB–2000035
[Phaeoceros carolinianus] WEEQ–2015086
[Phaeoceros carolinianus] RXEQ–2013192
[Phaeoceros carolinianus] WCZB–2008725|WCZB–2008726
[Phaeoceros carolinianus] ZFRE–2015560
[Azolla filiculoides] Azfi_s0113.g045986
[Marsilea vestita] Mvestita_S2812100–RA
[Marsilea vestita] Mvestita_S8904618–RA
[Salvinia cucullata] Sacu_v1.1_s0002.g000905
[Alsophila spinulosa] Aspi01Gene51405
[Alsophila spinulosa] Aspi01Gene51406
[Alsophila spinulosa] Aspi01Gene7973
[Ceratopteris richardii] Ceric.34G051400.1
[Adiantum capillus–veneris] Adc03778
[Adiantum capillus–veneris] Adc03782
[Lycopodium clavatum] EVM0006265.1
[Lycopodium clavatum] EVM0013107.1
[Isoetes taiwanese] Itaiw_v1_scaffold_4_t04344–RA_fr0
[Selaginella moellendorffii] Sm_74427
[Selaginella moellendorffii] Sm_424982
[Selaginella moellendorffii] Sm_421373
[Ginkgo biloba] Gbi_chr1.213
[Ginkgo biloba] Gbi_chr1.217
[Taxus chinensis] KAH9300019.1
[Torreya grandis] TG10g03246–mRNA1
[Torreya grandis] TG10g03245–mRNA1
[Torreya grandis] TG3g02947–mRNA1
[Torreya grandis] TG3g02946–mRNA1
[Torreya grandis] TG3g02945–mRNA1
[Torreya grandis] TG3g02948–mRNA1
[Torreya grandis] TG3g02943–mRNA1
[Sequoiadendron giganteum] SEGI_06034
[Sequoiadendron giganteum] SEGI_25804
[Sequoiadendron giganteum] SEGI_26040
[Sequoiadendron giganteum] SEGI_36411
[Taxus chinensis] KAH9300364.1
[Taxus chinensis] KAH9300326.1
[Taxus chinensis] KAH9291741.1
[Taxus chinensis] KAH9300332.1
[Taxus chinensis] KAH9307881.1
[Taxus chinensis] KAH9300328.1
[Taxus chinensis] KAH9291994.1|KAH9300327.1
[Sequoiadendron giganteum] SEGI_37043
[Ginkgo biloba] Gbi_chr4.302
[Ginkgo biloba] Gbi_chr1.82
[Ginkgo biloba] Gbi_chr6.514
[Gnetum montanum] TnS000842589t08
[Ginkgo biloba] Gbi_chr5.1171
[Ginkgo biloba] Gbi_chr5.1247
[Ginkgo biloba] Gbi_chr5.696
[Ginkgo biloba] Gbi_chr5.697
[Ginkgo biloba] Gbi_chr8.1873
[Ginkgo biloba] Gbi_chr5.947
[Picea abies] MA_94042g0010
[Torreya grandis] TG3g02880–mRNA1
[Torreya grandis] TG3g02881–mRNA1
[Taxus chinensis] KAH9301330.1
[Nymphaea colorata] Nycol.F00486.1
[Amborella trichopoda] AmTrH1.05G021500.1|AmTrH2.05G021400.1
[Amborella trichopoda] AmTrH1.05G067600.1
[Amborella trichopoda] AmTrH1.05G042400.1
[Amborella trichopoda] AmTrH2.05G041900.1
[Cinnamomum kanehirae] CKAN_00196800
[Liriodendron chinesis] Lchi03432
[Liriodendron chinesis] Lchi03433
[Brachypodium distachyon] Bradi1g37576.1
[Brachypodium distachyon] Bradi1g37560.1
[Brachypodium distachyon] Bradi1g37547.1
[Oryza sativa] LOC_Os06g37224.1_CYP701A9 (OsKOL5)
[Oryza sativa] LOC_Os06g37300.1_CYP701A8 (OsKOL4)
[Oryza sativa] LOC_Os06g37330.1_CYP701A19 (OsKOL3)
[Oryza sativa] LOC_Os06g37364.1_CYP701A6 (OsKO2)
[Populus trichocarpa] Potri.002G129700.1
[Arabidopsis thaliana] AT5G25900.1_CYP701A3 (AtKO1)
Clade
Moss
Liverwort
Hornwort
Lycophyte
Fern
Gymnosperm
Angiosperm
0.4

Supplemental Figure 8 Phylogenetic tree of KO homologs in land plants. Nodes were labelled with percentage support values from 1000 standard non-parametric bootstraps by IQ-TREE 2. Branch length represents the number of substitutions per site. *M. polymorpha* proteins of interest were indicated with red arrows. Related to Figure 4.

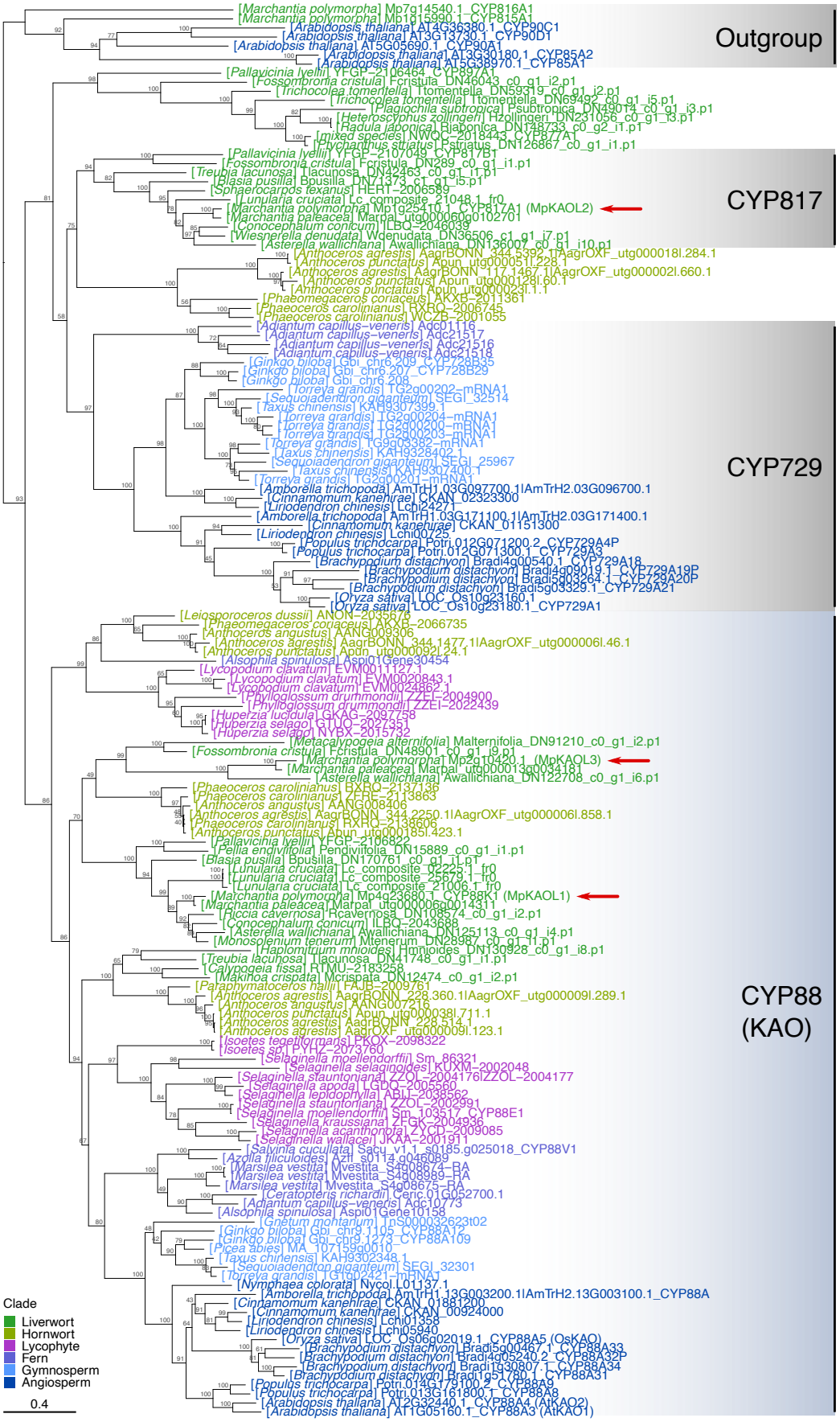
Outgroup
CYP817
CYP729
CYP88
(KAO)
Clade
Liverwort
Hornwort
Lycophyte
Fern
Gymnosperm
Angiosperm
0.4

Supplemental Figure 9 Phylogenetic tree of KAO and closely-related P450 enzymes in land plants. Nodes were labelled with percentage support values from 1000 standard non-parametric bootstraps by IQ-TREE 2. Branch length represents the number of substitutions per site. *M. polymorpha* genes of interest were indicated with red arrows. Related to Figure 4.

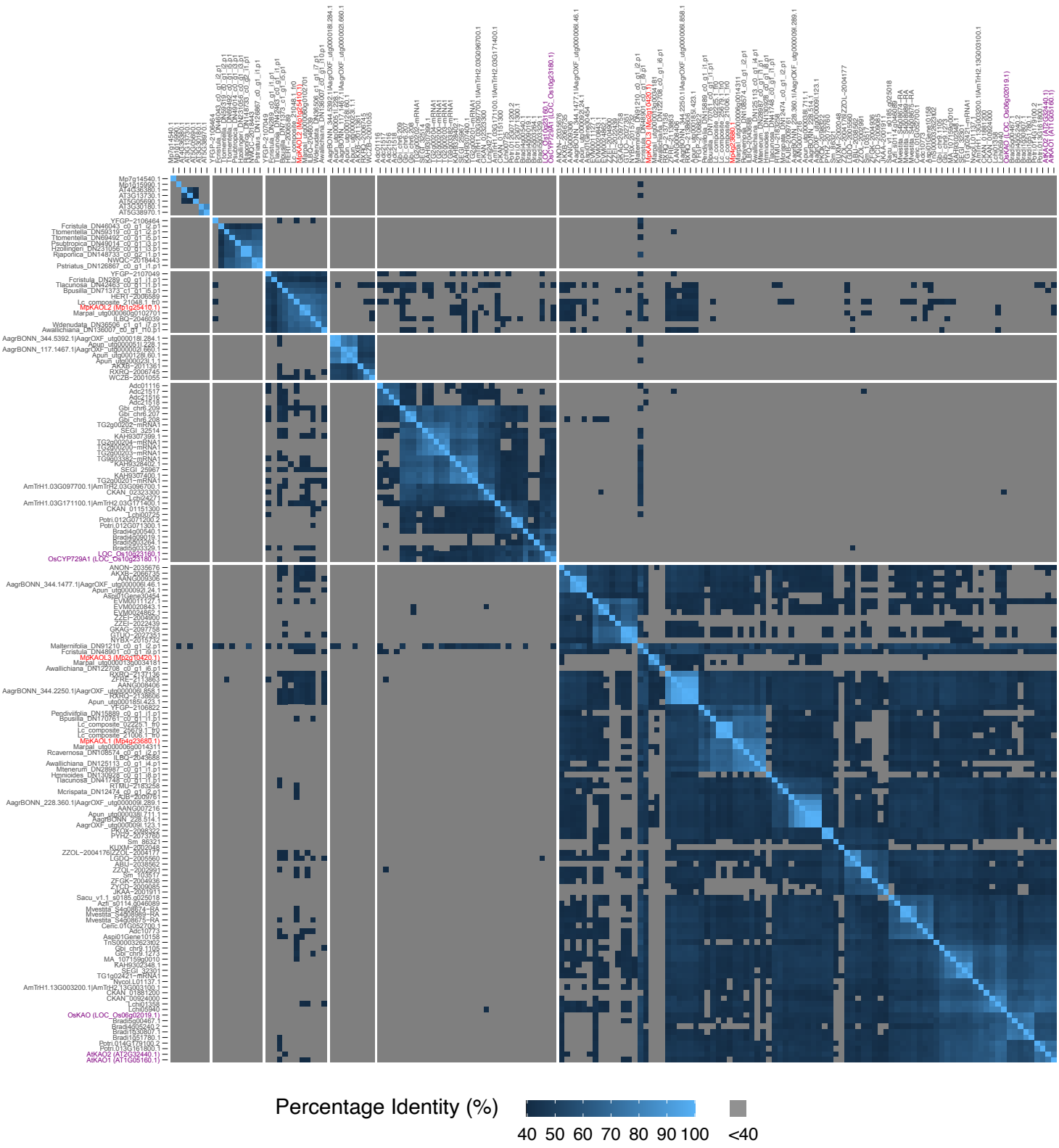

Supplemental Figure 10 Heatmap of percentage identity for KAO and closely-related CYP enzymes in land plants. Sequences shown in Supplemental Figure 9 were included in the analysis, and percentage identities were calculated by local alignment using BLAST. An arbitrary threshold of 40% was set for the visualization of protein identities, as it is the threshold for defining membership in a CYP family (Nelson, 2006). MpKAOL2 and its liverwort homologs showed limited similarity to CYP729 or

bona fide KAO (CYP88) family members. *M. polymorpha* genes of interest were colored in red, and their closely-related genes from *A. thaliana* or *O. sativa* were colored in purple. Related to Figure 4.

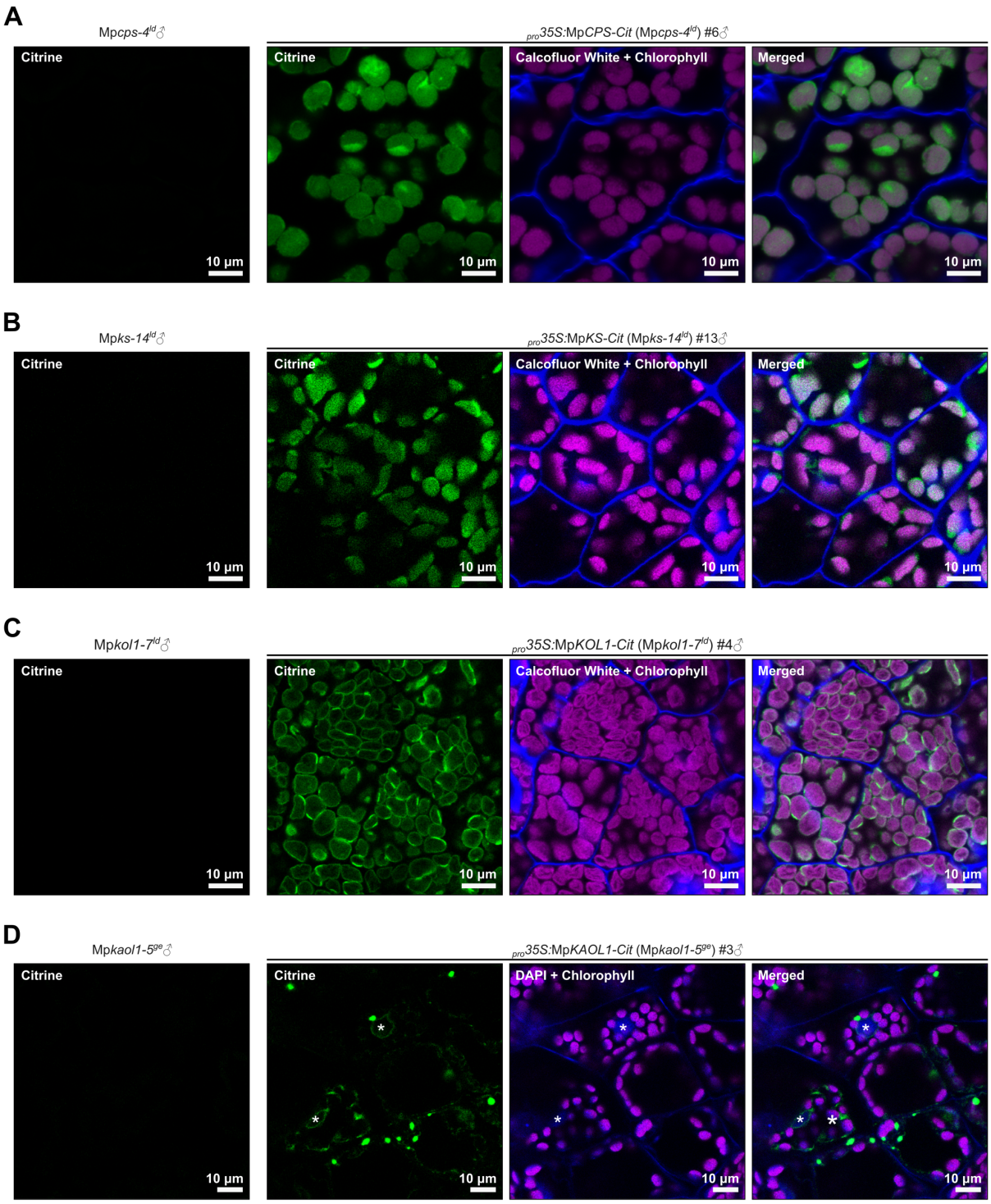

Supplemental Figure 11 Subcellular localization of GA biosynthesis enzymes in *M. polymorpha*. Representative images were taken from 7-day-old plants cultured under cW+cFR, fixed and stained with calcofluor white (A-C) or DAPI (D) to visualize the cell wall or the cell nuclei, respectively (shown in blue). Citrine signals were shown in green, and the autofluorescence of chlorophyll was shown in magenta. Asterisks (*) in D indicate the positions of cell nuclei. For each plant material, at least three different individuals were observed to confirm the protein localization patterns. Related to Figure 4.

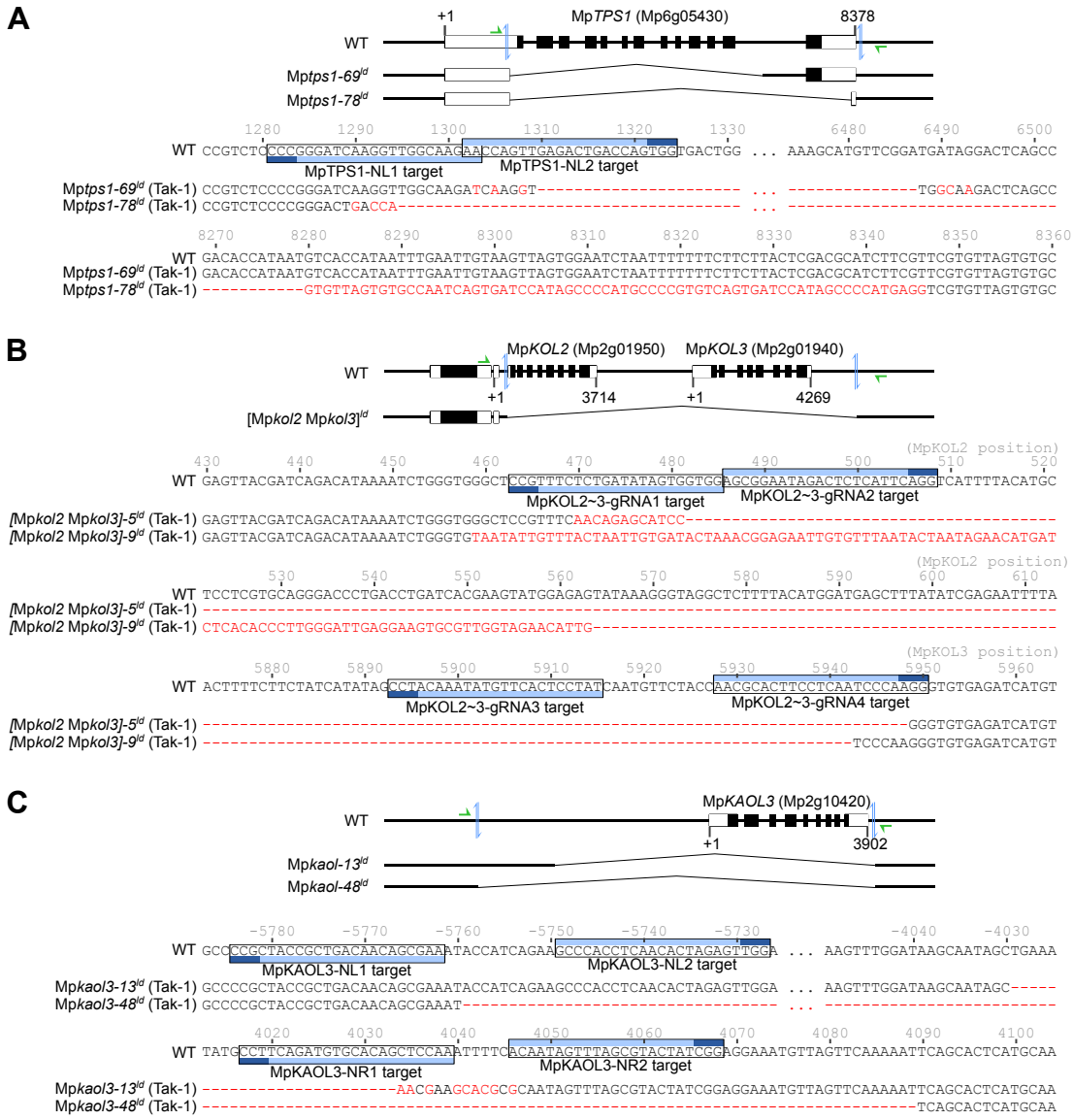

Supplemental Figure 12 Genotype information for Mp*tps1*^{ld}, [Mp*kol2* Mp*kol3*]^{ld} and Mp*kaol3*^{ld} mutants. WT refers to reference sequences from MpTak_v6.1 genome assembly. In the schematic presentations of genomic structures, white and black rectangles represent untranslated and coding regions of exons, respectively. Targets of guide RNAs are indicated by blue arrows in the scheme and frames in the sequence (dark blue: the protospacer adjacent motif). Green arrows indicate the binding sites of genotyping primers. Indels and substitutions are shown in red letters. Numbers above the sequences indicate positions relative to the transcription start sites (+1). Related to Figure 4.

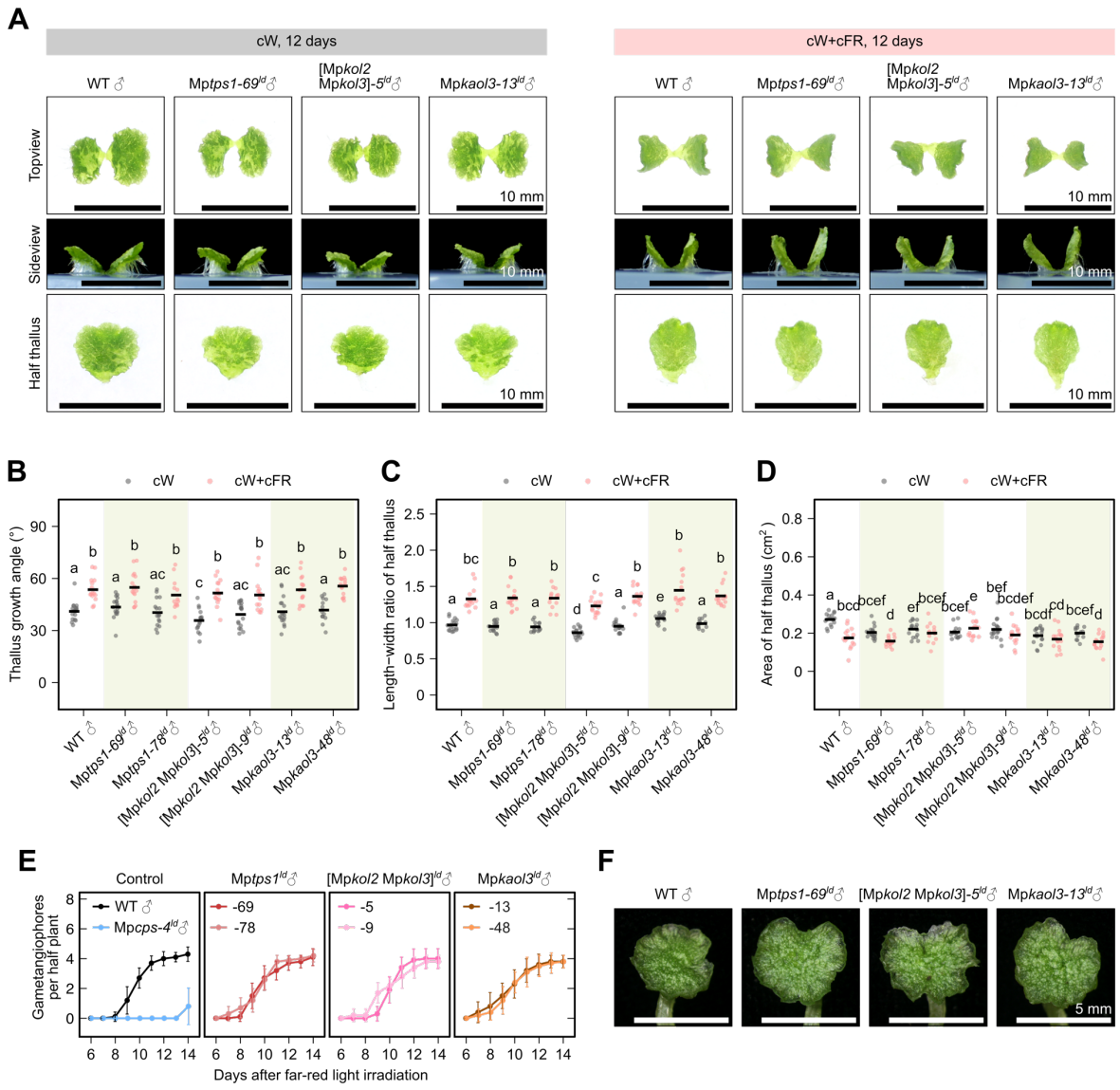

Supplemental Figure 13 Phenotypes of Mp*tps1*^{ld}, [Mp*kol2* Mp*kol3*]^{ld} and Mp*kaol3*^{ld} mutants. A-D, Morphology (A) and measurements (B-D) of 12-day-old thalli grown from gemmae under cW or cW+cFR. Each dot represent data from a "half thallus" developed from one apical meristem of the gemma. Horizontal lines represent mean values, and letters represent multiple comparisons with two-sided, non-pooled Welch's *t*-test and B-H adjustment (adjusted p<0.05 for non-overlapping letters, n=11-18). E-F, Gametangiophore formation progress (E) and morphology (F) of mutants, grown under cW for 7 days before transferred to cW+cFR in aseptic culture. Dots and error bars represent mean±SD in H (n=5). Bars = 5 mm in F. Related to Figure 4.

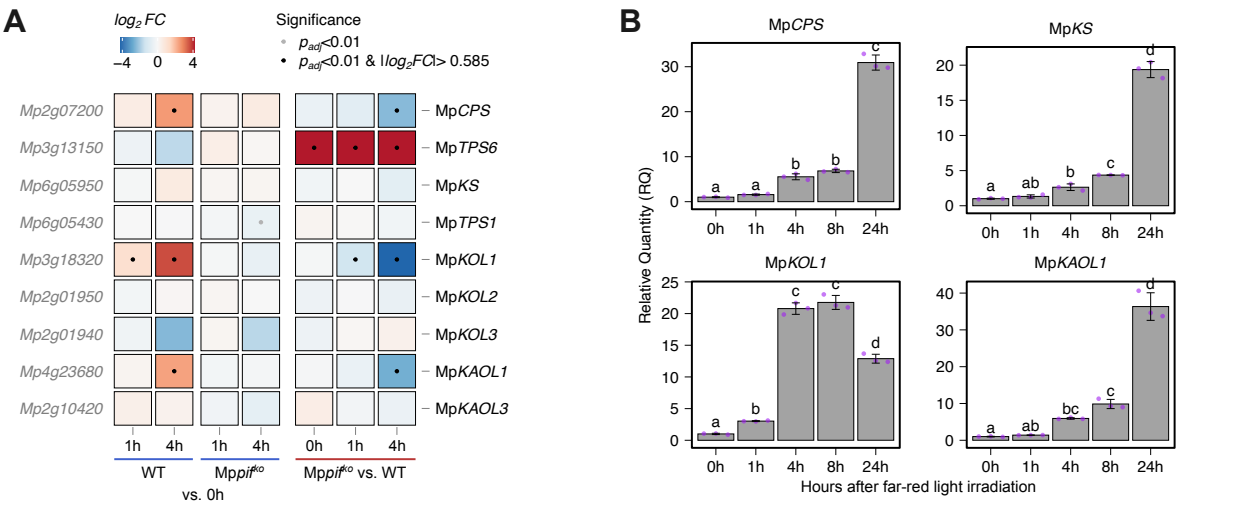

Supplemental Figure 14 Up-regulation of GA biosynthesis genes by FR irradiation. A, Heatmap of gene expression changes after FR irradiation, using data from (Hernández-García et al., 2021). The transcriptomes were sequenced from plants cultured under continuous red light for 7 days, then irradiated with FR light for 0, 1 or 4 hours. FC, fold change. p_{adj}, adjusted *p*-value. B, Relative expression level of GA biosynthesis genes in Tak-1 wild-type plants, quantified by qPCR from plants cultured under cW for 7 days and then transferred to cW+cFR for indicated hours. The plots represent mean±SD from 3 biological replicates. Related to Figure 5.

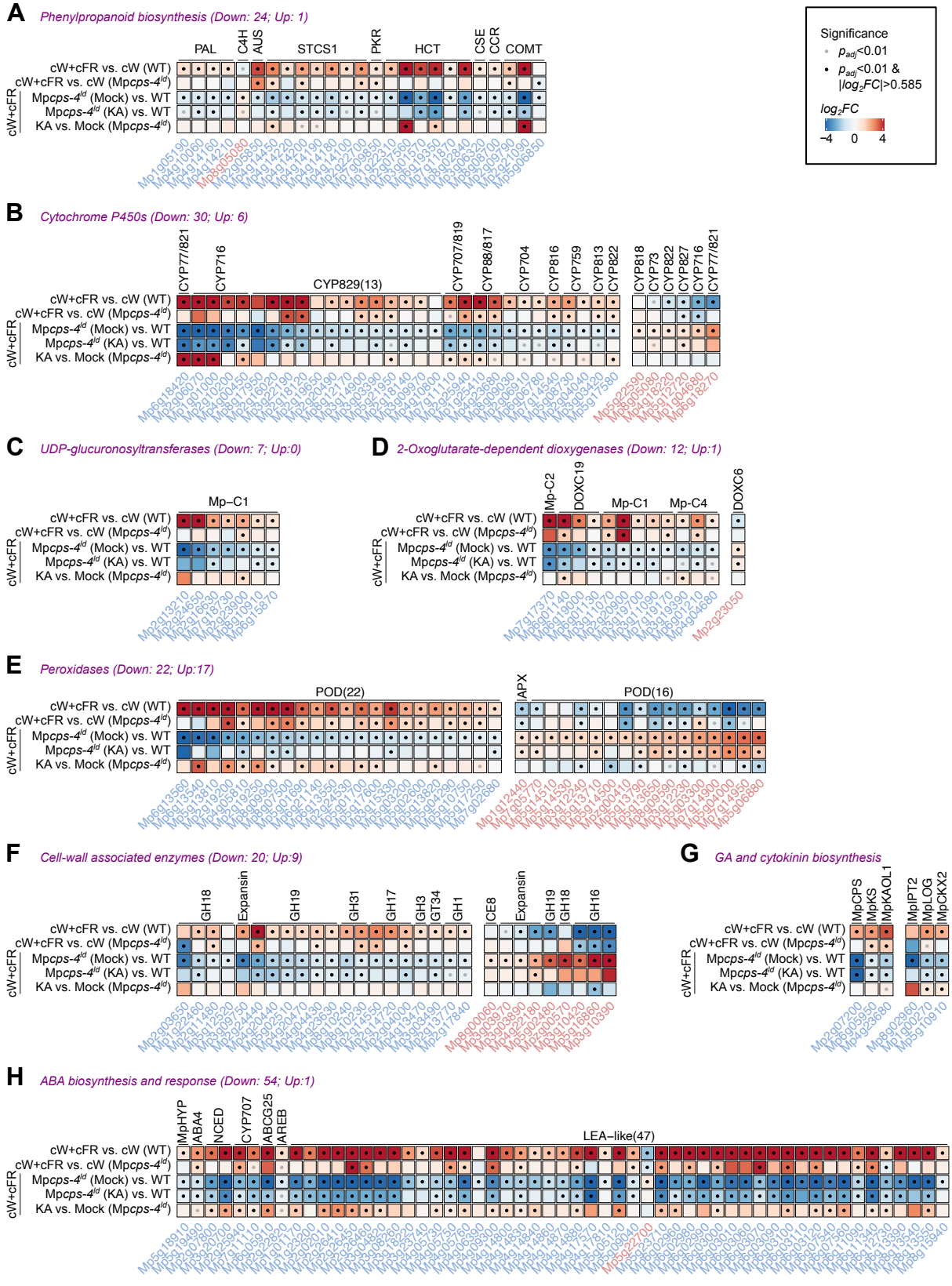

Supplemental Figure 15 Heatmaps of genes from selected pathways or gene families, showing differential expression in Mp*cps-4*^{ld} under cW+cFR. FC, fold change. p_{adj}, adjusted *p*-value. Related to Figure 5.

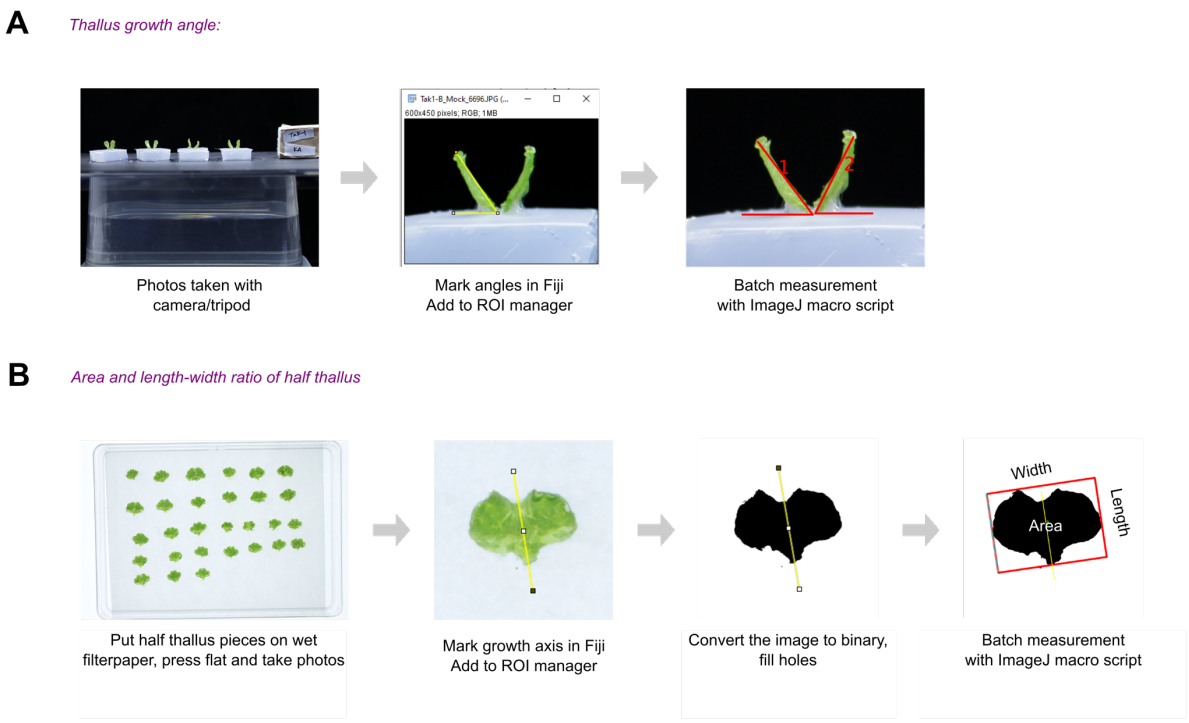

Supplemental Figure 16 Quantification method for thallus morphology. A, For the measurement of growth angles, blocks of agar medium with plants were cut out and aligned at certain distance to a fixed camera. After photos were taken from the side view, angles between the thallus and the medium surface were measured for each half thallus with Fiji/ImageJ. B, For the measurement of thallus area and length-width ratio, photos were taken from the top for half thalli flattened on a filter paper. A growth axis was defined manually for each half-thallus, pointing from the basal end to the first bifurcation point. A minimum bounding rectangle was created around the thallus along the direction of the growth axis, and the edges of this rectangle defined the length and width of the thallus. Related to methods.

Supplemental Table 1 List of plant materials

Name	Genetic background	Sex	Vector for construction	Source
Tak-1	-	Male	-	(Ishizaki et al., 2016)
Tak-2	-	Female	-	(Ishizaki et al., 2016)
Mp*cps-4*^{ld}	Tak-1	Male	pMpGE017-MpCPS-LD	This paper
Mp*cps-27*^{ld}	Tak-1	Male	pMpGE017-MpCPS-LD	This paper
$_{pro}$*35S*:Mp*CPS-Cit* (Mp*cps-4*^{ld}) #6	Mp*cps-4*^{ld}	Male	pMpGWB306-MpCPS-CDS	This paper
$_{pro}$*35S*:Mp*CPS-Cit* (Mp*cps-4*^{ld}) #7	Mp*cps-4*^{ld}	Male	pMpGWB306-MpCPS-CDS	This paper
Mp*cps-120*^{ld}	Tak-2	Female	pMpGE017-MpCPS-LD	This paper
Mp*cps-123*^{ld}	Tak-2	Female	pMpGE017-MpCPS-LD	This paper
$_{pro}$*35S*:Mp*CPS-Cit* (Mp*cps-120*^{ld}) #2	Mp*cps-120*^{ld}	Female	pMpGWB306-MpCPS-CDS	This paper
$_{pro}$*35S*:Mp*CPS-Cit* (Mp*cps-120*^{ld}) #6	Mp*cps-120*^{ld}	Female	pMpGWB306-MpCPS-CDS	This paper
Mp*cps-5*^{ld} (Mp*BNB-Cit* ♂)	Mp*BNB-Cit* ♂	Male	pMpGE018-MpCPS-LD	(Yamaoka et al., 2018)
Mp*cps-6*^{ld} (Mp*BNB-Cit* ♂)	Mp*BNB-Cit* ♂	Male	pMpGE018-MpCPS-LD	(Yamaoka et al., 2018)
Mp*cps-2*^{ld} (Mp*BNB-Cit* ♀)	Mp*BNB-Cit* ♀	Female	pMpGE018-MpCPS-LD	(Yamaoka et al., 2018)
Mp*cps-3*^{ld} (Mp*BNB-Cit* ♀)	Mp*BNB-Cit* ♀	Female	pMpGE018-MpCPS-LD	(Yamaoka et al., 2018)
Mp*ks-14*^{ld}	Tak-1	Male	pMpGE018-MpKS-LD	This paper
Mp*ks-19*^{ld}	Tak-1	Male	pMpGE018-MpKS-LD	This paper
$_{pro}$*35S*:Mp*KS-Cit* (Mp*ks-14*^{ld}) #13	Mp*ks-14*^{ld}	Male	pMpGWB106-MpKS-CDS	This paper
$_{pro}$*35S*:Mp*KS-Cit* (Mp*ks-14*^{ld}) #14	Mp*ks-14*^{ld}	Male	pMpGWB106-MpKS-CDS	This paper
Mp*kol1-7*^{ld}	Tak-1	Male	pMpGE018-MpKOL1-LD	This paper
Mp*kol1-13*^{ld}	Tak-1	Male	pMpGE018-MpKOL1-LD	This paper
$_{pro}$*35S*:Mp*KOL1-Cit* (Mp*kol1-7*^{ld}) #2	Mp*kol1-7*^{ld}	Male	pMpGWB106-MpKOL1-CDS	This paper
$_{pro}$*35S*:Mp*KOL1-Cit* (Mp*kol1-7*^{ld}) #4	Mp*kol1-7*^{ld}	Male	pMpGWB106-MpKOL1-CDS	This paper
Mp*kaol1-5*^{ge}	Tak-1	Male	pMpGE011-MpKAOL1-gRNA1	This paper
Mp*kaol1-7*^{ge}	Tak-1	Male	pMpGE011-MpKAOL1-gRNA1	This paper
$_{pro}$*35S*:Mp*KAOL1*^{mut}*-Cit* (Mp*kaol1-5*^{ge}) #3	Mp*kaol1-5*^{ge}	Male	pMpGWB106-MpKAOL1-CDSmut	This paper
$_{pro}$*35S*:Mp*KAOL1*^{mut}*-Cit* (Mp*kaol1-5*^{ge}) #4	Mp*kaol1-5*^{ge}	Male	pMpGWB106-MpKAOL1-CDSmut	This paper
Mp*tps1-69*^{ld}	Tak-1	Male	pMpGE018-MpTPS1-LD	This paper
Mp*tps1-78*^{ld}	Tak-1	Male	pMpGE018-MpTPS1-LD	This paper
*[*Mp*kol2* Mp*kol3]-5*^{ld}	Tak-1	Male	pMpGE018-MpKOL2/3-LD	This paper
*[*Mp*kol2* Mp*kol3]-9*^{ld}	Tak-1	Male	pMpGE018-MpKOL2/3-LD	This paper
Mp*kaol3-13*^{ld}	Tak-1	Male	pMpGE018-MpKAOL3-LD	This paper
Mp*kaol3-48*^{ld}	Tak-1	Male	pMpGE018-MpKAOL3-LD	This paper
Mp*pif*^{ko} #1	Tak-1×Tak-2 F1	Female	-	(Inoue et al., 2016)
*g*Mp*PIF*/Mp*pif*^{ko} #1	Mp*pif*^{ko} #1	Female	-	(Inoue et al., 2016)

Supplemental Table 2 List of plasmids

Name	Source	Identifier
pMpGE_En04	(Hisanaga et al., 2019)	-
pBCGE12	(Hisanaga et al., 2019)	-
pBCGE23	(Hisanaga et al., 2019)	-
pBCGE34	(Hisanaga et al., 2019)	-
pMpGE017	(Hisanaga et al., 2019)	-
pMpGE018	(Hisanaga et al., 2019)	-
pMpGE_En04-MpCPS-NL1	This paper	-
pBCGE12-MpCPS-NL2	This paper	-
pBCGE23-MpCPS-NR1	This paper	-
pBCGE34-MpCPS-NR2	This paper	-
pMpGE_En04-MpCPS-LD	This paper	-
pMpGE017-MpCPS-LD	This paper	-
pMpGE018-MpCPS-LD	This paper	-
pENTR/D-TOPO	Thermo Fisher	Cat#K240020
pENTR-MpCPS-CDS	This paper	-
pMpGWB306	(Ishizaki et al., 2015)	Addgene #68637
pMpGWB306-MpCPS-CDS	This paper	-
pMpGE_En04-MpKS-NL1	This paper	-
pBCGE12-MpKS-NL2	This paper	-
pBCGE23-MpKS-NR1	This paper	-
pBCGE34-MpKS-NR2	This paper	-
pMpGE_En04-MpKS-LD	This paper	-
pMpGE018-MpKS-LD	This paper	-
pENTR-MpKS-CDS	This paper	-
pMpGWB106	(Ishizaki et al., 2015)	Addgene #68560
pMpGWB106-MpKS-CDS	This paper	-
pMpGE_En04-MpKOL1-gRNA1	This paper	-
pBCGE12-MpKOL1-gRNA2	This paper	-
pBCGE23-MpKOL1-gRNA3	This paper	-
pBCGE34-MpKOL1-gRNA4	This paper	-
pMpGE_En04-MpKOL1-gRNA1~4	This paper	-
pMpGE018-MpKOL1-gRNA1~4	This paper	-
pENTR-MpKOL1-CDS-NoStop	This paper	-
pMpGWB106-MpKOL1-CDS	This paper	-
pMpGE_En03	(Sugano et al., 2018)	Addgene #71535
pMpGE011	(Sugano et al., 2018)	Addgene #71537
pMpGE_En03-MpKAOL1-gRNA1	This paper	-
pMpGE011-MpKAOL1-gRNA1	This paper	-
pENTR-MpKAOL1-CDS-NoStop	This paper	-
pENTR-MpKAOL1-CDSmut-NoStop	This paper	-
pMpGWB106-MpKAOL1-CDSmut	This paper	-
pMpGE_En04-MpTPS1-NL1	This paper	-
pBCGE12-MpTPS1-NL2	This paper	-
pBCGE23-MpTPS1-NR1	This paper	-
pBCGE34-MpTPS1-NR2	This paper	-
pMpGE_En04-MpTPS1-LD	This paper	-
pMpGE018-MpTPS1-LD	This paper	-
pMpGE_En04-MpKOL2/3-gRNA1	This paper	-
pBCGE12-MpKOL2/3-gRNA2	This paper	-
pBCGE23-MpKOL2/3-gRNA3	This paper	-
pBCGE34-MpKOL2/3-gRNA4	This paper	-
pMpGE_En04-MpKOL2/3-LD	This paper	-
pMpGE018-MpKOL2/3-LD	This paper	-
pMpGE_En04-MpKAOL3-NL1	This paper	-
pBCGE12-MpKAOL3-NL2	This paper	-
pBCGE23-MpKAOL3-NR1	This paper	-
pBCGE34-MpKAOL3-NR2	This paper	-
pMpGE_En04-MpKAOL3-LD	This paper	-

pMpGE017-MpKAOL3-LD	This paper	-
pPICZA	Thermo Fisher	Cat #V19020
pPICZA-AtKO	This paper	-
pPICZA-MpKOL1	This paper	-
pPICZA-MpKOL2	This paper	-
pPICZA-MpKOL3	This paper	-
pPICZA-AtKAO1	This paper	-
pPICZA-MpKAOL1	This paper	-
pPICZA-MpKAOL3	This paper	-

Supplemental Table 3 List of DNA oligos

Name	Sequence (5′→3′)	Used for
MpCPS-NL1-OligoA	CTCGATCAACCTTACGAACCGGAC	pMpGE_En04-MpCPS-NL1
MpCPS-NL1-OligoB	AAACGTCCGGTTCGTAAGGTTGAT	pMpGE_En04-MpCPS-NL1
MpCPS-NL2-OligoA	CTCGGATAACTGCCACAGCGAAGC	pBCGE12-MpCPS-NL2
MpCPS-NL2-OligoB	AAACGCTTCGCTGTGGCAGTTATC	pBCGE12-MpCPS-NL2
MpCPS-NR1-OligoA	CTCGTTCGGGTACAAGGGTTTGGA	pBCGE23-MpCPS-NR1
MpCPS-NR1-OligoB	AAACTCCAAACCCTTGTACCCGAA	pBCGE23-MpCPS-NR1
MpCPS-NR2-OligoA	CTCGGAATGTCTAGTACGGAGCTT	pBCGE34-MpCPS-NR2
MpCPS-NR2-OligoB	AAACAAGCTCCGTACTAGACATTC	pBCGE34-MpCPS-NR2
MpCPS-gt-F	GGAACCTATCCGGGGATCCT	Genotyping of Mp*cps*^{ld}
MpCPS-gt-R	ATGTGACGTTCGTTTGCTGC	Genotyping of Mp*cps*^{ld}
CACC-MpCPS-CDS-F	CACCATGGCATTCTCGTTAGCAGGT	pENTR-MpCPS-CDS
MpCPS-CDS-R	GGCCACAGGCTCGAAGAGTA	pENTR-MpCPS-CDS
MpKS-NL1-OligoA	CTCGTGTGGAACATAGAGTCTTGC	pMpGE_En04-MpKS-NL1
MpKS-NL1-OligoB	AAACGCAAGACTCTATGTTCCACA	pMpGE_En04-MpKS-NL1
MpKS-NL2-OligoA	CTCGTCCACAGAGTCTTGTTCGTC	pBCGE12-MpKS-NL2
MpKS-NL2-OligoB	AAACGACGAACAAGACTCTGTGGA	pBCGE12-MpKS-NL2
MpKS-NR1-OligoA	CTCGTGCTTGCTGTCCTGATGTCC	pBCGE23-MpKS-NR1
MpKS-NR1-OligoB	AAACGGACATCAGGACAGCAAGCA	pBCGE23-MpKS-NR1
MpKS-NR2-OligoA	CTCGCAAGCATACGTCCGCCACTA	pBCGE34-MpKS-NR2
MpKS-NR2-OligoB	AAACTAGTGGCGGACGTATGCTTG	pBCGE34-MpKS-NR2
MpKS-gt-F	ACTGTGAGCTGAAACTGCAGA	Genotyping of Mp*ks*^{ld}
MpKS-gt-R	GGACGGACATGGATCTAGCA	Genotyping of Mp*ks*^{ld}
CACC-MpTPS4-CDS-F	CACCATGATGATCCATCCAGCTATTGTG	pENTR-MpKS-CDS
MpTPS4-CDS-R	GGCCTGTTCACTTTCGATGG	pENTR-MpKS-CDS
Mapoly0140s0010-gRNA1-F	CTCGGATCATGGCTTTTCTCCCGC	pMpGE_En04-MpKOL1-gRNA1
Mapoly0140s0010-gRNA1-R	AAACGCGGGAGAAAAGCCATGATC	pMpGE_En04-MpKOL1-gRNA1
Mapoly0140s0010-gRNA2-F	CTCGGATGCTCGCTCCATAAAAAC	pBCGE12-MpKOL1-gRNA2
Mapoly0140s0010-gRNA2-R	AAACGTTTTTATGGAGCGAGCATC	pBCGE12-MpKOL1-gRNA2
Mapoly0140s0010-gRNA3-F	CTCGATCCGACAAATAATGTTTGT	pBCGE23-MpKOL1-gRNA3
Mapoly0140s0010-gRNA3-R	AAACACAAACATTATTTGTCGGAT	pBCGE23-MpKOL1-gRNA3
Mapoly0140s0010-gRNA4-F	CTCGGTTCAGTTTAGAAACCCTCC	pBCGE34-MpKOL1-gRNA4
Mapoly0140s0010-gRNA4-R	AAACGGAGGGTTTCTAAACTGAAC	pBCGE34-MpKOL1-gRNA4
Dseq-KOL1-gRNA1~4F	GGATTGATGTACTTGACGAG	Genotyping of Mp*kol1*^{ld}
Dseq-KOL1-gRNA1~4R	TTCGGCCTGAAGTCTAAGAG	Genotyping of Mp*kol1*^{ld}
CACC-MpKOL1-CDS-F	CACCATGAAATGCTTCGGTTTG	pENTR-MpKOL1-CDS
MpKOL1-CDS-ns-R	AATCTTCGCTGGACAG	pENTR-MpKOL1-CDS
MpKAO-gRNA1F	CTCGCCAGGCTCCTCTCCCCCC	pMpGE_En03-MpKAOL1-gRNA1
MpKAO-gRNA1R	AAACGGGGGGAGAGGAGCCTGG	pMpGE_En03-MpKAOL1-gRNA1
MpKAO-Dseq1-F	GAGGCATTGAGATCGAGAGG	Genotyping of Mp*kaol1*^{ge}
MpKAO-Dseq1-R	ATACTCTCGGCGGTCGTTGC	Genotyping of Mp*kaol1*^{ge}
Mapoly0020s0131-F	CACCATGTTGGAGATTTCGTCCAC	pENTR-MpKAOL1-CDS-NoStop
MpKAOL1-CDS-ns-R	CAATCGTGAGAAGTTTATAAGACAG	pENTR-MpKAOL1-CDS-NoStop
MpKAOL1-mut-F	GCTGCCGCCGGGAGACATGGGCTGG	pENTR-MpKAOL1-CDSmut-NoStop
MpKAOL1-mut-R	GGTGCTTGCCCTTTCTGAAGACTGGG	pENTR-MpKAOL1-CDSmut-NoStop
MpTPS1-NL1-OligoA	CTCGGTTCTTGCCAACCTTGATCC	pMpGE_En04-MpTPS1-NL1
MpTPS1-NL1-OligoB	AAACGGATCAAGGTTGGCAAGAAC	pMpGE_En04-MpTPS1-NL1
MpTPS1-NL2-OligoA	CTCGAACCAGTTGAGACTGACCAG	pBCGE12-MpTPS1-NL2
MpTPS1-NL2-OligoB	AAACCTGGTCAGTCTCAACTGGTT	pBCGE12-MpTPS1-NL2
MpTPS1-NR1-OligoA	CTCGACGTGACTGTGTTGAGTCTA	pBCGE23-MpTPS1-NR1
MpTPS1-NR1-OligoB	AAACTAGACTCAACACAGTCACGT	pBCGE23-MpTPS1-NR1
MpTPS1-NR2-OligoA	CTCGCAGTCACGTCACTACGAGAC	pBCGE34-MpTPS1-NR2
MpTPS1-NR2-OligoB	AAACGTCTCGTAGTGACGTGACTG	pBCGE34-MpTPS1-NR2
MpTPS1-gt-F	GGCCTCTCGTAGCTTTGA	Genotyping of Mp*tps1*^{ld}
MpTPS1-gt-R	CAGGAAGGTTTGCTTGCA	Genotyping of Mp*tps1*^{ld}
Mapoly0130s0002-0003-gRNA1-F	CTCGCCACCACTATATCAGAGAAA	pMpGE_En04-MpKOL2/3-gRNA1
Mapoly0130s0002-0003-gRNA1-R	AAACTTTCTCTGATATAGTGGTGG	pMpGE_En04-MpKOL2/3-gRNA1
Mapoly0130s0002-0003-gRNA2-F	CTCGAGCGGAATAGACTCTCATTC	pBCGE12-MpKOL2/3-gRNA2
Mapoly0130s0002-0003-gRNA2-R	AAACGAATGAGAGTCTATTCCGCT	pBCGE12-MpKOL2/3-gRNA2

Mapoly0130s0002-0003-gRNA3-F	CTCGATAGGAGTGAACATATTTGT	pBCGE23-MpKOL2/3-gRNA3
Mapoly0130s0002-0003-gRNA3-R	AAACACAAATATGTTCACTCCTAT	pBCGE23-MpKOL2/3-gRNA3
Mapoly0130s0002-0003-gRNA4-F	CTCGAACGCACTTCCTCAATCCCA	pBCGE34-MpKOL2/3-gRNA4
Mapoly0130s0002-0003-gRNA4-R	AAACTGGGATTGAGGAAGTGCGTT	pBCGE34-MpKOL2/3-gRNA4
Dseq-KOL2-3_gRNA1~4F	CTCCAAGTGTTGTGTAGCTG	Genotyping of *[Mpkol2 Mpkol3]*^{ld}
Dseq-KOL2-3_gRNA1~4R	CTCTTAGCAGATGTGACCAC	Genotyping of *[Mpkol2 Mpkol3]*^{ld}
MpKAOL3-NL1-OligoA	CTCGTTCGCTGTTGTCAGCGGTAG	pMpGE_En04-MpKAOL3-NL1
MpKAOL3-NL1-OligoB	AAACCTACCGCTGACAACAGCGAA	pMpGE_En04-MpKAOL3-NL1
MpKAOL3-NL2-OligoA	CTCGGCCCACCTCAACACTAGAGT	pBCGE12-MpKAOL3-NL2
MpKAOL3-NL2-OligoB	AAACACTCTAGTGTTGAGGTGGGC	pBCGE12-MpKAOL3-NL2
MpKAOL3-NR1-OligoA	CTCGTTGGAGCTGTGCACATCTGA	pBCGE23-MpKAOL3-NR1
MpKAOL3-NR1-OligoB	AAACTCAGATGTGCACAGCTCCAA	pBCGE23-MpKAOL3-NR1
MpKAOL3-NR2-OligoA	CTCGACAATAGTTTAGCGTACTAT	pBCGE34-MpKAOL3-NR2
MpKAOL3-NR2-OligoB	AAACATAGTACGCTAAACTATTGT	pBCGE34-MpKAOL3-NR2
MpKAOL3-gt-F	GGCACACACGAGACTCCC	Genotyping of Mp*kaol3*^{ld}
MpKAOL3-gt-R	TCGCGAGGAGTAGGCTTT	Genotyping of Mp*kaol3*^{ld}
pPICZA-AtKO-IF-F	ATTCGAAACGAGGAA ATGGCCTTCTTCTCCATGA	pPICZA-AtKO
pPICZA-AtKO-IF-R	CCCAAGCTGGCGGCC AGAACGCCTTGGATTGAT	pPICZA-AtKO
pPICZA-MpKOL1-IF-F	ATTCGAAACGAGGAA ATGAAATGCTTCGGTTTGTC	pPICZA-MpKOL1
pPICZA-MpKOL1-IF-R	CCCAAGCTGGCGGCC AATCTTCGCTGGACAG	pPICZA-MpKOL1
pPICZA-MpKOL2-IF-F	ATTCGAAACGAGGAA ATGACCAGACACTTGGGTGA	pPICZA-MpKOL2
pPICZA-MpKOL2-IF-R	CCCAAGCTGGCGGCC AGCTGGCAAAATATTTTTCA	pPICZA-MpKOL2
pPICZA-MpKOL3-IF-F	ATTCGAAACGAGGAA ATGGAGAGTACAGAGAAATC	pPICZA-MpKOL3
pPICZA-MpKOL3-IF-R	CCCAAGCTGGCGGCC AGATGGCAGAACACCTTTGA	pPICZA-MpKOL3
pPICZA-AtKAO1-IF-F	ATTCGAAACGAGGAA ATGGCGGAGACAACGAGTTG	pPICZA-AtKAO1
pPICZA-AtKAO1-IF-R	CCCAAGCTGGCGGCC CTGATAACTAATTCTTGCCA	pPICZA-AtKAO1
pPICZA-MpKAOL1-IF-F	ATTCGAAACGAGGAA ATGTTGGAGATTTCGTCCAC	pPICZA-MpKAOL1
pPICZA-MpKAOL1-IF-R	CCCAAGCTGGCGGCC CAATCGTGAGAAGTTTATAA	pPICZA-MpKAOL1
pPICZA-MpKAOL3-IF-F	ATTCGAAACGAGGAA ATGGCTGCGATTGTTCTCA	pPICZA-MpKAOL3
pPICZA-MpKAOL3-IF-R	CCCAAGCTGGCGGCC GCTGCACACACGACGAGT	pPICZA-MpKAOL3
MpEF1−qPCR_F	AAGCCGTCGAAAAGAAGGAG	qPCR for MpEF1 (reference)
MpEF1−qPCR_R	TTCAGGATCGTCCGTTATCC	qPCR for MpEF1 (reference)
MpCPSKS_qPCR-F	TCTTACACGGTTCTCGGGATG	qPCR for MpCPS
MpCPSKS_qPCR-R	GGATTGCGTTTTGAGGAAGATG	qPCR for MpCPS
MpKS-RT-F	CAAGCAAGGATAGCAATCCAG	qPCR for MpKS
MpKS-RT-R	TCGCATCATTCCCAACCAG	qPCR for MpKS
MpKO_qPCR-F1	TGCAGCACTTCGAGTTGACC	qPCR for MpKOL1
MpKO_qPCR-R1	TGCAGTTTGTGGGAGGTGAC	qPCR for MpKOL1
MpKAO_qPCR-F1	GCCCTATGCGTTCAAACCTG	qPCR for MpKAOL1
MpKAO_qPCR-R1	GCTCGATGCCGATACAACTC	qPCR for MpKAOL1

Red letters indicate adapter sequences, and start codons are indicated with underline.

Supplemental References

Albone, K.S., Gaskin, P., MacMillan, J., Phinney, B.O., and Willis, C.L. (1990). Biosynthetic Origin of Gibberellins A_3 and A_7 in Cell-Free Preparations from Seeds of *Marah macrocarpus* and *Malus domestica*. Plant Physiol. **94**: 132–142.

Fujioka, S., Yamane, H., Spray, C.R., Phinney, B.O., Gaskin, P., MacMillan, J., and Takahashi, N. (1990). Gibberellin A_3 Is Biosynthesized from Gibberellin A_{20} via Gibberellin A_5 in Shoots of *Zea mays* L. Plant Physiol. **94**: 127–131.

Hernández-García, J., Sun, R., Serrano-Mislata, A., Inoue, K., Vargas-Chávez, C., Esteve-Bruna, D., Arbona, V., Yamaoka, S., Nishihama, R., Kohchi, T., and Blázquez, M.A. (2021). Coordination between growth and stress responses by DELLA in the liverwort *Marchantia polymorpha*. Current Biology.

Hisanaga, T., Okahashi, K., Yamaoka, S., Kajiwara, T., Nishihama, R., Shimamura, M., Yamato, K.T., Bowman, J.L., Kohchi, T., and Nakajima, K. (2019). A *cis*-acting bidirectional transcription switch controls sexual dimorphism in the liverwort. The EMBO Journal **38**: 1–12.

Inoue, K., Nishihama, R., Kataoka, H., Hosaka, M., Manabe, R., Nomoto, M., Tada, Y., Ishizaki, K., and Kohchi, T. (2016). Phytochrome signaling is mediated by PHYTOCHROME INTERACTING FACTOR in the liverwort *Marchantia polymorpha*. The Plant Cell **28**: 1406–1421.

Ishizaki, K., Nishihama, R., Ueda, M., Inoue, K., Ishida, S., Nishimura, Y., Shikanai, T., and Kohchi, T. (2015). Development of Gateway binary vector series with four different selection markers for the liverwort *Marchantia polymorpha*. PLoS ONE **10**: e0138876.

Ishizaki, K., Nishihama, R., Yamato, K.T., and Kohchi, T. (2016). Molecular genetic tools and techniques for *Marchantia polymorpha* research. Plant and Cell Physiology **57**: 262–270.

Nelson, D.R. (2006). Cytochrome P450 Nomenclature, 2004. In Cytochrome P450 Protocols, I.R. Phillips and E.A. Shephard, eds, Methods in Molecular Biology. (Humana Press: Totowa, NJ), pp. 1–10.

Sugano, S.S., Nishihama, R., Shirakawa, M., Takagi, J., Matsuda, Y., Ishida, S., Shimada, T., Hara-Nishimura, I., Osakabe, K., and Kohchi, T. (2018). Efficient CRISPR/Cas9-based genome editing and its application to conditional genetic analysis in Marchantia polymorpha. PLoS ONE **13**: e0205117.

Yamaoka, S. et al. (2018). Generative Cell Specification Requires Transcription Factors Evolutionarily Conserved in Land Plants. Current Biology **28**: 479-486.e5.